Development of On-site Environmental Analytical Methods for Nitrogen Compounds Using Microfluidic Paper-based Analytical Devices

マイクロ流体ペーパー分析デバイスによる窒素化合物の現場環境分析法の開発

Mika ISOYAMA

Graduate School of Natural Science and Technology

(Doctoral program)

OKAYAMA UNIVERSITY

March 2025

Contents

Chapter 3. Development of μPADs for Measuring Ammonium Ions

Abstract

Water analysis is essential for ensuring the safety of the water supply. Currently, around 2 billion people worldwide lack access to safe drinking water, and 3.6 billion people are using water without proper treatment of waste. The World Health Organization (WHO) has reported that safe Water, Sanitation, and Hygiene (WASH) practices could prevent 1.4 million deaths annually. The Sustainable Development Goals (SDGs) proposed in 2015 address water pollution, a significant issue in many regions, including developing countries. In areas with insufficient infrastructure and power supply, cost-effective, simple analytical techniques are crucial for continuous water quality management via on-site analysis. Simple analytical techniques are useful not only in developing countries but also for businesses and individuals to reduce costs through basic measurements. In settings where frequent checks are necessary, like manufacturing process management and quality control, such analytical techniques could likely achieve continuous monitoring and simple screening. Furthermore, the application of these analytical techniques in environmental education in schools holds great promise.

Microfluidic paper-based analytical devices (μPADs) offer advantages such as low cost, portability, and the absence of the need for external equipment. They are gaining attention as simple analytical tools in various fields, including environmental analysis, food analysis, and clinical testing. Thus, this thesis reports on the development of μPADs for the simple on-site analysis of environmental water samples. The target compounds are inorganic nitrogen compounds, specifically nitrite ions, nitrate ions, and ammonium ions, which are substances with regulated limits in wastewater and contribute to environmental harm as nutrients. Additionally, the thesis discusses a simple method for the fabrication of μPADs. While the most common method for fabricating μPADs is using a wax printer, which can be difficult to obtain, the thesis explores a new approach for more accessible fabrication.

This thesis comprises five chapters.

Chapter 1 introduces the global water resources and the history of simple analysis methods using paper. It also provides an overview of μPADs, including their general fabrication methods.

Chapter 2 reports on the development of μPADs for measuring nitrite ions and nitrate ions. These nitrogen compounds are the causative agents of methemoglobinemia. Additionally, they react with amines to form nitrosamines, which are carcinogenic substances. Therefore, we need to regulate the discharge of these compounds into environmental waters.

This study involved the fabrication of layered PADs, optimization of the analytical conditions, and application to practical analysis. The same design of PADs could measure both nitrite and nitrate ions. The Greiss reaction served as the colorimetric method for the detection of nitrite ions. The Greiss reaction similarly detected nitrate ions after reduction using zinc powder. Thus, the μPADs for measuring nitrate ions contained zinc powder as a reducing agent.

The presence of zinc not only partially reduced nitrate ions but also lowered their detection sensitivity. Three calibration curves were constructed to address these issues: one for nitrite ions, one for nitrite ions treated with zinc, and one for nitrate ions treated with zinc. These curves corrected the influence of zinc on the insufficient reduction of nitrate ions and the degradation of sensitivity for nitrite ions. The developed μPADs permitted the measurements of environmental water samples that demonstrated the practical applicability of the method.

Chapter 3 reports on the μPADs developed for measuring ammonium ions. In our daily lives, we use ammonia as an essential material for industrial products and fertilizers. However, the emission of ammonia in industrial, agricultural, and living processes causes contamination of natural water and soil. Ammonium-nitrogen is converted into nitrite nitrogen and nitrate nitrogen by microorganisms.

Ammonium ions were detected by generating indophenol-type dye using α-naphthol. The reaction uses harmless or low-toxic substances, so it would be suitable for green chemistry. The conditions for the colorimetric reaction were optimized to apply it to μPADs. The calibration curve was constructed by plotting the color intensity against the concentrations of ammonium ions using the optimized μPADs. The calibration curve showed good linearity in the low concentration range of 0.01–0.05 mg L^{-1}.

Chapter 4 presents the results of investigating a facile fabrication method for μPADs. Rosin, a natural resin, was used as a hydrophobic barrier because of its easy availability. The coating method was spray application, which easily allowed for the formation of fluidic channels. We determined the optimal conditions by varying the concentration of the rosin, heating temperature and time, spraying distance, number of sprayings, and thickness of the mask.

The chemical resistance of the fabricated channels was evaluated using acids and bases. It was found that strong bases caused the channels to collapse. However, it was concluded that the μPADs could be used for samples under conditions with a pH of 9 or lower.

Chapter 5 provides a general conclusion of the study.

Chapter 1

General Introduction

Chapter 1. General Introduction

1.1 The world’s water environment

The United Nations Summit in 2015 established the Sustainable Development Goals (SDGs) with the aim of realizing a sustainable and better society. The SDGs consist of 17 goals, with No. 6 goal being "Clean water and sanitation". The goal is to ensure access to and sustainable management of water and sanitation for all. Currently, 2 billion people around the world do not have access to safe drinking water, and 3.6 billion people (about half of the world's population) use water that has not been treated with excrement. According to a 2020 report, only 74% of the world's population has access to a safely managed drinking water supply that is uncontaminated and available on-site when needed, while 2 billion people have limited access or are forced to rely on unprotected drinking water sources [1]. 115 million people use water directly from ponds, rivers, irrigation canals, etc. [2]. Furthermore, 3.4 billion people lack access to a hygienic toilet at home, and 419 million of these individuals urinate outdoors, often in grassy areas, as reported [2].

It has been reported that 4.9 million children die before their fifth birthday each year [3]. In other words, one young life is lost somewhere in the world every six seconds due to various causes. The WHO has reported that safe WASH (Water, Sanitation, and Hygiene) services could prevent 1.4 million deaths per year [4]. However, many people currently lack access to safe WASH services when they need them most. Contamination of domestic water, such as drinking water, has a serious impact on human health. For this reason, routine monitoring of water quality is extremely important. Achieving No. 6 Goal by promoting the widespread use of sanitary toilets, ensuring the safety of drinking water, and providing continuous water quality management will help solve this critical problem. The first step in improving water quality is for residents to understand how contaminated the water they use in daily life is and to become aware of the problems with water pollution.

The problem of water pollution is prominent in developing countries, especially among the least developed countries, and water quality testing is essential to establish safe WASH in these regions. The majority of water quality testing generally requires experts who have acquired knowledge and skills at specialized institutions equipped with

expensive equipment. However, in many regions, major issues such as cost, insufficient personnel and power sources, and a lack of facilities and environment pose significant challenges to daily water quality testing. Official methods for testing water quality necessitate cooling samples for transportation to the laboratory after collection. However, immediate analysis of the sample is preferable to prevent degradation or change in chemical species during transportation. Furthermore, conducting the analysis requires a significant number of man-hours and typically takes a considerable amount of time to complete. The issue of wastewater treatment for samples also arises during wet analysis. In order to solve these problems, microfluidic paper-based analytical devices (μPADs) have been attracting attention in recent years and are expected to become an extremely promising tool for simple analysis.

1.2 History of simple analysis using paper and μPADs

Since ancient times, people have used paper as a familiar material and as a simple substrate in chemical analysis. Paper is an excellent material for many purposes due to its lightweight, flexibility, and low cost. It also serves as an excellent absorbent for liquids, boasting a high specific surface area owing to its porous fibrous structure. Solutions spontaneously permeate and diffuse through it by capillary action without the need for external devices such as pumps. It can be burned, making the waste process simple and straightforward. Trees, the raw material of paper, absorb carbon dioxide during their growth, thereby fixing carbon. For this reason, people accept the idea that paper is carbon neutral, meaning it does not emit new carbon dioxide. These excellent characteristics have led to its use as a green material for a variety of purposes from ancient times to the present.

In the early 1800s, Gay-Lussac introduced litmus paper for acids [5]. Researchers have developed simple analyses, such as dry chemistry and dipsticks, using paper as a substrate, including litmus paper and pH paper. As mentioned above, paper sensors have excellent characteristics such as being lightweight, inexpensive, and disposable, making them particularly useful for point-of-care testing (POCT). For example, the first paper device for measuring glucose in urine was reported in 1956 [6], and familiar items such as urine test strips [7] and pregnancy test kits that patients can use at home [8] are useful for simple and rapid measurement. During the COVID-19 pandemic that became a

major epidemic around 2020, self-diagnosis and rapid measurement at home are still fresh in our memories. The demand for POCT is increasing year by year, but all of these tests mentioned above are mainly intended for qualitative analysis and show positive or negative results or are used as a rough guide.

In 1937, Yagoda created a ring-shaped hydrophobic pattern on filter paper, deposited a colorimetric reagent inside the ring, and dropped a sample onto it to detect nickel and iron in a solution [9, 10]. A mold press and paraffin hydrophobic ink were used to form the flow channels. In this research, the detection limit improved as the ring diameter decreased. Applying this technology, Müller et al. created long and thin flow channels on filter paper in 1949, which developed into microfluidic channels [11]. The application of paper-based analytical methods subsequently progressed with the development of chromatography.

Research on microfluidic devices [12] and lab-on-a-chip [13, 14] emerged in the 1990s. The microfluidic devices use glass, silicon, resin, etc., as substrates. In 2007, Whitesides et al. proposed a method of fabricating channels on filter paper to achieve flow analysis. They named the devices as microfluidic paper-based analytical devices (μPADs) [15, 16]. This report prompted many researchers to develop new devices using filter paper as a substrate [17], i.e., the μPADs have attracted much attention as an alternative to microfluidics using glass and plastic substrates. In μPADs, capillary action guides a sample into a hydrophilic channel, where it reacts with a pre-deposited reagent. In many cases, colorimetry is used to detect the color change caused by the reaction, and the target substance can be quantified from the color intensity. Unlike classical test paper strips, colorimetry yields results in the form of numerical values. Thus, the μPADs have led to the expansion of research into quantitative analysis and have entered a new phase.

The World Health Organization (WHO) Sexually Transmitted Disease Diagnostics Initiative (SDI) has proposed the ASSURED criteria in response to the growing demand for analytical devices capable of conducting on-site environmental chemical measurements and home health examinations in recent years. It is a set of standards required for testing and measurement devices intended for point-of-care testing (POCT) in environments with insufficient facilities and is composed of the initial letters of seven items that describe the characteristics of the devices. Specifically, testing and measurement devices must meet the following seven criteria: Affordable, Sensitive,

Specific, User-friendly, Rapid and robust, Equipment-free, and Deliverable to end-users. Due to their characteristics and recent attention, we expect the μPADs to meet these requirements. Particularly in the field of environmental analysis, quantitative measurement of measured substances is often required because of emission standards, so the μPADs would be a promising tool for achieving on-site analysis with simple operations. The characteristics of the μPADs are described in Chapter 1.2.1.

1.2.1 The characteristics of μPADs

Since μPAD is made of paper, it has the following characteristics (1) to (10).

(1) It is inexpensive, so manufacturing costs can be kept low.
(2) It is lightweight, so it is highly portable.
(3) Because it has a porous structure and is hydrophilic, when a solution is dropped, it spreads spontaneously by capillary action, so no external devices such as pumps are required.
(4) The reagent can be immobilized on paper and stored and transported.
(5) Pretreatment of samples that require filtration is also not required.
(6) The color of the substrate is white, so color changes are easy to confirm. (Basically, detection of the measured substance is performed by colorimetric analysis.)
(7) Only a small amount of reagent is required.
(8) It can be disposed of by incineration, so no waste liquid treatment is required.
(9) Depending on the design, multiple results can be obtained at once, allowing for high throughput.
(10) It is also possible to measure several substances simultaneously by changing the reaction of the branched detection parts.

These characteristics give μPADs many advantages. The high specific surface area of paper allows many enzymes and dye molecules to be immobilized. Cellulose, the main component of paper, is highly compatible with molecules such as proteins, making it easy to apply analytical methods such as enzyme reactions that utilize them [18]. In addition, because the surface has hydroxyl groups and a small number of carboxyl groups [19], various analytical reagents can be immobilized [18]. Since the reagents are pre-added, end users only need to introduce the reagent solution, making the measurement user-

friendly. Measurements can be performed without handling chemicals or by carrying minimal reagents, and even people without analytical skills can easily obtain measurement results.

As the fabrication methods are simple, facile, and inexpensive, mass production is possible using a printer and cutting machine. It can also be easily produced by hand, so anyone can readily make it. The thin, compact device can be carried to the site and mailed by regular mail, making it simple to transport. It is a device that considers the environmental impact and safety from the perspective of waste liquid treatment. Additionally, it is a green analytical device because it uses paper, a carbon-neutral material.

Many μPADs have been developed for the purpose of diagnosis and measurement, especially in developing countries, because they are suitable for on-site environmental analysis and POCT and are inexpensive to manufacture. Our laboratory has also developed a variety of μPADs to date [20-32].

1.2.2 The relationship between μPAD and the SDGs

The United Nations Summit adopted the SDGs in 2015, international goals aimed at a sustainable and better world by 2030. The SDGs, which aim to leave no one behind on the planet, consist of 17 goals and 169 targets. The 17 goals of the SDGs are shown in Table 1.1.

The development of portable, simple, rapid, and safe measurement devices is crucial in recent chemical measurements, and it closely correlates with some of the SDGs. The environment relates to all 17 SDGs and directly associates with 13 goals. The environment also indirectly relates to the remaining four goals. The inexpensive, portable, and rapid measurement realized by μPADs enables on-site analysis and continuous monitoring and is expected to improve environmental problems. Figure 1.1 displays the goals deemed particularly relevant. The most relevant goals are No. 6: clean water and sanitation; No. 13: climate action; No. 14: life below water; and No. 15: life on land. Rapid measurement in clinical trials is useful for the early detection of diseases. Therefore, it is also related to No. 3: Good health and well-being. Furthermore, because anyone can easily obtain analysis results, μPADs can be used in educational settings as teaching

materials for elementary and junior high school students who have not acquired analytical skills, and it is possible to provide quality education. We believe that aiming to commercialize simple measurements using μPADs will also lead to supporting the SDGs.

Table 1.1 The relationship between SDGs goals and the environment [33]

SDGs goals		Related to the environment
1	No poverty	
2	Zero hunger	○
3	Good health and well-being	○
4	Quality education	○
5	Gender equality	
6	Clean water and sanitation	○
7	Affordable and clean energy	○
8	Decent work and economic growth	○
9	Industry, innovation and infrastructure	○
10	Reduced inequalities	
11	Sustainable cities and communities	○
12	Responsible consumption and production	○
13	Climate action	○
14	Life below water	○
15	Life on land	○
16	Peace, justice and strong institutions	
17	Partnerships for the goals	○

Figure 1.1 SDGs related to μPADs

1.2.3 General method for fabricating μPADs

The fabrication methods for μPADs can be classified into four types: photolithography, printing, cutting, and equipment-free methods [17]. This chapter summarizes the characteristics of each method.

(1) Photolithography methods

Photolithography is a microfabrication technique that creates patterns by partially exposing the surface of a material coated with a photosensitive substance to light. The manufacture of semiconductors and liquid crystal displays generally uses it to fabricate electronic circuits on a substrate. This method can produce patterns of various sizes with high precision, making it suitable for mass production [18].

The first reported method for fabricating μPADs was optical lithography using a photomask [34]. Initially, filter paper is soaked in photoresist such as SU-8. A patterned photomask covers it to protect it from light, which solidifies the photoresist. Thus, the unmasked regions form a hydrophobic solid. Thereafter, the uncured photoresist is removed by washing with an organic solvent in the masked regions that form hydrophilic channels. So, aqueous solutions flow only through those regions.

An alternative method is the irradiation of plasma or ultraviolet light to create hydrophilic channels. The photoresist makes the entire filter paper hydrophobic and then irradiates plasma or ultraviolet light through a photomask to remove the hydrophobic functional groups. In this case, unmasked regions work as hydrophilic channels.

Li et al. made the entire filter paper hydrophobic using an alkyl ketene dimer, sandwiched it between metal plate masks, and irradiated it with plasma to create a hydrophilic channel [35]. Conversely, Asano et al. employed octadecyltrichlorosilane to create the hydrophobic paper substrate. The hydrophobic paper substrate was irradiated with ultraviolet light under covering with a photomask [36]. The photomasks were prepared using a 3D printer in this study. Kao et al. reported a method to directly form the hydrophobic surface of filter paper using fluorocarbon plasma [37]. Channels were formed using a stainless-steel metal mask. In this case, the surface of the filter paper can be hydrophobic without pretreatment.

However, the photolithography method requires an individual photomask for

each design, a large number of steps, and equipment for sources generating light or plasma. Currently, researchers rarely use it due to its complexity and difficulty.

(2) Printing methods

There are fabrication methods that use wax printers or inkjet printers to pattern channels on filter paper. Fabrication using a printer is simple and mass-produced, with excellent reproducibility.

Wax printers use solid wax ink to print paper and function as printing machines in offices. They also work for industrial design and packaging [18]. Conventional inkjet printers use liquid ink, but wax printers melt solid ink to transfer it to paper. The wax printer has advantageous characteristics that permit printing on any paper independent of its quality and high-speed printing. Since the ink is solidified wax, no plastic containers, such as cartridges or ink tanks, are required, and no cartridges are discarded. Many researchers employ wax printers for the fabrication of μPADs because it simplifies printer preparation and maintenance, allowing for quick and simple channel fabrication. A method for fabricating μPADs using a wax printer was first reported in 2009 [38]. When the channel designed using computer drawing software is printed onto filter paper and then heated, the wax melts and soaks into the filter paper, forming the channel.

The American company Xerox once manufactured wax printers, but due to the declining demand for wax printers and the price down of laser printers, they no longer manufacture them. The only way to obtain a wax printer is to look for one secondhand. Additionally, the ink's sales have ended in Japan, making it difficult to obtain. As the number of wax printer users declines, the discontinuation of the ink supply is unavoidable.

Inkjet printing is widely used because it ejects ink droplets with high precision, prints without touching the substrate, does not contaminate the channel, and produces repeatedly. We can fill ink cartridges with hydrophobic substances and analytical reagents to print them on paper. Commercial inkjet printers easily produce μPADs when suitable hydrophobic materials are available. Generally, we add reagents to μPADs using a micropipette, but inkjet printers can also incorporate reagents to form reaction zones on μPADs, if the ink of the reagent smoothly ejects.

Others use piezo-driven inkjet printers from Microjet companies [39, 40]. The

process involves soaking filter paper in polystyrene, drying it, and then spraying toluene on the inkjet printer to remove the polystyrene and form a hydrophilic channel. In response to this, a method has been reported in which the contents of an ink cartridge are replaced with ultraviolet light-curing resin as UV ink that does not contain volatile organic solvents and printed on filter paper [41]. A design is printed on filter paper using a mixture of octadecyl acrylic acid and 1,10-decanediol diacrylic acid and then irradiated with ultraviolet light, where the ink hardens as the components in the ink polymerize. Furthermore, reports suggest that you can fill an ink cartridge with a heptane solution of alkyl ketone dimer as ink, print it, and then heat it to form a channel [42].

(3) Cutting methods

The channels are created by cutting filter paper into the shape of the channel. In this method, the entire cut filter paper becomes the channel, so the design is more limited than with other methods. A cutting plotter or laser cutter performs the cutting. The cutting plotter becomes less reproducible as the shape becomes more complex, necessitating adjustments to the blade angle and pressure. After cutting, the paper pieces are sandwiched between laminate film or attached to a plastic or glass substrate, depending on its thickness. There have also been instances where an XY plotter replaced the pen part with a knife to cut out the channels [43]. A carbon dioxide laser [44] or a craft cutter [45] also cut filter paper to form flow channels.

(4) Equipment-free methods

Methods for making channels by hand without using special equipment include flexographic printing [46], stamping [47], screen printing [48], handwriting, wax dipping [49], and the use of the resin ink filled in an XY plotter pen [50]. Reports suggest that one can make channels by hand using wax pens [51, 52], eyeliner, or oil-based markers [53]. Making channels by hand is the easiest method, but it is difficult to make precise and accurate channels reproducibly.

1.2.4 Channel formation using wax printer

Chapter 1.2.3 provided an explanation of the wax printer. Figure 1.2 shows the appearance of the wax printer and the wax ink, a solid ink consisting of carbamates and hydrocarbons that serves as a hydrophobic barrier. When heated, the wax that forms a channel pattern on the paper surface melts and penetrates into the backside of the filter paper (Figure 1.3). Figure 1.4 shows the photographs of filter paper with wax-printed channels before and after heating. Figure 1.4 (a) and (b) indicate the frontside and backside of the printed paper before heating. The backside is white and has no wax, but the design is faintly visible. Therefore, we can know that the wax is printed only on the front side prior to heating. Conversely, Figure 1.4 (c) and (d), which represent the front side and backside after heating, show the channel design appearing on the backside as a result of ink penetration. After the wax has melted, clear tape covers the bottom side to prevent the reagent and sample solutions from leaking out of the filter paper when they are added to the μPAD. To prepare for analyte measurements, we cut the μPADs into individual devices. A micropipette adds specific amounts of reagents to the reaction and detection parts of the μPADs, and after drying, the assembled μPAD measures the analytes.

Figure 1.2 Wax printer and wax ink appearance

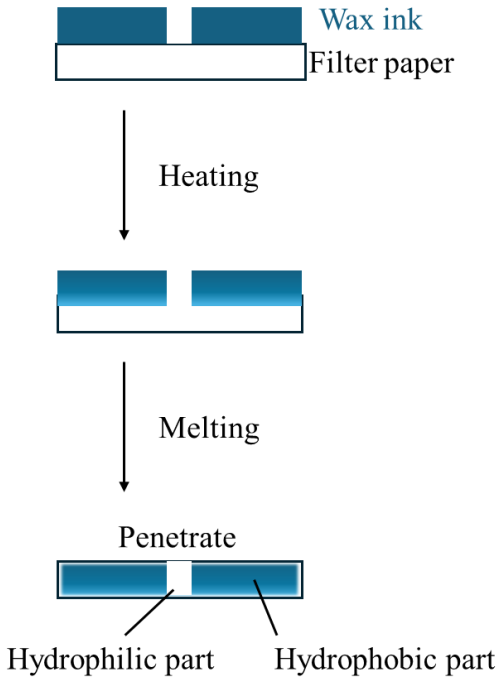

Figure 1.3 Illustration of melting wax ink applied to filter paper

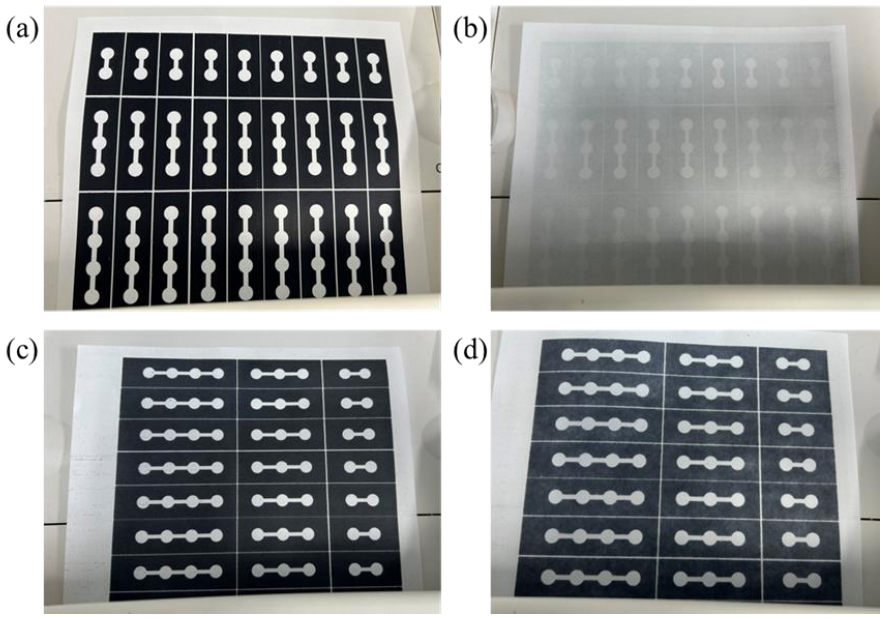

Figure 1.4 Printed μPADs channel

(a: front side before heating, b: back side before heating, c: front side after heating, d: back side after heating)

1.3 References

[1] WHO World health statistics 2023 : monitoring health for the SDGs, sustainable development goals **2023**, 53.

[2] Progress on household drinking water, sanitation and hygiene (WASH) 2000-2022: Special focus on gender, WHO/UNICEF JMP **2023**.

[3] Levels and trends in child mortality 2023, UNICEF **2024**.

[4] WHO Global water, sanitation and hygiene Annual report 2022 **2023**, 1.

[5] Crosland, M. Gay-Lussac Scientist and Bourgeois, Cambridge University Press **1978**.

[6] Comer, J. P. *Anal. Chem.* **1956**, *28*, 1748.

[7] Schiff, H. *Annalen der Chemie* **1866**, *140* (1), 92-137.

[8] Liu, H.; Xiang, Y.; Lu, Y.; Crooks, R. M. *Angew. Chem. Int. Ed.* **2012**, *51*, 6925.

[9] Yagoda, H. *Anal. Chem*. **1937**, *2*, 9.

[10] Yagoda, H. *US Pat.*, **1938**, 2129754.

[11] Müller,R. H.; Clegg, D. L. *Anal.Chem.* **1949**, *21* (9), 1123–1125.

[12] Whitesides, G. M. *Nature* **2006**, *442* (7101), 368–373.

[13] Janasek, D.; Franzke, J.; Manz, A. *Nature* **2006**, *442* (7101), 374–380.

[14] P. Yager,; Edwards, T.; Fu, E; Helton, K.; Nelson, K.; Tam, M. R.; Weigl, B.H. *Nature* **2006**, *442* (7101), 412–418.

[15] Martinez, A.W.; Phillips, S.T.; Butte, M.J; Whitesides, G. M. *Angew. Chem. Int. Ed.* **2007**, *46*, 1318-1320.

[16] Martinez, A.W.; Phillips, S.T.; Butte, M.J; Whitesides, G. M. *Proc. Natl. Acad. Sci. U.S.A.* **2008**, *105*, 19606–19611.

[17] Kaneta, T. *Bunseki* **2015**, *11*, 499-500.

[18] Yamada, K.; Suzuki, K.; Citterio, D. *Electrochemistry*, **2015**, *83* (1), 30-35.

[19] Alila, S.; Boufi, S.; Belgacem, M. N.; Beneventi, D. *Langmuir* **2005**, *21*, 8106.

[20] Karita, S.; Kaneta, T. *Anal. Chem.* **2014**, *86*, 12108.

[21] Karita, S.; Kaneta, T. *Anal Chim. Acta* **2016**, *924*, 60.

[22] Ogawa, K.; Kaneta, T. *Anal. Sci.* **2016**, *32*, 31.

[23] Alahmad, W.; Uraisin, K.; Nacapricha, D.; Kaneta, T. *Anal. Methods* **2016**, *8*, 5414.

[24] Shimada, Y.; Kaneta, T. *Anal. Sci.* **2018**, *34*, 65.

[25] Buking, S.; Suedomi, Y.; Nacapriicha, D.; Kaneta, T. *ACS Omega* **2019**, *4*, 15249-15254.

[26] Hashimoto, Y.; Kaneta, T. *Analytical Methods* **2019**, *11*, 179.

[27] Muhammed, A.; Hussen, A.; Kaneta, T. *Anal. Bioanal. Chem.* **2021**, *413*, 3339.

[28] Muhammed, A.; Hussen, A.; Redi, M.; Kaneta, T. *Anal. Sci.* **2021**, *37*, 585.

[29] Muhammed, A.; Hussen, A.; Kaneta, T. *Anal. Sci.* **2022**, *38*, 123.

[30] Muhammed, A.; Hussen, A.; Kaneta, T. *S. Afr. J. Chem.* **2023**, *77*, 1.

[31] Muhammed, A.; Hussen, A.; Kaneta, T. *Anal. Sci.* **2024**, *40*, 709.

[32] Umeda, M. I.; Danchana, K.; Fujii, T.; Hino, E.; Date, Y.; Aoki, K.; Kaneta, T. *Talanta Open* **2024**, *10*, 100347.

[33] Transforming our world: the 2030 Agenda for Sustainable Development, United Nations **2015**.

[34] Martinez, A. W.; Phillips, S. T.; Butte, M. J.; Whitesides, G. M. *Angew. Chem., Int. Ed.* **2007**, *46*, 1318.

[35] Li, X.; Tian, J.; Nguyen, T.; Shen, W. *Anal. Chem.* **2008**, *80*, 9131.

[36] Asano, H.; Shiraishi, Y. *Anal. Chim. Acta* **2015**, *883*,55.

[37] Kao, P.-K.; Hsu, C.-C. *Microfluid. Nanofluid.* **2014**, *16*, 811.

[38] Lu, Y.; Shi, W.; Jiang, L.; Qin, J.; Lin, B. *Electrophoresis* **2009**, *30*, 1497.

[39] Abe, K.; Suzuki, K.; Citterio, D. *Anal. Chem.* **2008**, *80*, 692.

[40] Abe, K.; Kotera, K.; Suzuki, K.; Citterio, D. *Anal. Bioanal. Chem.* **2010**, *398*, 885.

[41] Maejima, K.; Tomikawa, S.; Suzuki, K.; Citterio, D. *RSC Adv.* **2013**, *3*, 9258.

[42] Li, X.; Tian, J.; Garnier, G.; Shen, W. *Colloids Surf., B* **2010**, *76*, 564.

[43] Fenton, E.M.; Mascarenas, M. R.; Lopez, G. P.; Sibbett, S. S. *ACS Appl. Mater. Interfaces* **2009**, *1*, 124.

[44] Fu, E.; Lutz, B.; Kauffman, P.; Yager, P. *Lab Chip* **2010**, *10*, 918.

[45] Cassano, C. L.; Fan, Z. H. *Microfluid. Nanofluid.* **2013**, *15*, 173.

[46] Olkkonen, J.; Lehtinen, K.; Erho, T. *Anal. Chem.* **2010**, *82*, 10246.

[47] Lu, Y.; Shi, W.; Jiang, L.; Qin, J.; Lin, B. *Electrophoresis* **2009**, *30*, 1497.

[48] Zhang, Y.; Zhou, C.; Nie, J.; Le, S.; Qin, Q.; Liu, F.; Li, Y.; Li, J. *Anal. Chem.* **2014**, *86*, 2005.

[49] Songjaroen, T.; Dungchai, W.; Chailapakul, O.; Laiwattanapaisal, W. *Talanta* **2011**, *85*, 2587.

[50] Pomanholo, P. V. V.; Andrade, L. M.; Silva-Neto, H. A.; Coltro, W. K. T.; Sgobbi, L. F. *Anal. Chem.* **2024**, *96*, 5349-5356.

[51] Li, Z.; Li, F.; Xing, Y.; Liu, Z.; You, M.; Li, Y.; Wen, T.; Qu, Z.; Li, X. L.; Xu, F. *Biosensors and Bioelectronics* **2017**, *98*, 478-485.

[52] Dungchai, W.; Chailapakul, O.; Henry, C. S. *Analyst* **2011**, *136*, 77.

[53] Aementa, S.; Turrillas, F. A. E.; Martinez, J. M. H. *J. Chem. Educ.* **2020**, *97*, 3852-3857.

Chapter 2

Development of μPADs for Measuring Nitrite and Nitrate ions

Chapter 2. Development of μPADs for Measuring Nitrite and Nitrate ions

2.1 Introduction

2.1.1 Nutrient salts in environmental waters

In water bodies such as the sea and lakes, phytoplankton are responsible for primary production. The nutrients required by phytoplankton include nitrogen, phosphorus, silicon, and trace metals. These salts are collectively called nutrients. These parameters significantly influence the ecosystem of aquatic areas. The growth and reproduction of plankton and seaweed require nutrients, whereas their high concentrations lead to eutrophication, which is a cause of red tides. We know that domestic and industrial wastewater, water runoff from farms, precipitation, and the decomposition of organic matter on the seabed are the primary sources of nutrients.

In this study, we focused on nitrogen compounds in nutrients and attempted to develop μPADs to easily measure them. Nitrogen exists in environmental water as nitrite nitrogen, nitrate nitrogen, and ammonia nitrogen. The purpose of this study was to develop μPADs for analysis of these types.

2.1.2 Nitrite nitrogen and Nitrate nitrogen

Nitrite and nitrate nitrogen are present at low concentrations in the natural environment, and trace amounts of nitrates are essential nutrients for plants and animals. These salts are known to be present in soil, water, and plants. However, due to their high solubility in water, their presence in soil is limited. Various factors like nitrogen-based fertilizers, animal waste, and industrial wastewater can cause them to dissolve and pollute groundwater, river water, etc. The sources of contamination are diverse, and it often occurs over a wide area, making it difficult to completely eliminate the burden on the soil.

When nitrite reaches the acidic environment of the stomach, it has been reported that it can combine with amines or amides to form toxic and carcinogenic compounds such as nitrosamines and nitrosamides [1, 2]. Furthermore, nitrate nitrogen can cause methemoglobinemia if consumed in excess. Salivary microorganisms can convert nitrates

to nitrites, which can be absorbed into the blood. Nitrite reacts with the iron in hemoglobin, irreversibly converting it to methemoglobin. Methemoglobin cannot bind to oxygen, so if the methemoglobin concentration in the blood exceeds 10%, the supply of oxygen becomes insufficient [2, 3]. This reaction is known to occur particularly in infants [4]. This is because the pH of gastric juice in infants is higher than in adults, making it easier for nitrite nitrogen to be produced by nitrate-reducing bacteria than usual. People with this constitution are more likely to develop methemoglobinemia. Since nitrates are tasteless, odorless, and colorless, there is a risk of ingesting too much of it without realizing it is in drinking water. For these reasons, emissions of all forms of these nitrogen compounds into the environment must be strictly regulated.

2.1.3 Nitrate nitrogen and nitrite nitrogen pollution in Japan

The Water Pollution Prevention Law designated nitrate nitrogen and nitrite nitrogen as harmful substances in 1999. Environmental quality standards were established for these chemical species, and continuous monitoring of groundwater quality also started simultaneously. Environmental standards establish the levels required for these species to protect human health and the living environment. The environmental quality standards for nitrate nitrogen and nitrite nitrogen are set at 10 mg L-1 or less. However, according to the results of groundwater measurements conducted by the national and local governments, nitrate nitrogen and nitrite nitrogen continue to show the highest exceedance rate of environmental standards among the monitored substances (Figure 2.1) [5]. In addition, wells in 442 municipalities across the country have been reported in which nitrate nitrogen and nitrite nitrogen were detected at levels above the standard (Figure 2.3) [5]. Figure 2.2 shows the number of wells that exceeded the standard in the continuous monitoring survey [5]. Although the number is currently decreasing, it is still large. We can also see that the number is higher than other substances for which environmental standards are set.

The national government regulates groundwater through legal systems, including the Water Pollution Control Law (factory and business wastewater), the Livestock Wastewater Law, the Septic Tank Law (domestic wastewater), and fertilization standards, with groundwater environmental standards at the core. The Water Pollution Control Law governs the discharge of wastewater into public water areas and the release of water into

the ground. The law also specifies measures for groundwater, including constant monitoring of water quality, prohibiting the emission of harmful substances to the ground, implementing emergency measures, and purifying contaminated groundwater.

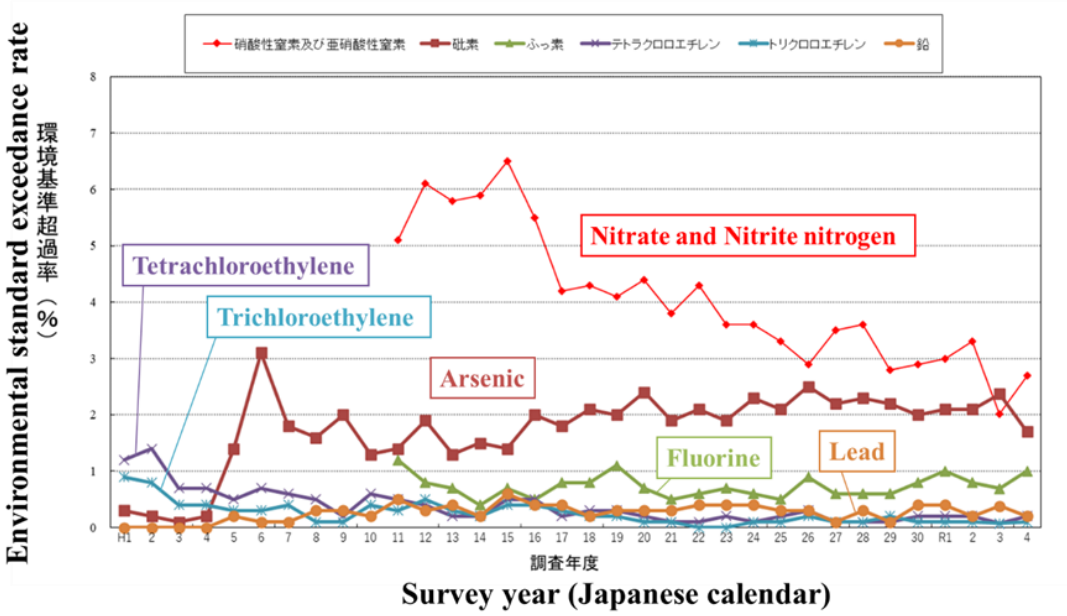

Figure 2.1 Survey results of Environmental standard exceedance rate

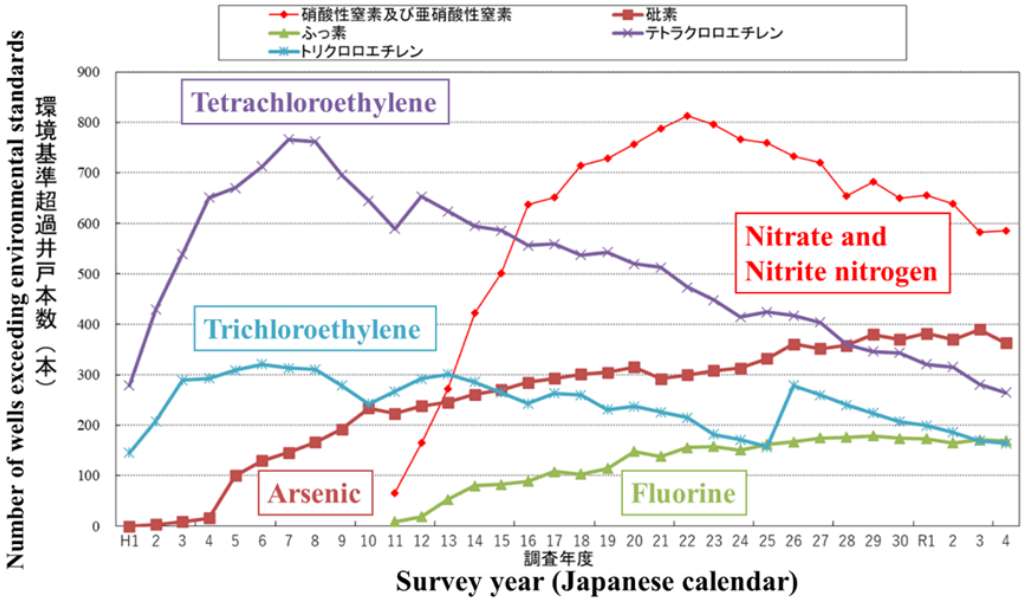

Figure 2.2 Survey results of number of wells exceeding environmental standards

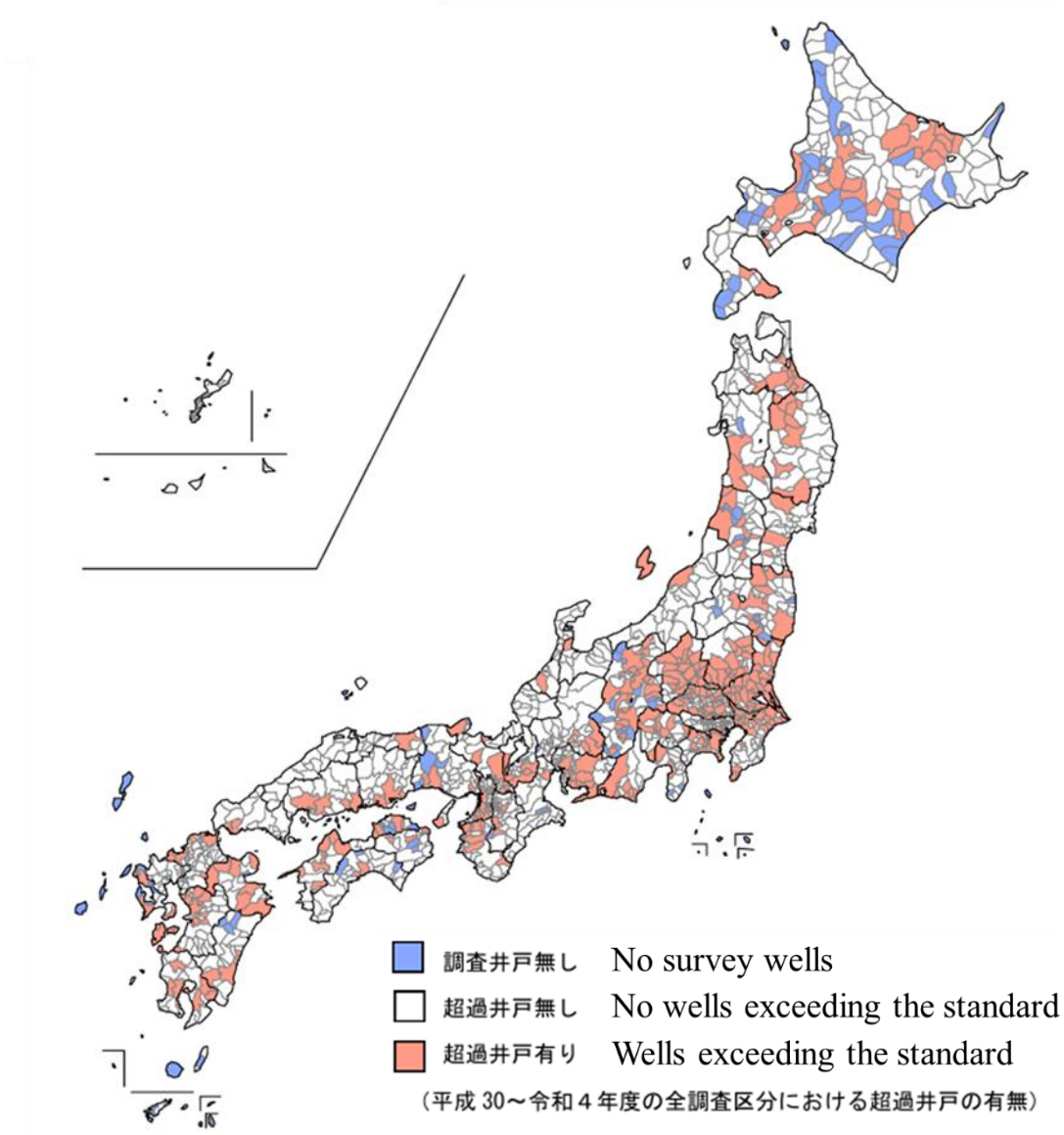

Figure 2.3 Survey results of exceeding environmental standards area

2.1.4 Measurement of nitrite and nitrate nitrogen

Several analytical methods that include spectrophotometry [6, 7], ion chromatography [8], flow injection analysis [9], capillary electrophoresis [10], and electrochemical techniques [11] can measure the concentrations of nitrite and nitrate ions. All of these techniques require extensive instrumentation that must be operated in a laboratory. However, oxidation during transportation and storage easily changes the concentration of nitrite ions, necessitating rapid measurements. Therefore, nitrite ions should be measured before they are converted to nitrate ions.

A common spectrophotometric method employs Griess reagent to measure nitrite and nitrate ions by coupling with a reducing reaction. If there is no reductant, nitrite ions react directly with Griess reagent. On the other hand, reductants like cadmium [12], cadmium-copper [13–15], zinc [16], and nitrate reductase convert nitrate ions into nitrite ions. However, the spectrophotometric method requires a large and expensive spectrophotometer and large volumes of reagents, samples, and waste.

Although many researchers have reported μPADs to determine the nitrite and nitrate levels, the reduction of nitrate still presents challenging issues due to the varying reduction efficiencies of different devices, and the influence of zinc on the simultaneous determination of nitrite and nitrate levels remains unclear. Therefore, the present study demonstrated a novel design of a layered PAD for determining nitrite and nitrate ions in natural water samples. The developed μPADs also clarified the effect of zinc in a colorimetric reaction using Griess reagent. Zinc degrades the sensitivity of nitrite ions, so we need to construct the calibration curves for nitrite ions both with and without zinc reduction. A correction method was proposed to measure the accurate concentrations of both nitrite and nitrate ions. Therefore, the developed μPADs simultaneously measured nitrite and nitrate ions in natural water samples, and the results were compared with those of conventional UV-VIS spectrophotometry.

2.2 Experiment

2.2.1 Materials and Equipment

Sulfanilamide, citric acid, N-(1-naphthyl)-ethylenediamine dihydrochloride, zinc dust, nitrate nitrogen standard solution (N 0.1 mg mL^{-1}), nitrite ion standard solution (NO_2^- 1000 ppm), and an ammonia assay kit (LabAssay Ammonia) were purchased from FUJIFILM Wako Pure Chemical Corporation (Osaka, Japan). A zinc suspension containing 0.2 g mL^{-1} of zinc was prepared by suspending zinc dust in water. The Griess reagent contained 50 mM sulfanilamide, 330 mM citric acid, and 10 mM N-(1-naphthyl)-ethylenediamine dihydrochloride. Chromatography paper (200×200 mm, 1CHR, Whatman™) served as the substrate for the μPADs. Filter paper, (5B or 5C, ADVANTEC, Tokyo, Japan) was used to remove zinc powder from the solutions in spectrophotometric measurements. PARAFILM (Bemis Company, Inc., WI, USA) controlled the time for the reduction of nitrate ions on the μPADs.

Natural water samples were collected from wells, ponds, and a brackish lake in and nearby the National Institute of Technology, Yonago College and Okayama University. The amounts of nitrite and nitrate ions were measured via both the μPADs and a spectrophotometer.

The μPADs were designed using Microsoft Office Power Point 2016. The μPADs were printed using a wax printer, Color Qube 8580N (Xerox, CT, USA), and heated in an oven (EO-300V, AS ONE, Tokyo, Japan). The images of the detection zones on the μPADs were scanned using a CanoScan LiDE400 scanner (Canon, Tokyo, Japan). We used a V-730 spectrophotometer (JASCO, Tokyo, Japan) to measure the absorbance of the reaction product with Griess reagent for conventional absorption spectrophotometry. A Synergy Neo2 microplate reader (Agilent BioTek, CA, USA) was employed for the measurement of ammonia.

2.2.2 Detection of nitrite and nitrate ions

The Griess reaction is the most common method for detecting nitrite, which has been used since 1879 [17]. Under acidic conditions, nitrite reacts with a primary aromatic amine to form a diazonium salt. The diazonium salt then reacts with an aromatic compound containing an amino group to form a diazonium salt (Scheme 2.1). The resulting diazonium salt is an azo dye that absorbs at around 520 nm.

The Griess reagent was prepared with citric acid, sulfanilamide as a primary aromatic amine, and N-(1-naphthyl)ethylenediamine dihydrochloride as an aromatic compound containing an amino group. Since nitrate ions do not react with the Griess reagent, a reductant reduced them to nitrite. Zinc was used as the reductant in this study because of its lower toxicity to the human body, although reductants such as metallic Cd and Cu-Cd were known to be more efficient reductants.

The concentrations of each were measured simultaneously using two μPADs with the same channel design; one measures nitrite ions, and another measures nitrate ions. The μPAD, which contained zinc layers for the reduction of nitrate to nitrite ions, was used to determine the total concentration of nitrite and nitrate ions.

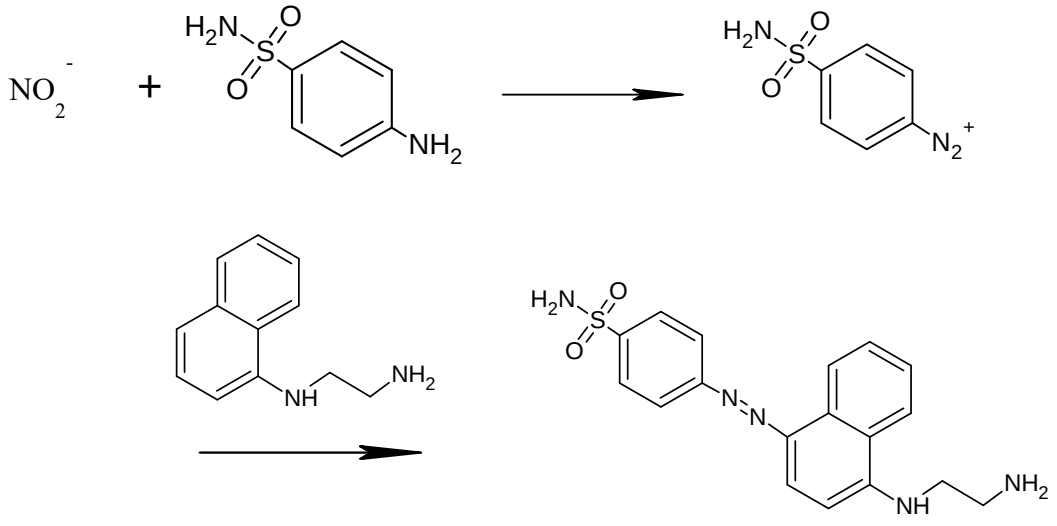

Scheme 2.1 Reaction mechanism of Griess reaction

2.2.3 Design and fabrication of µPADs

The µPADs were designed using Microsoft Office PowerPoint. Two types of µPADs, 2D and 3D, were designed in this study as shown in Figure 2.4 (a) and (b, c). Both types of µPADs were composed of a sample introduction zone, reduction zones, and detection zones. In the measurement of nitrite ions, no reducing agent was added to the reduction zones. Griess reagent, which reacts with nitrite ions to produce color, was added to the detection zone.

In the 2D-µPADs, the sample introduction zone, the reduction zone, and the detection zone were horizontally connected to flow the sample solution. Two reduction zones were aligned successively, and each contained 2 mg of zinc (5 µL of 0.2 g mL-1 zinc suspension was added 2 times). Each of the four detection zones contained 2 µL of Griess reagent. Forty40 µL volumes of sample solutions were added at the center of the µPADs.

In the 3D-µPADs, the two reduction zones were layered with untreated zones to prevent their contact (Figure 2.4 (b, c)). A suspension of 0.2 g mL^{-1} zinc powder was prepared, and 5 µL aliquots were dropped twice to the reduction zones using a micropipette. The detection zones contained 2 µL of Griess reagent, which was similar to the 2D-µPADs.

A wax printer printed the designed µPADs onto filter paper. The filter paper printed with wax ink was heated in an oven set at 120 °C for 1.5 min to permit penetration of the wax to the backside to form the channels. Following the heating process, the backside of the printed filter paper was covered with clear tape to prevent the leaking of solutions, and individual µPADs were cut to separate them into pieces.

In the 3D-µPADs, to facilitate folding, a knife traced the lines on both sides of the µPADs. This operation ensured excellent contact between the layers. The reduction zone contained zinc powder as a reducing agent.After the reagent solutions had dried, the µPAD was folded into a bellows shape, and the top and bottom layers were fixed onto two glass slides by sealing the surroundings with tape to prevent the solution from leaking. Due to the rectangular shape of the µPAD (Figure 2.4 (c)), layers were not firmly contacted without any support. Thus, two glass slides sandwiched the µPAD and were clamped with clothespins to maintain the flat shape.

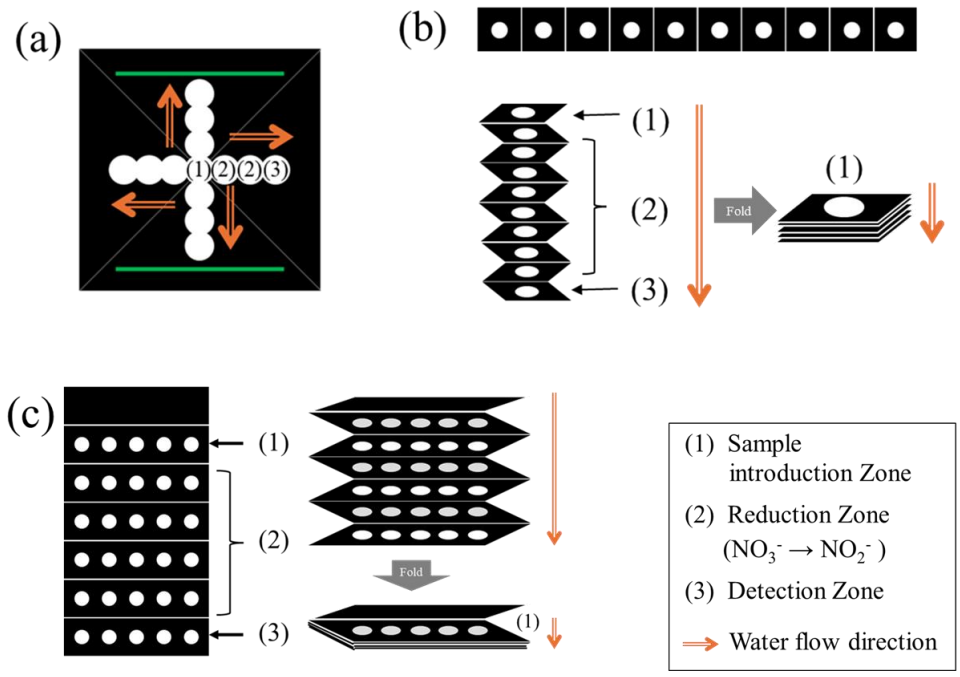

Figure 2.4 The design of μPADs
(a: Design 1 (2D-μPADs), b: Design 2 (3D-μPADs), c; Design 3 (3D-μPADs))

2.2.4 Measurement procedure using 3D-μPADs

A micropipette introduced a 40 μL sample solution into the μPAD. When the sample solution reached the detection zone, nitrite ions reacted for 30 min with the Griess reagent to develop the color. Subsequently, the detection zone was scanned using a scanner, and the color intensity was quantified using image analysis software, ImageJ. Section 2.2.4 provides details of the image processing.

Nitrate ions require reduction, of which the yield may depend on the reaction time. Therefore, the process of measuring nitrate ions requires a series of steps. Initially, the detection zone was placed on the top, and a hydrophobic film was inserted between the detection and reaction zones so as not to contact them, as shown in Figure 2.5. A sample solution was introduced into the reaction zone to reduce nitrate ions to nitrite ions with zinc powder for a certain time. After leaving the μPAD for 20 min for the reduction, the μPAD was turned over to face the detection zone downward. The hydrophobic film was then removed, and 10 μL of water was introduced from the sample introduction zone. The water flushed the nitrite ions in the reaction layers, enabling them to reach the detection

zone. The subsequent procedures for the colorimetric reaction and image processing are identical to those for nitrite ions.

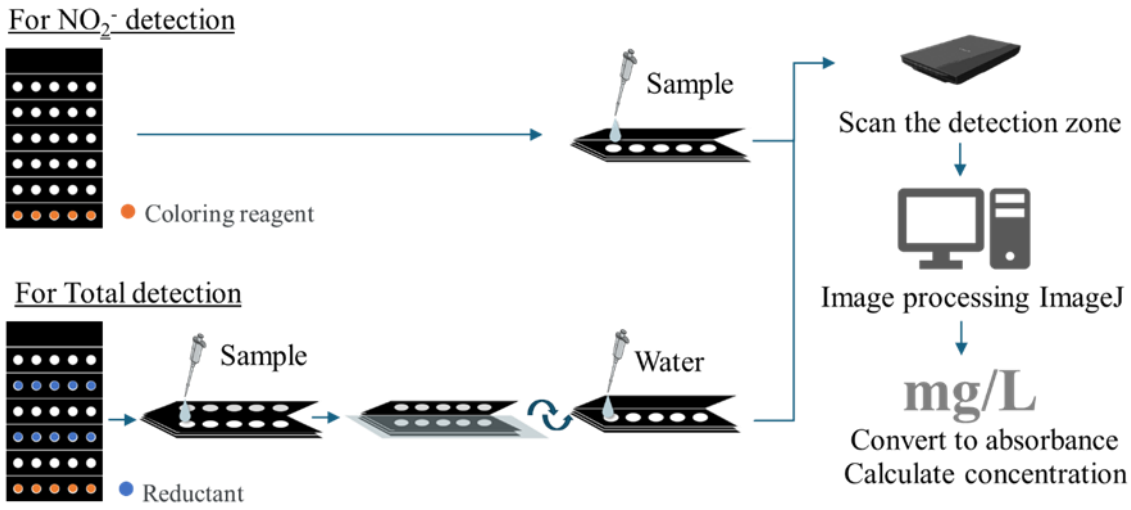

Figure 2.5 Schematic illustration of the measurement procedure

2.2.5 Image processing

The images of the detection zones were captured as JPG files by a scanner to obtain the color intensity after the reaction was completed. The image processing software ImageJ (National Institutes of Health) [18] processed the acquired images to quantify the color intensities of the detection zones.

Several color systems, like RGB and XYZ, express color information through the spectral intensity of incident light, the spectral intensity of reflected and transmitted light, and the overlap integral of color matching functions defined by the International Commission on Illumination (Commission internationale de l'éclairage: CIE) [19]. Since the color intensity of RGB and XYZ corresponds to the photometric intensity, it is possible to measure absorbance and reflection based on the Beer-Lambert law. In this study, the color of the detection zone was divided into three colors, red, green, and blue, using RGB in the quantification of intensity.

Whitesides et al. calculated pseudo-absorbance in immunoassays using RGB values

in digital images [20]. As referred to in the method by Whitesides et al., this study also calculated absorbance using Equation (2.1), where I_0 and I were the intensity of the green color for a blank and a sample, respectively. The green color was the most suitable for quantifying the color intensity in this study because the reaction product had a pink color and absorbed the green color region.

$$\text{Absorbance} = -\log_{10}\frac{I_0}{I} \qquad (2.1)$$

2.2.6 Spectrophotometric measurement

In the spectrophotometric method, nitrate ions were reduced using the following procedure: 5 mL aliquots of a 0.2 g mL^{-1} zinc suspension were added to 10 mL of nitrate ion solutions in the centrifuge tubes. The solutions were shaken for 10 s more than 5 or 6 times, and were then filtered with filter paper after 10 min. A 1 mL or 7 mL aliquot of the filtrate was transferred to a microtube, and 50 µL or 350 µL of the Griess reagent was added to react with the resultant nitrite ions. After 30 min, absorbance was measured at a wavelength of 520 nm [21].

2.3 Results and discussion

2.3.1 Selection of conditions for reduction

Cadmium or a mixture of cadmium and copper is often used as a reducing agent, but cadmium is highly toxic, and a safer reducing agent is desired. On the other hand, zinc has been reported as a reducing agent with minimal impact on human health. Additionally, nitrate reductase-mediated reduction has been reported [22]. Considering safety, zinc or enzymes were investigated as candidate reducing agents. A solution was prepared by adding 10 µL of grease reagent to 100 µL of 1 mM nitrate solution, then mixing it with a reducing agent, and the color of the solution was observed immediately and approximately 3-5 min later. Zinc suspension at 0.05 g mL^{-1} or nitrate reductase solution at 1.5 U mL^{-1} was used as the reducing agent.

Figure 2.6 shows photographs of the solution after the reaction when 1 µL or 10 µL

of zinc suspension was added as the reducing agent. Immediately after mixing, both solutions showed sufficient coloration, but in the solution with 10 μL of zinc suspension, the red-purple color disappeared after 3 min. Immediately after adding the zinc suspension, nitrate ions were reduced, and nitrite ions formed, reacting with the grease reagent to turn red purple. After 3 min, it is possible that this color reaction was inhibited by the presence of zinc. This is supported by the results from the colorimetric experiment using μPADs shown in Chapter 2.3.3. Furthermore, the results of investigating additional conditions are shown in Figure 2.7. The higher the amount of zinc suspension, the faster the color disappeared. Additionally, the higher the concentration of nitrate, the more intense the red-purple color of the solution, and when there was a higher amount of zinc, the color changed. At this point, the color of the solution changed from reddish purple to red and then from red to yellow, depending on the amount of zinc. The change in color suggests that the excessive amount of zinc caused the azo compound to be converted into other compounds.

Figure 2.8 shows the results when 1 μL and 5 μL of nitrate reductase were added. The solution immediately after adding the enzyme remained colorless but gradually developed a light pink color. In this experiment, the reaction was carried out at room temperature, but enzyme reactions are sensitive to pH and temperature conditions, so the color change may have been weak due to the complexity of optimizing the conditions. In this study, zinc powder, which showed a quicker and stronger color change, was chosen as the reducing agent.

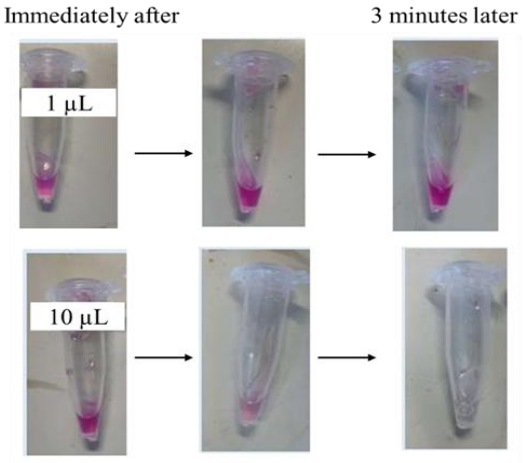

Figure 2.6 Color changes of the sample solution after the addition of the zinc suspension.

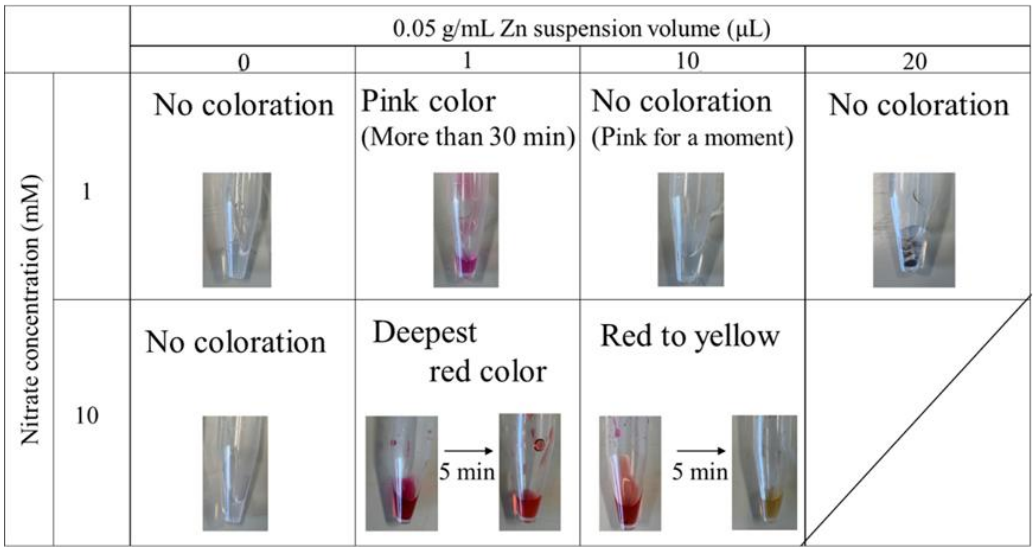

Figure 2.7 Color changes based on the amount of zinc and the concentration of nitrate ions.

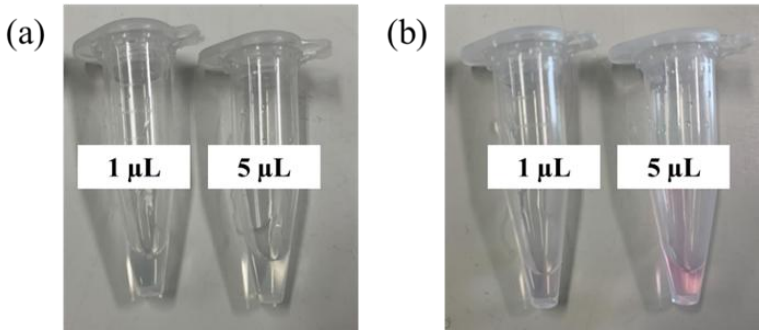

Figure 2.8 Color changes of the sample solution after the addition of the nitrate reductase.

2.3.2 Optimization of analytical conditions

To quantify the color intensity, each color value with a red, green, and blue value (RGB value) was extracted from the images. For this purpose, 2D-μPADs were used. In Figure 2.9, we can see how the RGB values change when nitrite ion solutions in the range of 0 to 350 μM are added to the μPADs.

When a calibration curve was constructed using the green value, a steep slope was observed, indicating the highest sensitivity with good linearity. The detection zone

reacts with nitrite ions to produce a red color, which results in the absorption of green light, the complementary color on the color wheel (Figure 2.10). Therefore, the green value of the RGB showed the largest variation. These findings confirmed that the green value changes linearly with concentration. Thus, in the actual analysis, the green value was used to quantify the color intensity, which was then applied to calculate absorbance.

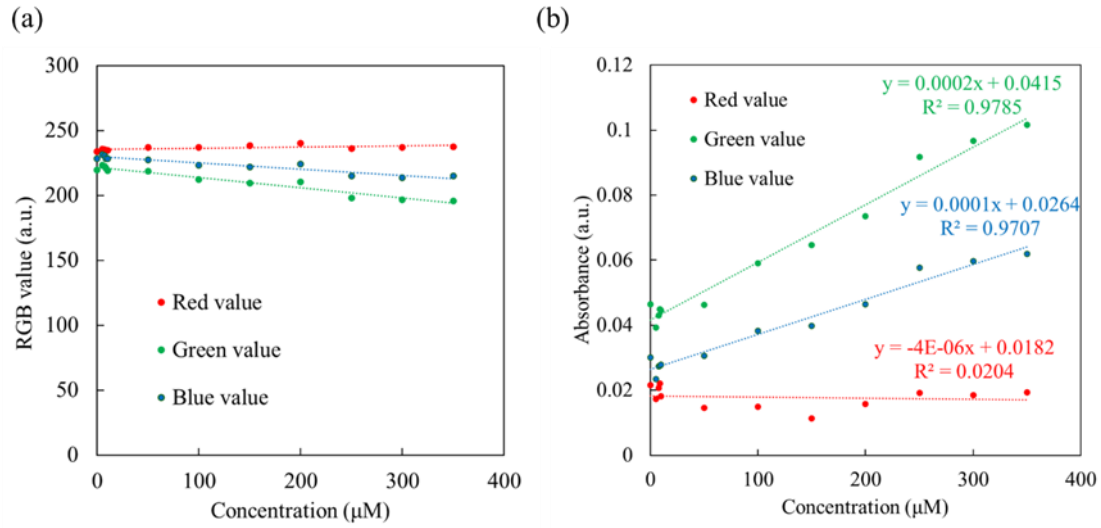

Figure 2.9 Measured value and calibration curve for each RGB

(a: RGB value, b: absorbance)

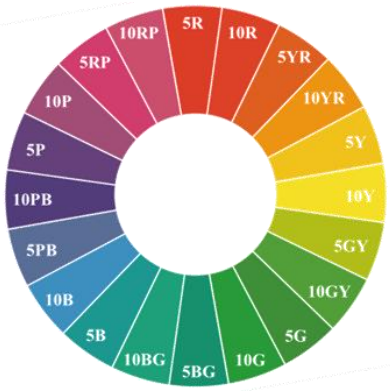

Figure 2.10 Munsell color wheel

2.3.3 Design Optimization

This chapter investigates (1) the types of designs developed, (2) optimization near the detection zone, (3) the number of layers in the reduction zone, and (4) The optimized design.

(1) The types of designs developed

Design 1 (Figure 2.4 (a)) is a 2D structure, where the introduced sample solution flows horizontally through the channels. Design 2 (Figure 2.4 (b)) is a 3D structure formed by folding the μPAD into a bellows shape, with the sample solution flowing vertically through the channels. A 0.2 mM nitrite ion solution was prepared and introduced into each of the channels.

In Design 1, since the sample flows from the center to the outer edges, the color reagent applied in advance was washed away by the flow of the introduced solution, causing the color to become stronger toward the edge, resulting in uneven coloring in the detection zone (Figure 2.11 (a)).

Figure 2.12 shows the results of testing concentration dependence. In Design 1, the absorbance was approximately 0.05 at 10 μM, which was higher than that of Design 2. Kitagawa et al. reported that when a nitrite ion-containing solution and purified water were stored in a sealed space, the purified water was contaminated by nitrite ions in the air [23]. In Design 1, the exposed detection zone may have reacted with the nitrite ions in the air and the Griess reagent, resulting in a higher absorbance than Design 2. Therefore, Design 2 was chosen, and the entire μPAD was covered with tape to isolate it from the air. As a result, at 10 μM, a lower absorbance was obtained.

Furthermore, it was found that the 3D structure showed better uniformity in coloring. Since the solution flows vertically from the top in the 3D structure, it is believed to result in more uniform coloring, as shown in Figure 2.11 (b). Figure 2.12 shows that the 3D structure exhibited a larger change in absorbance, and at higher concentrations, the absorbance was generally higher than Design 1. By using the 3D structure, more uniform coloring and higher sensitivity detection were achieved.

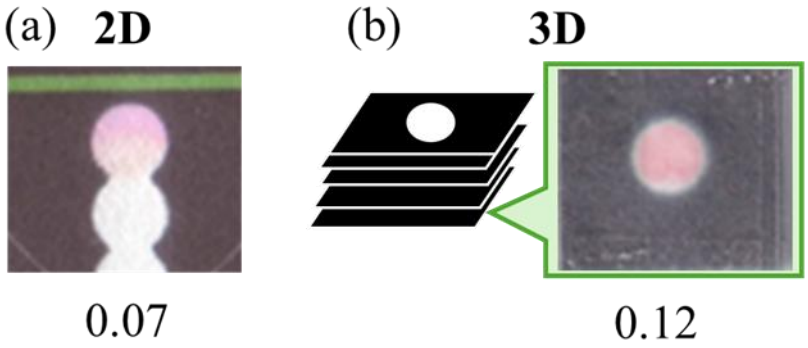

Figure 2.11 Photographs of the detection zone when introduced sample (a: 2D structure, b: 3D structure)
The numbers shown below the photographs are the absorbance of the detection zone.

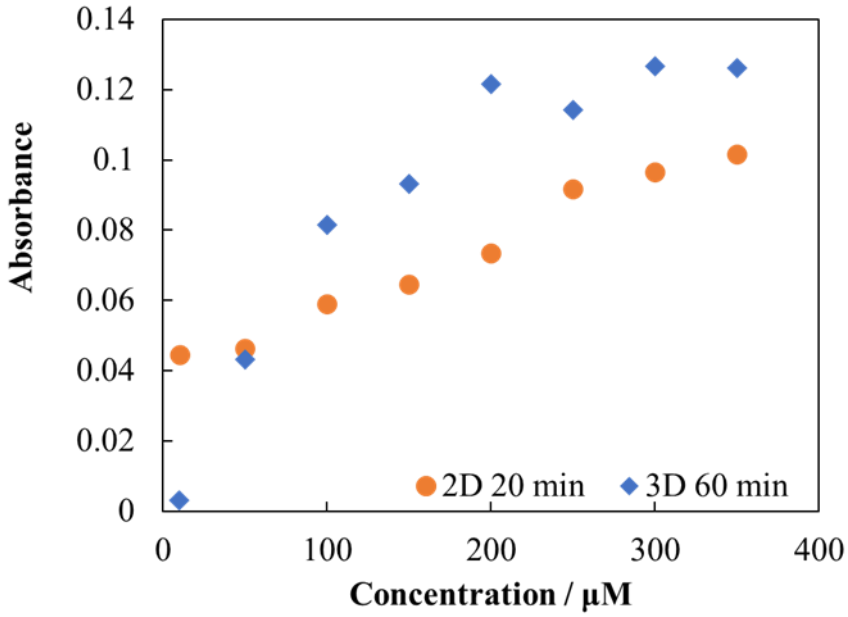

Figure 2.12 Concentration dependence (10 μM~350 μM nitrite solution)

(2) Configuration of the reduction and detection zones

To optimize the reduction and detection conditions, the μPADs were fabricated as shown in Figure 2.13. The design of Figure 2.13(a) consists of a two-layer structure for the entire μPAD, where zinc and the Griess reagent are in contact, while Figure 2.13(b) shows a three-layer structure for the entire μPAD, where zinc and the Griess reagent are not in contact. The Griess reagent was applied to the lower layer,

while the reducing agent was added to the upper layer, and then these layers were folded so that each was on the inside. The zinc suspension was designed to be placed inside the μPAD to prevent the zinc powder applied to the surface from peeling off when the suspension dries.

When a 0.7 mM nitrate ion solution was introduced as the sample solution into these μPADs, it was found that when zinc and the Griess reagent were in contact, no color developed (Figure 2.14(a)). This was also the case in the batch method (Chapter 2.3.1). These results indicate that zinc inhibits the Griess reaction. Therefore, the developed μPADs were designed with separate layers for the zinc and the Griess reagent.

Additionally, in the design shown in Figure 2.14(a), the black color of the zinc powder was visible through the detection zone. Based on these results, it was determined that at least three layers were necessary. To avoid contact between the reductant and the Griess reagent, the channels were created between the detection zone and the reduction zone without any applied material.

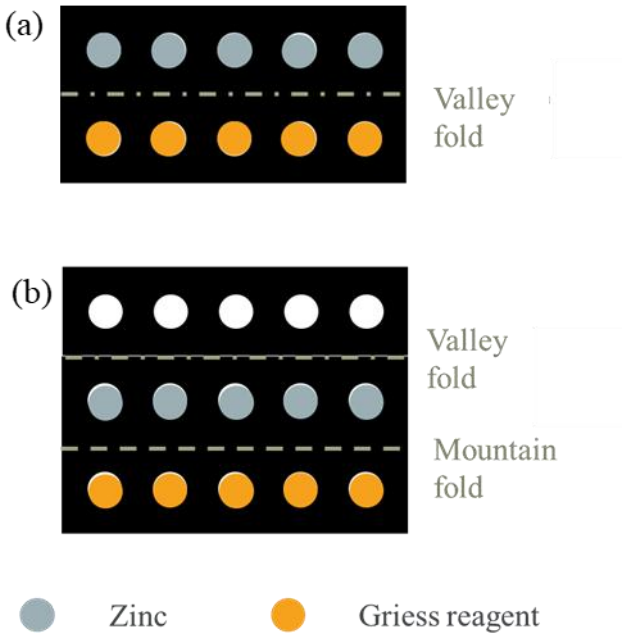

Figure 2.13 Design used in this experiment
(a: two-layer, b: three-layer)

(a)

(b)

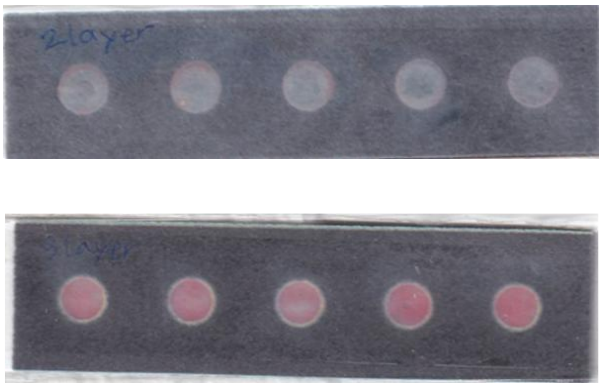

Figure 2.14 Photographs of the detection zone after reaction
(a: two-layer, b: three-layer)

(3) The number of layers in the reduction zone

To optimize the number of layers in the reduction zone, four different μPADs were fabricated, and the number of layers for the zinc addition was tested. A 0.2 g mL^{-1} zinc suspension was used as the reducing agent, and the number of layers in the reductant zone was varied from 1 to 4. The μPADs used had the same design, with a total of 10 layers (Figure 2.15(c)). The strongest color change occurred when the reductant layer consisted of 2 layers. When 3 and 4 layers were used, the absorbance decreased, likely due to the influence of zinc. As mentioned earlier, the reaction between nitrite ions and the Griess reagent can be inhibited in the presence of zinc. Therefore, it was predicted that the higher zinc content in the 3-layer and 4-layer designs would result in a decrease in absorbance compared to the 2-layer design. Based on these results, the reduction zone was optimized to 2 layers, and the overall thickness of the μPAD was minimized. The reason for minimizing the thickness is that increasing the number of layers can lead to poor contact between the channels, which is expected to worsen the coloring intensity in the detection zone.

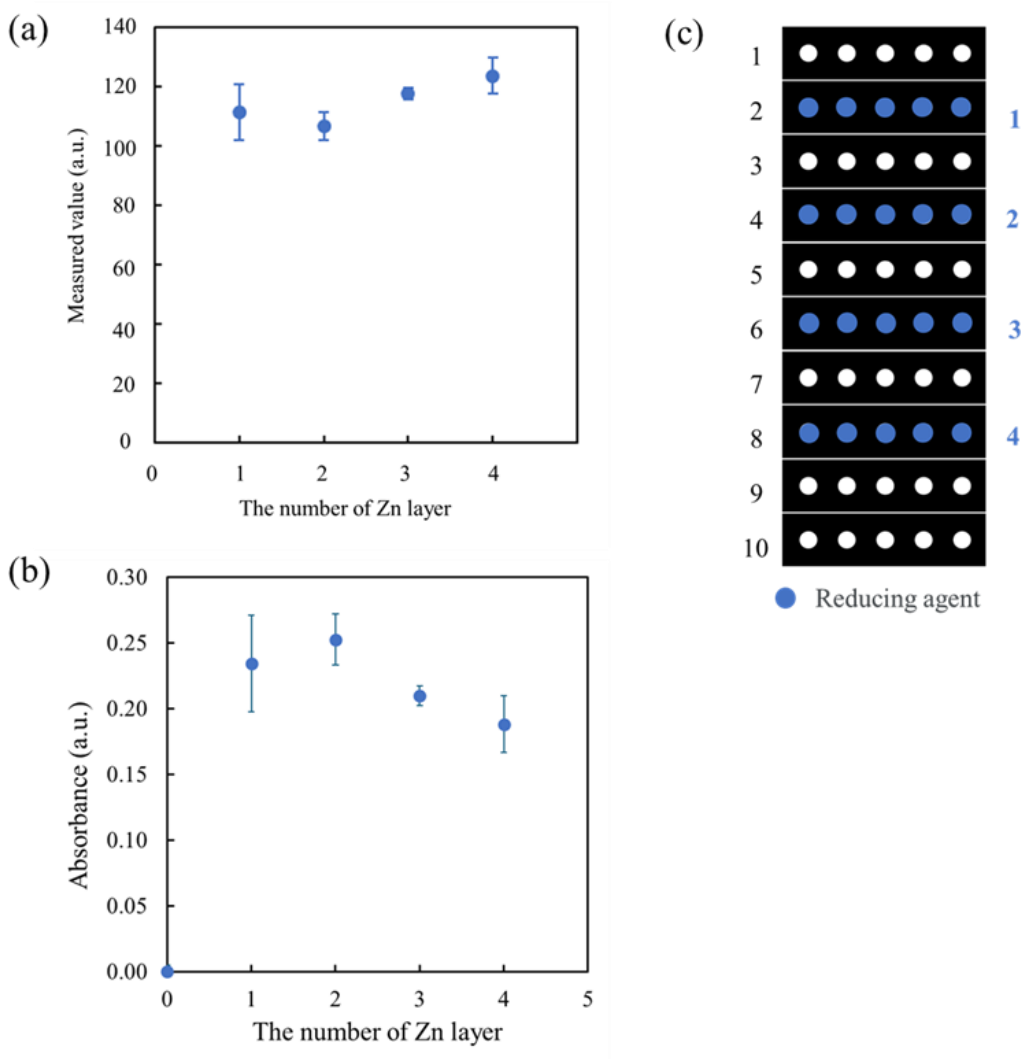

Figure 2.15 Color intensity due to zinc layer
(a: Measured value, b: Absorbance, c: Design used)

(4) The optimized design

Figure 2.16 displays the optimized channel design that actually measures nitrite and nitrate ions. The layered structure consists of the sample introduction zone, the reduction zones, and the detection zone from the top to the bottom layers. Figure 2.16 (c) shows the image of the opened μPAD. This design can measure five samples in one operation to enhance the throughput of the analysis.

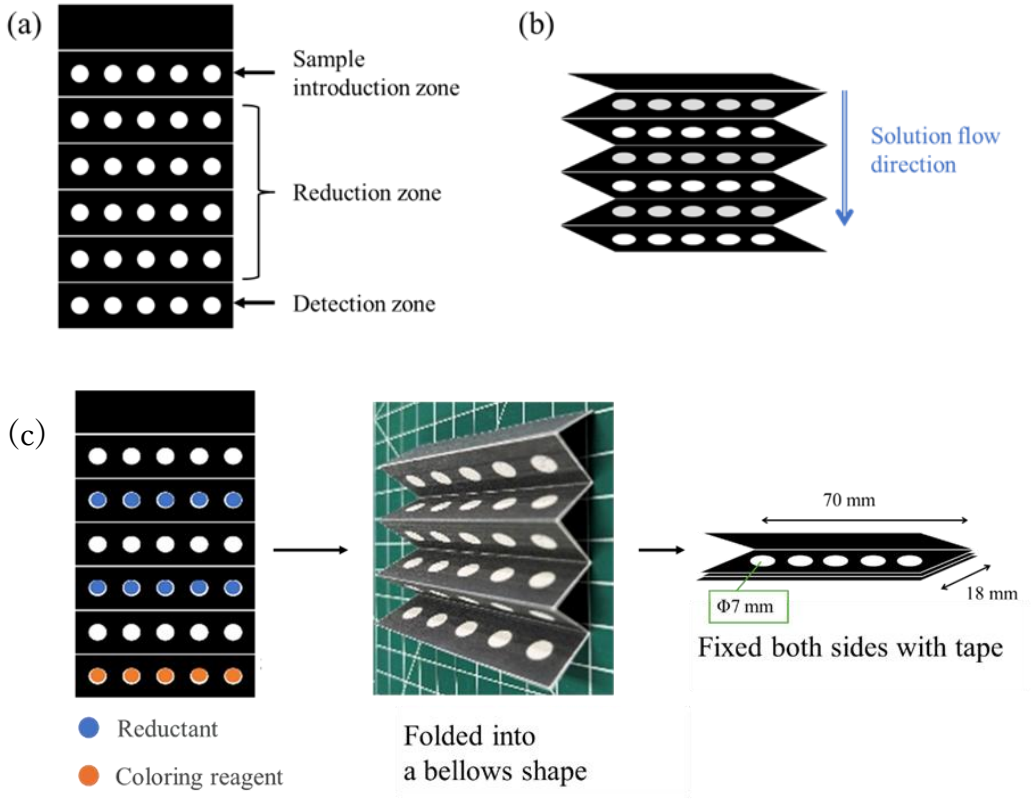

Figure 2.16 Optimized μPAD Design

(a: The location of each zone, b: Flow direction of sample solution, c: Reagent drop location and folded μPAD)

2.3.4 pH conditions of Griess reagent

The effect of changing the pH condition on the color intensity was investigated using the μPADs. Griess reagent was prepared by mixing 50 mM sulfanilamide, citric acid, and 10 mM N-1-naphthylethylenediamine dihydrochloride, and the pH was adjusted by changing the amount of citric acid (Table 2.1). A sample solution containing 1 mM nitrite was introduced into the μPAD at a volume of 40 μL.

The relationship between the pH of the Griess reagent and the green value is shown in Figure 2.17. Note that the small green value indicates an intense color. Figure 2.17 shows that the green value was slightly lower at pH 2.37 while it remained constant in other pHs. The results suggest that the concentration of citric acid should be 330 mM to obtain the most intense color, although the reason is unclear yet. Conversely, a citric acid

solution with a concentration lower than 165 mM could not be employed because it did not dissolve sulfanilamide in the preparation of the Griess reagent. When the amino group of sulfanilamide is protonated in acidic conditions, a hydrophilic cation species is formed. So, an increased acidity enhanced the solubility of sulfanilamide in water. Therefore, a high pH solution, that is, a low concentration of citric acid solution, reduced the solubility of sulfanilamide.

Table 2.1 Citric acid concentration and pH of Griess reagent

Concentration / mM	pH
165	2.55
248	2.41
330	2.37
495	2.20
660	2.16

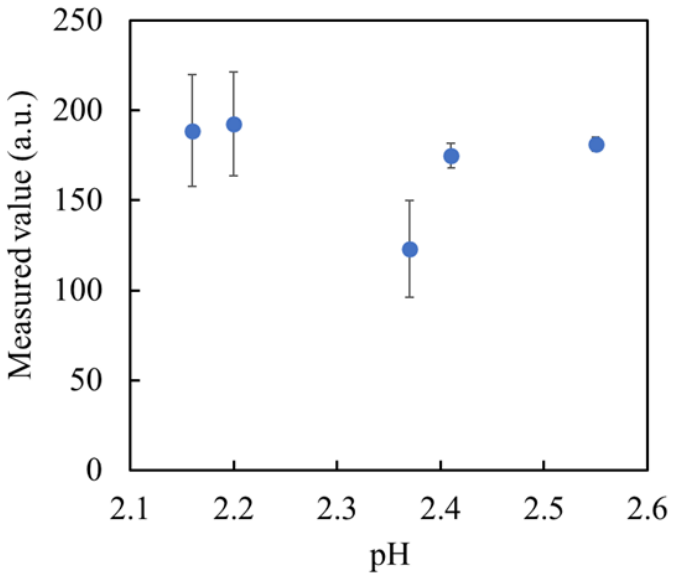

Figure 2.17 Effect of pH of Griess Reagent on Green Value

2.3.5 Investigating storage conditions for Greiss reagent

The storage temperature of the Griess reagent was investigated using (1) spectrophotometry and (2) the μPADs..

(1) Measurements using spectrophotometry

A UV-visible spectrophotometer (JASCO, V750) measured the absorbance of the reaction product for a nitrite ion solution with a nitrogen concentration of 14 mg L^{-1} at 520.0 nm. The absorbance was monitored at specified intervals for three weeks using the Griess reagents stored at room temperature (approximately 20 °C) and in a refrigerator (4 °C) to clarify the effect of storage temperature.

The results in Figure 2.18 confirmed that the absorbance was independent of the storage temperature. Therefore, Griess reagent can be stored at room temperature. Griess reagent would be stable even at room temperature because of its low pH, approximately 2.37. It is expected that such an acidic condition will suppress the growth of bacteria and microorganisms. Furthermore, the antioxidant properties of citric acid would prevent degradation of the colorimetric reagents even at room temperature. However, the absorbance suddenly decreased at 21 days.

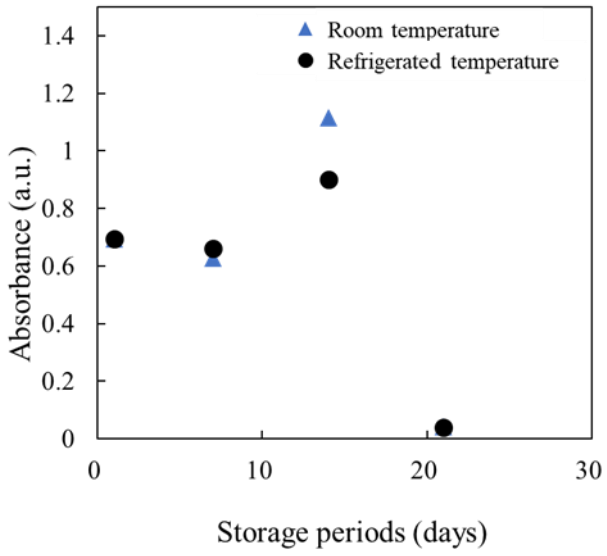

Figure 2.18 Comparison of storage temperatures for Griess reagent measured by spectrophotometry

(2) Measurements using μPADs

Taking into account the results in Figure 2.19, a freshly prepared Griess reagent was compared with one stored for two weeks at room temperature using μPADs. The absorbance was measured for nitrite solutions of 0, 0.5, 1, 2.5, and 5 mg L^{-1}. At a low concentration range, the calibration curve showed no significant difference between the fresh reagent and the stored one. However, at 5 mg L^{-1}, the absorbance was slightly smaller for the stored reagent than that of the fresh one. However, the large standard deviation led to the conclusion that there is no significant difference between the first day and two weeks later.

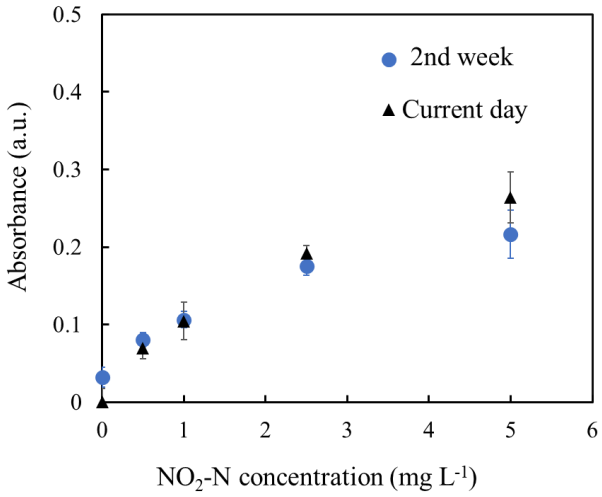

Figure 2.19 Effect of storage temperature for Griess reagent measured by μPADs

After depositing the Griess reagent in the detection zones, the prepared μPADs were sealed in a plastic bag and stored in either refrigerated (4 °C) or frozen (-20 °C) conditions in the dark to assess their stability. The PADs measured a nitrite ion solution with a nitrogen concentration of 14 mg L^{-1} after a month of storage. Figure 2.20 displays the images of the detection zones, while Figure 2.21 illustrates the impact of the storage period on the green color intensity-measured absorbance. As expected based on the results obtained by spectrophotometry, there is no significant difference in absorbance between refrigerated and frozen storage. According to the results of Figures 2.18 and 2.21, the shelf life of the grease reagent is approximately 2 weeks in solution and about 3 weeks on the μPAD, regardless of the storage temperature. This is also confirmed by the fact that the detection zone showed slight

coloration even before the addition of nitrite ions after four weeks of storage, indicating that deterioration progressed during the three weeks. Oxidation of sulfanilamide and/or light-induced degradation of n-1-naphthylethylenediamine dihydrochloride would be responsible for the deterioration.

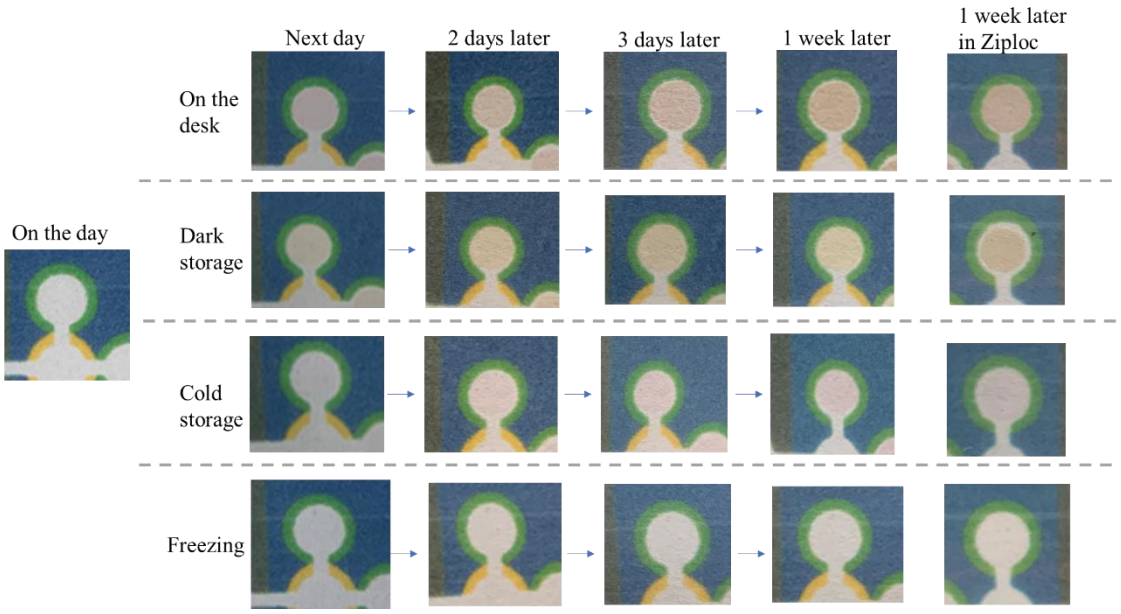

Figure 2.20 Time degradation of Griess reagent

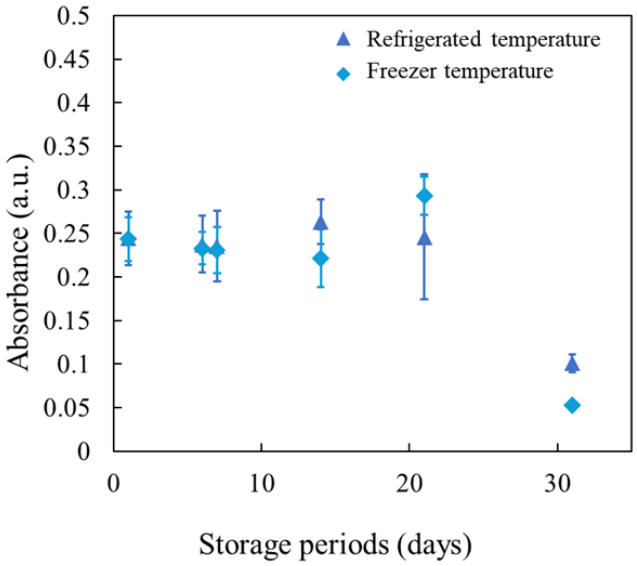

Figure 2.21 Measurement results using a μPAD stored for a certain period of time

2.3.6 Optimization of reaction time and sample volume for colorimetric detection

The time for scanning the detection zone after sample introduction was optimized to obtain intense color intensity. The color intensity was observed at 5-min intervals from the time of sample introduction up to 90 min. The μPADs used a 10-layer design (with 4 layers for the reducing agent). A 2 mM nitrite ion solution was introduced as the sample in volumes of either 25 μL or 40 μL, and the results were compared. As shown in Figure 2.22, the larger sample volume of 40 μL exhibited a stronger color intensity. For the 40-μL sample, absorbance increased significantly over 20–30 min, and after 30 min, it started to decrease. Therefore, 30 min was optimal for the time from sample introduction to scanning.

The sample volume can also influence the color intensity, so it was varied from 10 to 60 μL using a 7-layer design (with 2 layers for the reducing agent) and a 5 mg L^{-1} nitrite ion solution. The results are shown in Figure 2.23, where a smaller green value indicates stronger color intensity. The increase in green value at 60 μL would be caused by the solution leaking out. Since introducing more than 40 μL could result in overflow from the channels, the sample introduction volume was set to 40 μL.

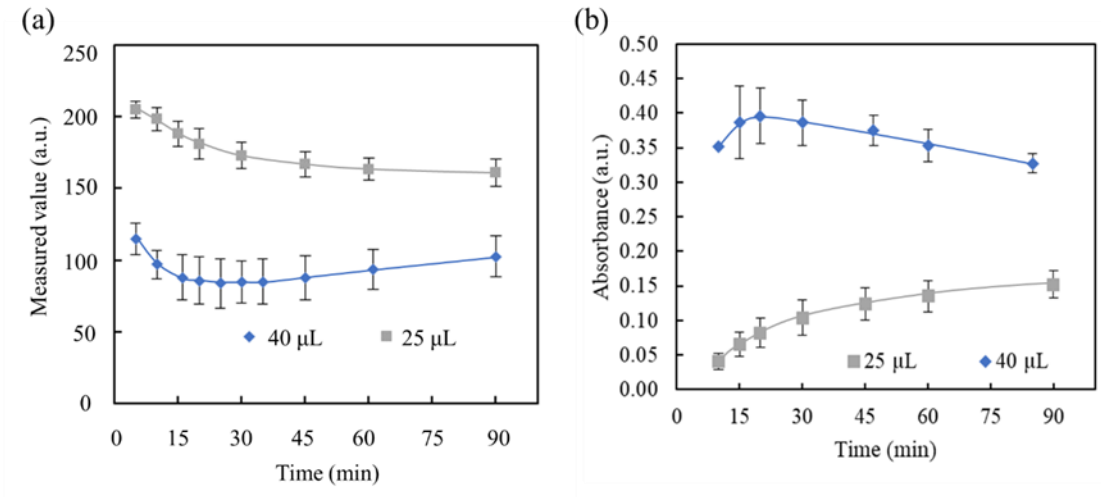

Figure 2.22 Color intensity after sample introduction (a: green value, b: absorbance)

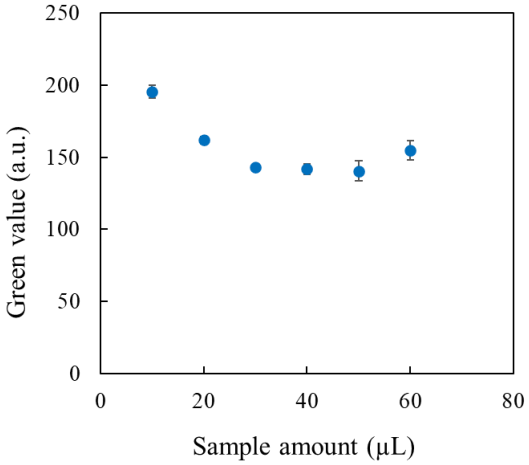

Figure 2.23 green value depending on sample amount

2.3.7 Reduction reaction time

The optimal reduction reaction time was investigated. In this experiment, a hydrophobic film was used to separate the reduction zone and the detection zone to prevent the sample solution introduced into the reduction zone from reacting with the Griess reagent added to the detection zone. After introducing the sample solution and allowing it to react for a set time, the hydrophobic film was removed, and the reduction zone and detection zones were brought into contact. The reduction reaction times were compared at 1, 5, 10, 15, 25, and 30 min. The sample used was a 10 mg L^{-1} nitrite solution. The results are shown in Figure 2.24.

When the reduction reaction time was 1 min, the color change was minimal, and the standard deviation was large. The most significant color change occurred when the reduction reaction time was 15 min and 25 min. Figure 2.25 shows the appearance of the detection zone when measuring a sample of nitrate ion from 1 to 15 mg L^{-1}. When no reduction time was set, there was a lot of uneven coloring. When a reduction time of 20 min was set, it was confirmed that the coloring was uniform. Figure 2.26 shows the calibration curves for reduction times of 10 min and 20 min. The linearity was obtained in the range of 0 to 15 mg L^{-1}. In both cases, the slopes were almost the same, but the R^2 value was better for the 20 min reduction reaction time. Therefore, a reduction time of 20 min was chosen for use.

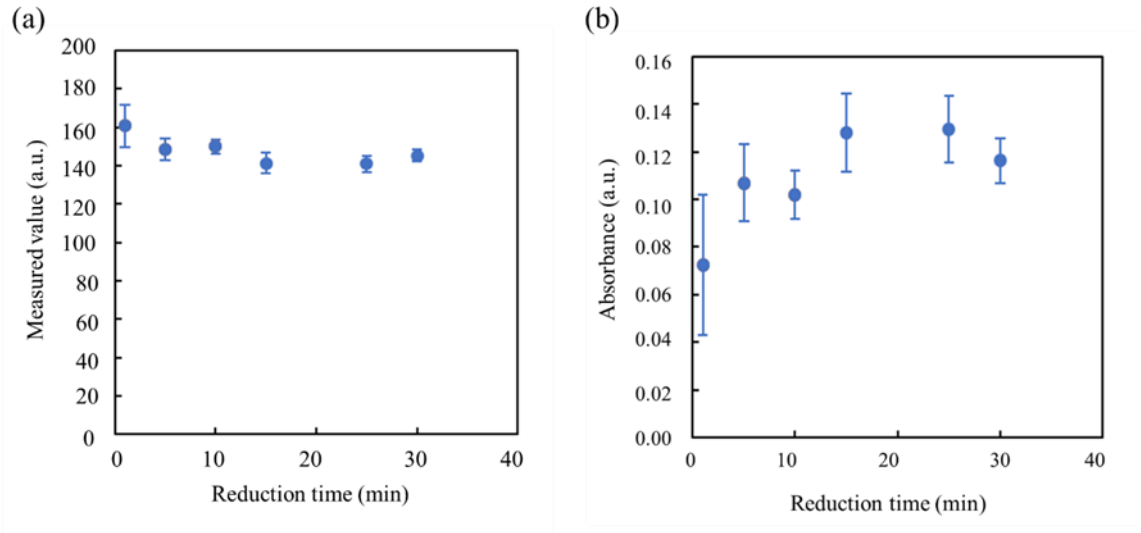

Figure 2.24 Color intensity over reduction reaction time

(a: measured value, b: absorbance)

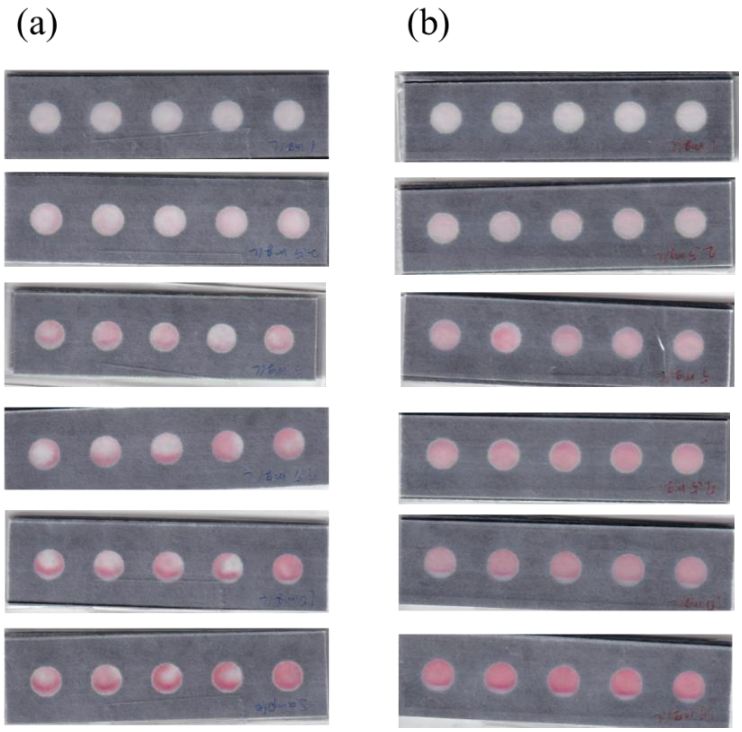

Figure 2.25 Photographs of the detection zone according to reduction reaction time

(a: immediately after, b: 20 min later)

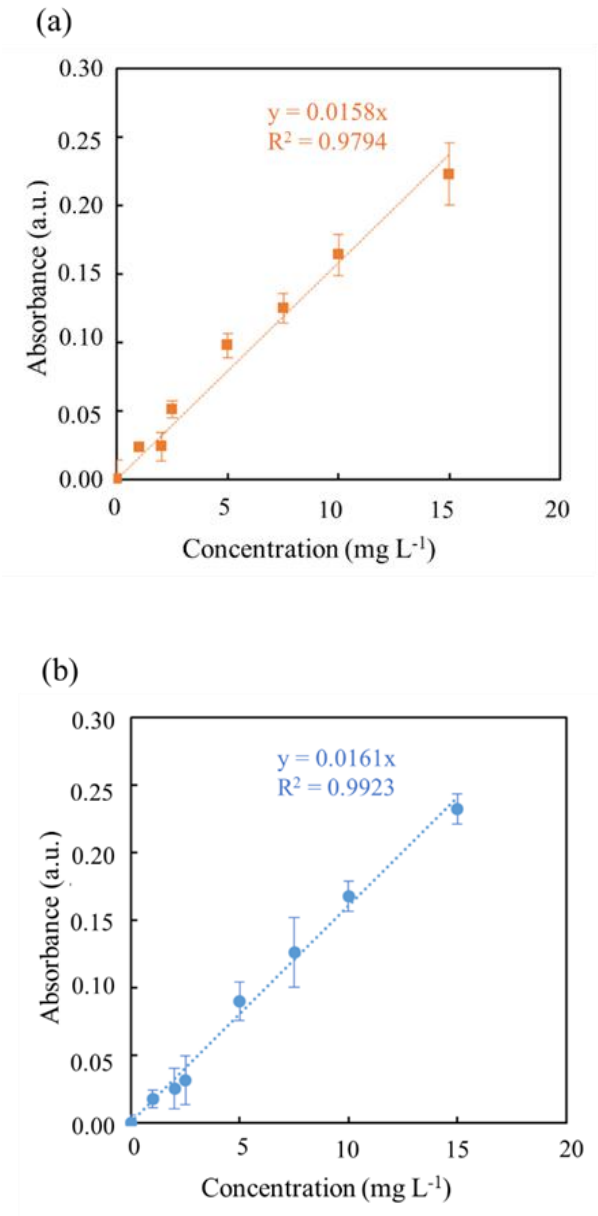

Figure 2.26 Calibration curve of nitrate ion for each reaction time

(a: 10 min, b: 20 min)

2.3.8 Confirmation of selectivity

The selectivity to nitrite ions was investigated using the optimized μPAD. A solution containing a mixture of nitrite ions and nitrate ions, as well as a solution containing only nitrite ions, were employed for samples. Figure 2.27 shows the results of the absorbance measurements against nitrite ion concentration. No significant difference in absorbance was observed between the two samples at each concentration. This confirms that the Griess reaction can detect only nitrite ions without interference from nitrate ions.

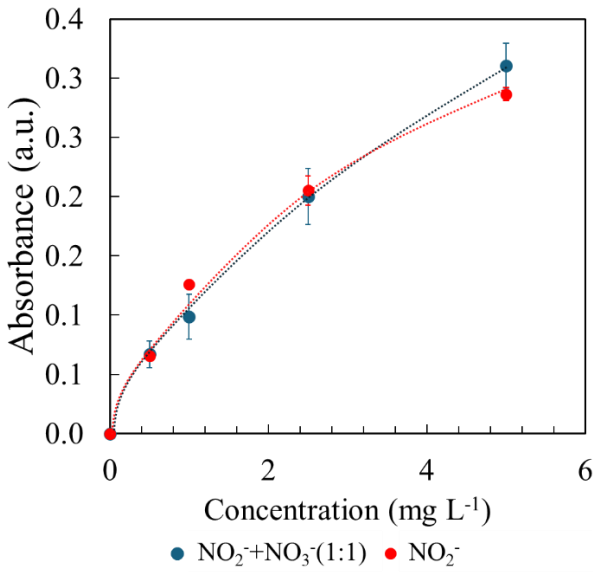

Figure 2.27 Absorbance relative to nitrite ion concentration

2.3.9 Effect of zinc on detection sensitivity

To investigate the effect of zinc on detection sensitivity, the following experiments were conducted using the μPAD and spectrophotometry: (1) the effect of zinc on the color intensity of nitrite ions on μPADs; (2) calibration curves for nitrite and nitrate ions in the presence and absence of zinc; and (3) calibration curves for total nitrogen concentration at different ratios of nitrite and nitrate ions.

(1) Effect of zinc on the color intensity of nitrite ions on μPADs

Using the μPAD shown in Figure 2.28(a), the effect of zinc on the color intensity was investigated with a 10 mM nitrite solution as the sample. When adding zinc, 10 μL of a 0.2 mg mL^{-1} zinc suspension was added to the location shown in Figure 2.28(a). As can be seen in Figure 2.28(b), the color of the detection zone differed depending on the presence or absence of zinc. In the presence of zinc, the blue tint of the reddish-purple color disappeared, and it appeared as a red color with a stronger yellowish hue. From Figure 2.28(c), until 30 min after the sample introduction, the absorbance was similar, but after that, it gradually decreased when measured with the μPAD containing zinc. The difference in color and absorbance suggests that zinc powder also affects the nitrite ions. Furthermore, to verify the results, calibration curves for nitrite ions and nitrate ions were constructed with and without zinc using both spectrophotometry and μPADs.

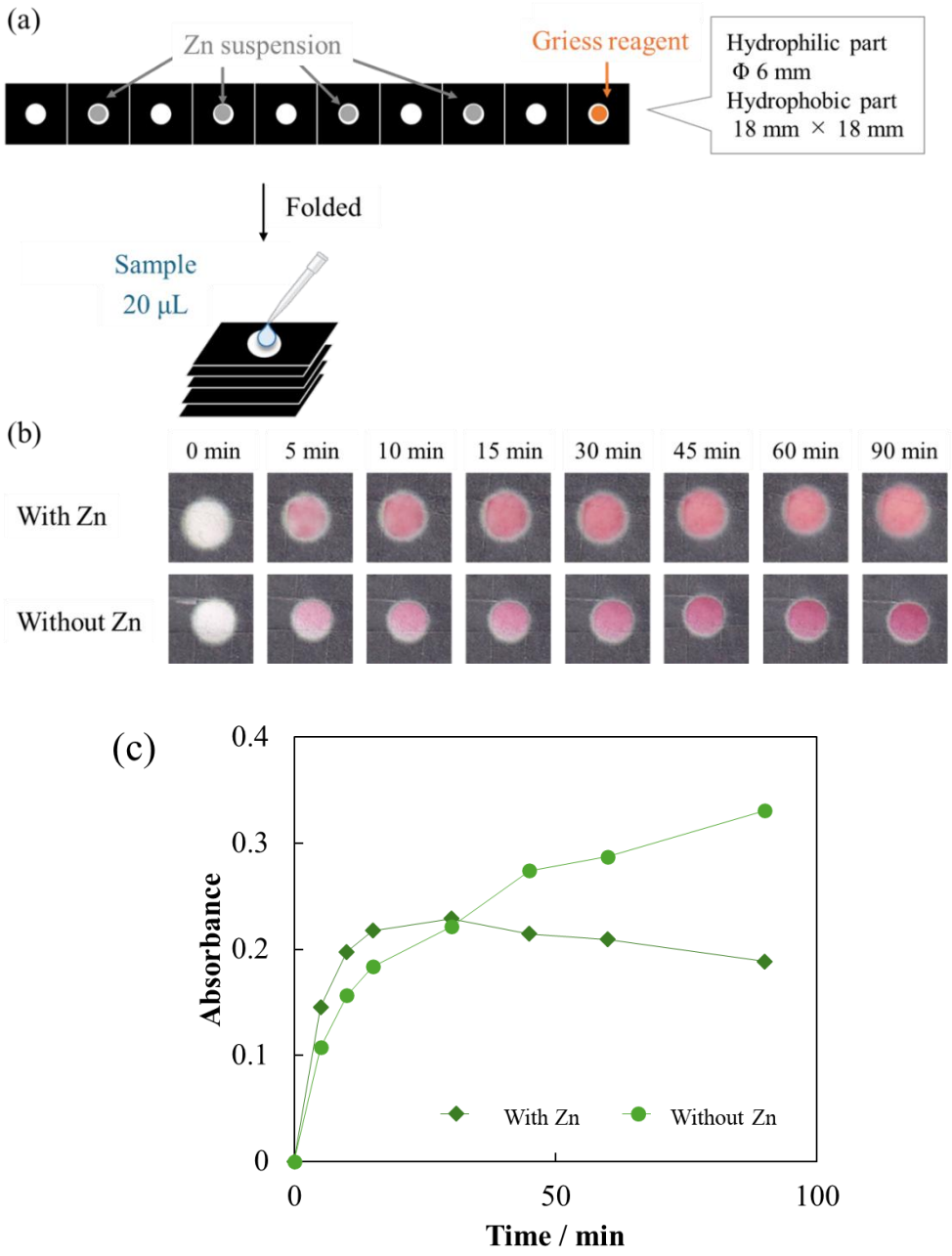

Figure 2.28 Comparison of 10 mM nitrite with and without Zn
(a: Design used, b: Photographs of the detection zone, c: Absorbance comparison)

(2) Calibration curves for nitrite and nitrate ions in the presence and absence of zinc

The calibration curves for nitrite and nitrate were constructed in wide ranges of concentrations via the use of reduction with zinc. Figure 2.29(a) shows the calibration curves for nitrate with zinc reduction and for nitrite, both with and without zinc reduction, using the μPADs. Note that adding zinc to the reduction zones reduced the sensitivity to nitrite to 68%. Figure 2.29(b) shows similar results obtained using conventional spectrophotometry, where the sensitivity was decreased to 48%, which is more significant than the decrease observed when using the μPADs. These results indicate that zinc incompletely converts nitrate to nitrite ions and also decreases the amount of nitrite ions.

Although many studies have reported simultaneous determinations of nitrite and nitrate using μPADs, only Jayawardane et al. reported that zinc showed no effect on the quantification of nitrite ions [24]. Unfortunately, the other reports could have simply assumed that zinc resulted in no change in the sensitivity to nitrite ions [25-28]. In the present study, the sensitivity to nitrite ions decreased to 68% after treatment with zinc. Merino reported a similar decrease in the sensitivity using conventional spectrophotometry, although the decrease in sensitivity was much smaller (9%) than that observed in the present study when the slopes of the calibration curves are compared [16]. Therefore, the sensitivity to nitrite ions was obviously decreased after pretreatment with zinc. The inconsistency with Merino [16] and Jayawardane et al. [24] would have been caused by different conditions, such as the concentration range of nitrite ions, the amounts of zinc, and the reaction time. Zinc would have no, or even less, influence on the determination of nitrate ions if the concentrations of nitrite ions were sufficiently low to negate the effect on the measurement of nitrate ions.

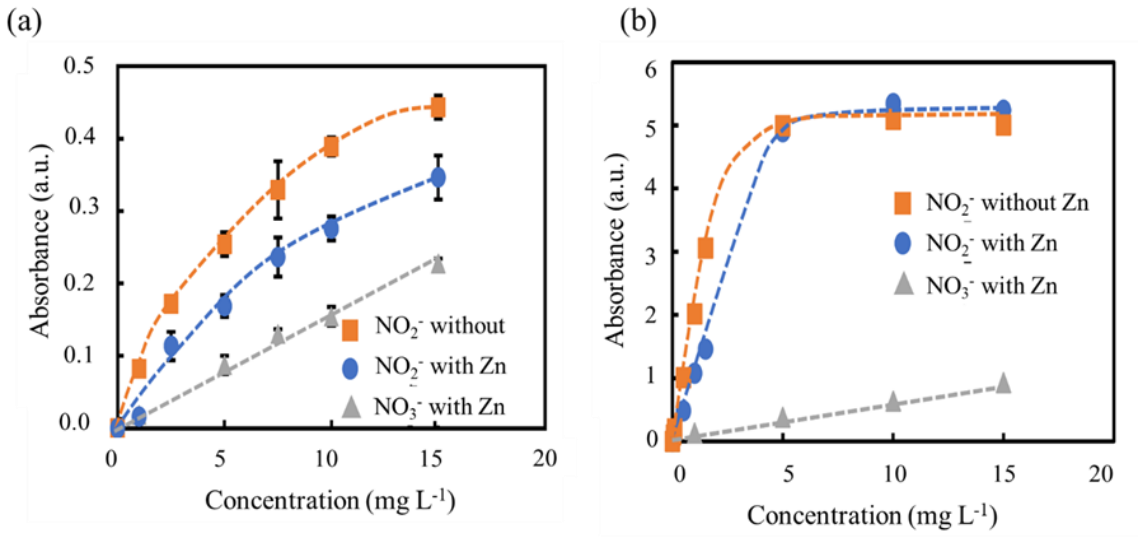

Figure 2.29 Calibration curves of nitrite and nitrate obtained by μPADs and spectrophotometry. (a: μPADs, b: spectrophotometry)

(3) Calibration curves for total nitrogen concentration at different ratios of nitrite and nitrate ions

The absorbance of the mixed samples was measured using both a spectrophotometer and μPADs. The samples were prepared in the proportions shown in Table 2.2. From Figure 2.30, it was confirmed that the sensitivity varied according to the mixing ratio in both methods, where the mixing ratio is defined as $C_{Nitrite}$ / ($C_{lNitrite}$+$C_{Nitrate}$). Compared to the solution containing only nitrate ions, the sensitivity increased as the proportion of nitrite ions increased. Subsequently, the results were replotted with the mixing ratio on the x-axis (Figure 2.31). It was found that as the amount of nitrite ions in the sample increased, the absorbance increased proportionally to the ratio. Based on these results, when calculating the concentration using a calibration curve, it was determined that if both nitrite and nitrate ions are present in the sample, the concentration must be corrected according to their ratio. The correction method will be discussed in Chapter 2.3.10.

Table 2.2 Mixture ratio (%)

Sample	NO_2^-	NO_3^-
1	100	0
2	75	25
3	50	50
4	25	75
5	0	100

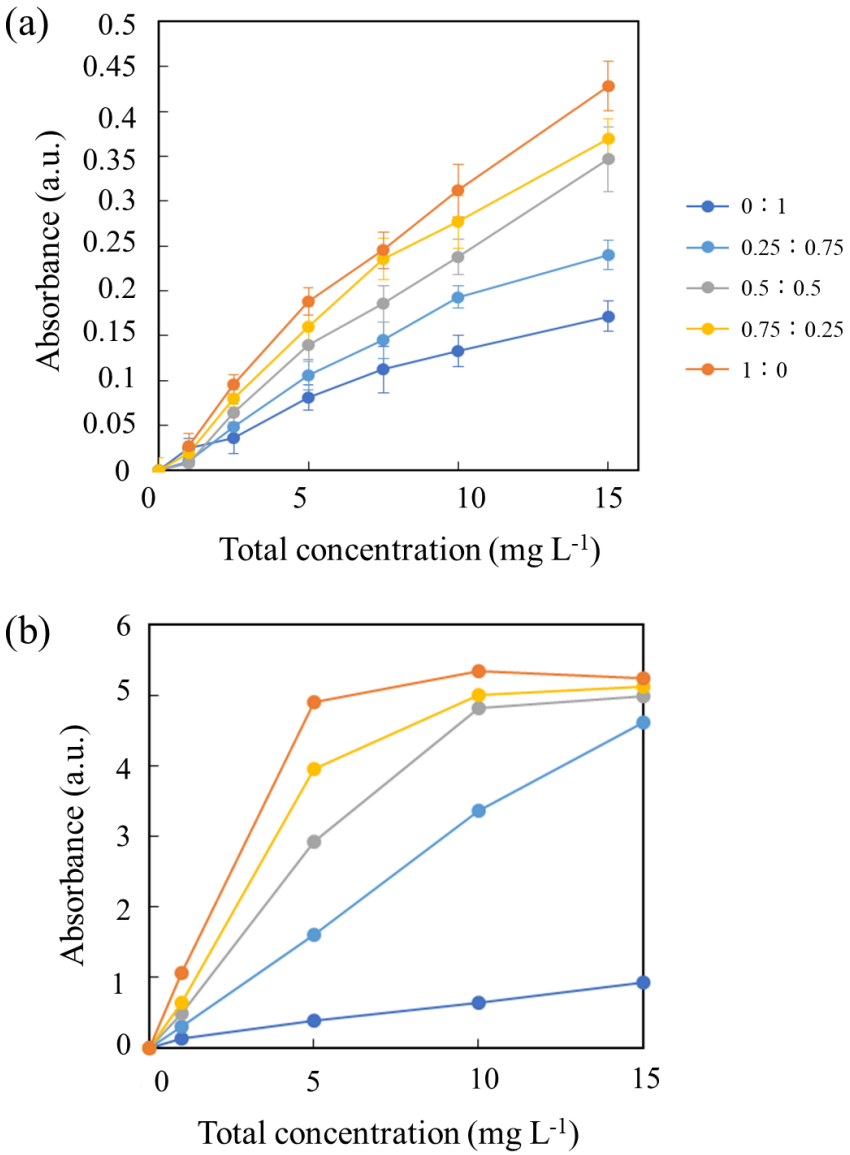

Figure 2.30 Absorbance of mixed sample (a: μPADs, b: spectrophotometry)

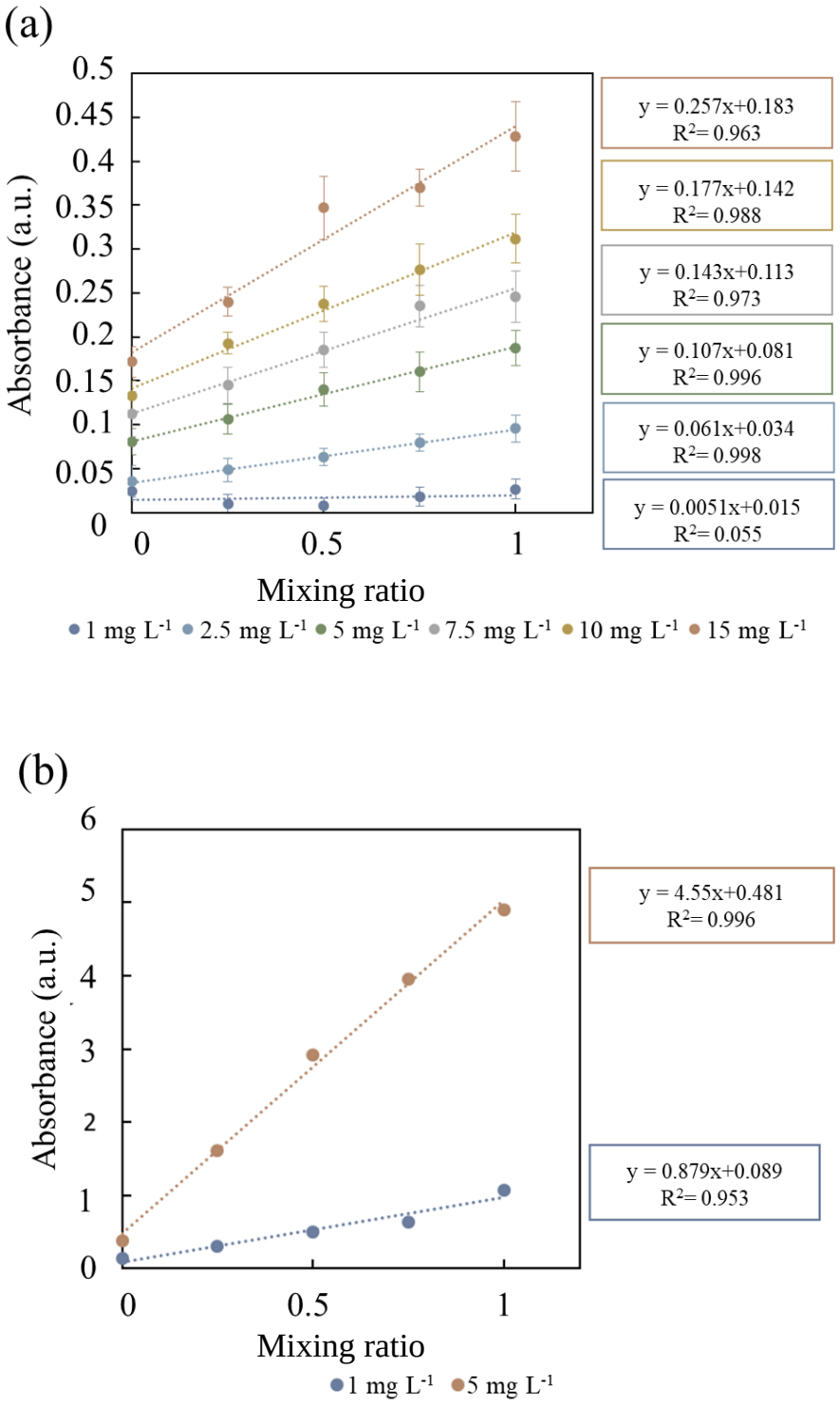

Figure 2.31 Absorbance relative to the mixing ratio

(a: μPADs, b: spectrophotometry)

2.3.10 Calculation of concentrations for nitrite and nitrate ion

When the sample contains both nitrite and nitrate ions, the simultaneous determination of nitrite and nitrate necessitates a correction of the total concentration, as zinc reduction yields only 53% of the apparent conversion efficiency. In addition, the results of Chapter 2.3.9 suggest that the zinc treatment also decreases the sensitivity of nitrite. Thus, the concentration ratio of nitrate and nitrite in the sample influences the total nitrite and nitrate concentrations.

To develop the correction method, the experimental results were reproduced using the calibration curves of nitrite and nitrate ions with zinc treatment. Absorbance for a mixture of nitrite and nitrate ions can be expressed by Equation (2.2).

$$A = S_{NO_2} C_{total}\left(1 - X_{NO_3}\right) + I_{NO_2} + S_{NO_3} C_{total} X_{NO_3} + I_{NO_3} \qquad (2.2)$$

In Equation (2.2), *S* and *I* indicate the slopes and intercepts of the calibration curves for nitrite and nitrate in the presence of zinc, and X_{NO_3} is the ratio of nitrate ions ($0 \leq X_{NO_3} \leq 1$) to the total concentration of nitrite and nitrate ions.

The absorbance obtained for the mixture of nitrite and nitrate ions (Figure 2.29(b) of Chapter 2.3.9(3)) was compared with the absorbance calculated using Equation (2.2), which is shown in Figure 2.31 The circle markers indicate the experimental data. It should be noted that linear relationships were obtained in the range of absorbance, A < 5, and, therefore, data higher than 5 were removed from the graph. Equation (2.2) calculated the absorbance indicated by the triangle markers.

Obviously, the equation reproduces the calibration curves that were experimentally obtained, as seen in Figure 2.32. Therefore, Equation (2.2) must be employed for the determination of the total concentration if the concentration of nitrite ions is too high to be ignored against that of the nitrate concentration. In practical analyses, therefore, Equation (2.4) should be employed to determine the concentration of nitrate ions. The concentration of nitrite ion is calculated using Equation (2.3).

$$A = S_{NO_2} C_{NO_2} + I_{NO_2} \quad (2.3)$$

$$A = S_{NO_2}{}' C_{NO_2} + I_{NO_2}{}' + S_{NO_3} C_{NO_3} + I_{NO_3} \quad (2.4)$$

In Equation (2.4), A is the absorbance with zinc treatment and C_{NO_2} is the concentration of nitrite ions, which must be measured without zinc treatment. In addition, $S_{NO_2}{}'$, $I_{NO_2}{}'$, S_{NO_3}, and I_{NO_3} also must be measured by constructing calibration curves for nitrite and nitrate with zinc treatment.

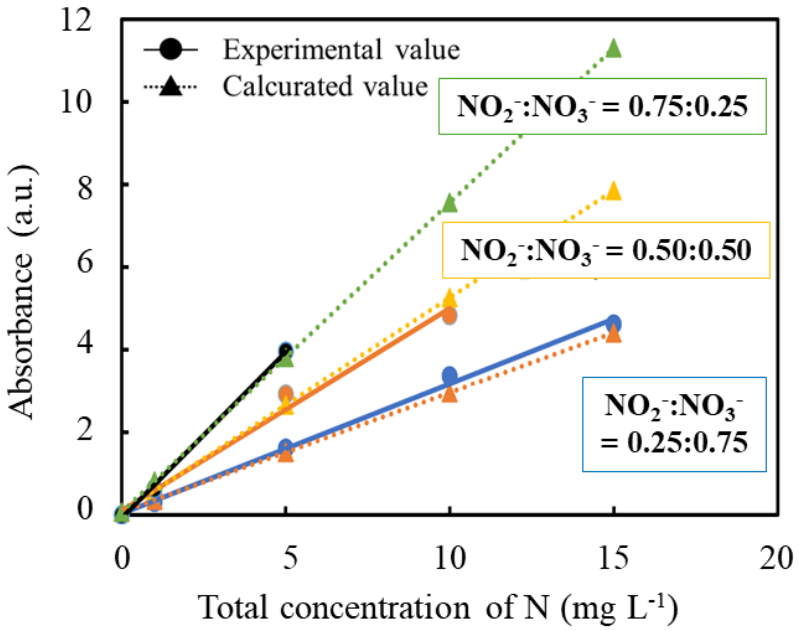

Figure 2.32 Calibration curves of nitrite and nitrate at different ratios of nitrite and nitrate.

The circles represent the data experimentally obtained, and the triangles and the dashed lines indicate the values calculated from the calibration curves only for nitrite and nitrate after zinc treatment according to Equation (2.2).

2.3.11 Analytical performance of the μPADs

A calibration curve for nitrate ions was constructed using 40 μL samples with reaction times of 20 min. Nitrate showed a linear relationship that ranged from 1 to 10 mg L^{-1} of nitrogen ($y = 0.0151x + 0.006$, $R^2 = 0.994$) whereas the calibration curves for nitrite deviated from a linear relationship when the concentration range exceeded 10 mg L^{-1}. A linear relationship for nitrite was obtained within a range of from 0.05 to 1.5 mg L^{-1} in the absence of zinc ($y = 0.0421x + 0.0327$, $R^2 = 0.960$). The limit of detection (LOD) and limit of quantification (LOQ) were calculated from concentrations calculated using the IUPAC recommendation [29]. The LODs and LOQs were 0.03 mg L^{-1} and 0.21 mg for $N\text{-}NO_2^-$ (0.1 and 0.7 mg L^{-1} in the form of NO_2^-) and 0.9 mg L^{-1} and 3.9 mg L^{-1} for $N\text{-}NO_3^-$ (4.2 and 17 mg L^{-1} in the form of NO_3^-).

2.3.12 Investigation of decreased sensitivity for nitrate ions

The lower sensitivity of nitrate ions compared to nitrite ions is attributed to (1) the potential for adsorption of nitrite or nitrate ions to zinc and (2) the potential for reduction to ammonia. This chapter reports the results of the investigation of these factors.

(1) The possibility of adsorption of nitrite or nitrate ions to zinc

To investigate the possibility of nitrite or nitrate ions adsorbing zinc, Raman spectra were measured by passing nitrite and nitrate ions through zinc powder. Figure 2.33 shows the Raman spectra when sodium nitrite, potassium nitrate, and zinc powder were used as samples. It was confirmed that the peaks obtained from the actual samples of sodium nitrite and potassium nitrate matched the literature values [30] (Table 2.3). Subsequently, the spectra of samples passed through zinc powder with each ion solution were measured. The results are shown in Figure 2.34. The results were very similar, and no peaks corresponding to nitrites or nitrates were observed. These peaks may have been buried or not detected. Figure 2.35 shows the measurement results after passing the ion solutions through zinc powder and washing twice with water. No differences in the peaks were observed with or without washing. Based on these results, it was concluded that the possibility of nitrite or nitrate ions adsorbing to zinc is low.

Table 2.3 Vibrational frequencies

	NO_2^-	$K[NO_3]$
$\tilde{\nu}_1$ (cm^{-1})	1327	1049
$\tilde{\nu}_2$ (cm^{-1})	806	-
$\tilde{\nu}_3$ (cm^{-1})	1286	1390
$\tilde{\nu}_4$ (cm^{-1})	-	716
Ref. (cm^{-1})	338	705

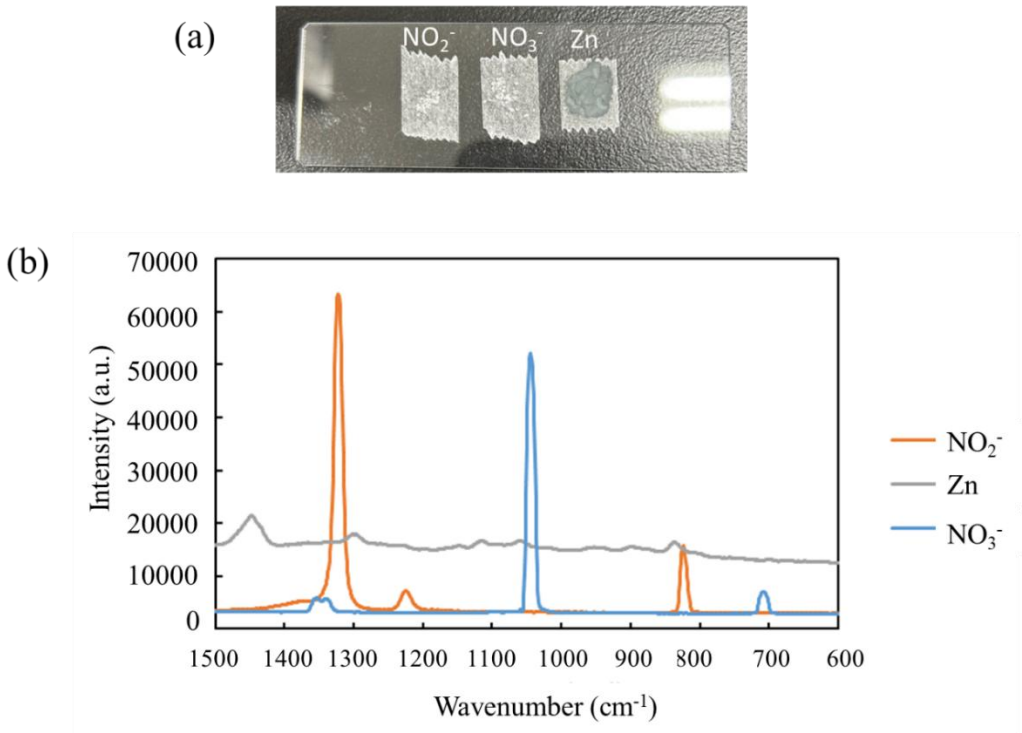

Figure 2.33 Raman spectra results

(a: photograph of measurement sample, b: obtained spectrum)

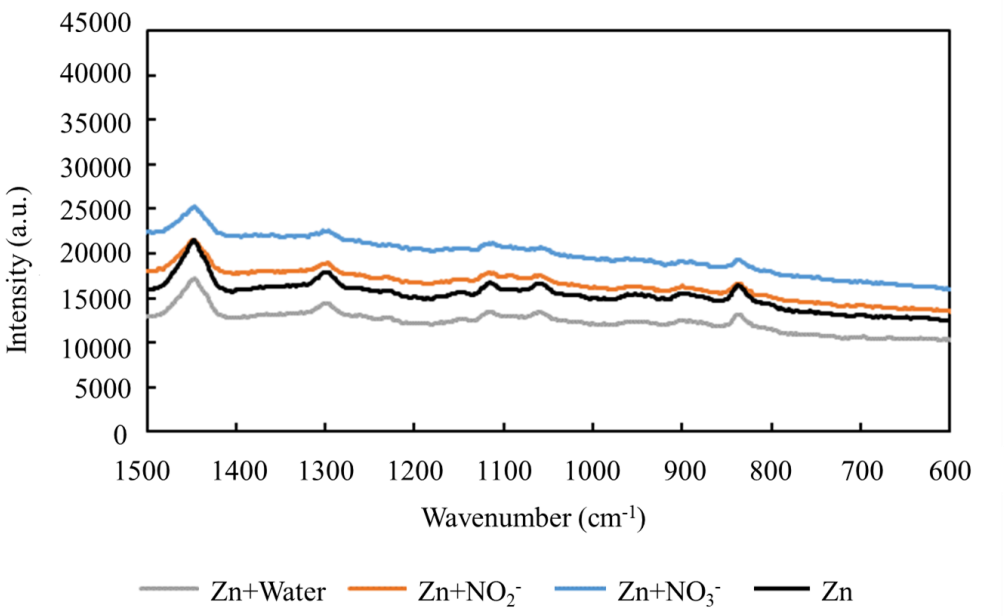

Figure 2.34 Raman spectra results of zinc powder through each ion

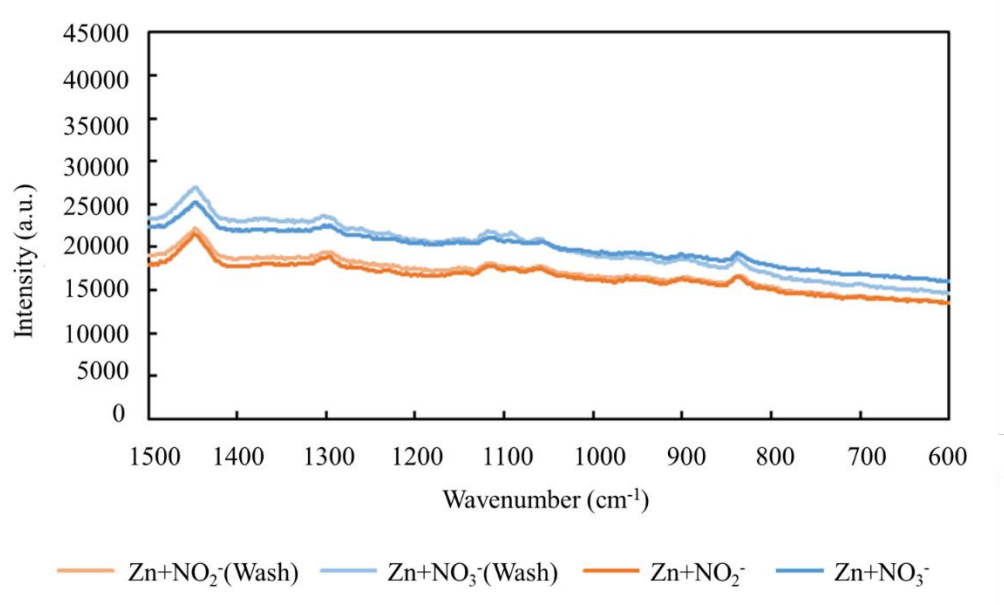

Figure 2.35 Raman spectra results for zinc powder before and after washing

(2) The possibility of reduction to ammonia

Zinc reduces nitrite to ammonia and nitrogen gas, as described in the literature [31,32]. To elucidate the cause for the decrease in sensitivity to nitrite ions in the presence of zinc, ammonia was measured after the reaction with zinc. Table 2.4 shows the production of ammonia at 100 mg L^{-1} of nitrite and nitrate ions using different amounts of zinc. When reacting with zinc, both nitrite and nitrate generated ammonia due to their reduction. So, one of the possible reasons for the decrease in sensitivity to nitrite ions is attributed to the reduction of nitrite ions to ammonia. However, the amount of ammonia was too small (1-2% of nitrite and nitrate ions) to explain the decrease in sensitivity. Therefore, further investigation is needed to clarify the complete mechanism of the decreased sensitivity.

Next, the potential formation of a complex between ammonia and zinc ions was investigated. Zinc chloride was added to an ammonia aqueous solution, and ammonia concentration was measured. As shown in Figure 2.36, no decrease in ammonia concentration was observed due to zinc ions. In fact, when a higher concentration of zinc ions was present, the absorbance increased. This suggests that ammonia and zinc ions are unlikely to form a complex. Furthermore, when 10 mM of zinc chloride was added, the absorbance was approximately 0.7, even though ammonia was not present. This high absorbance is believed to be due to the reaction between zinc ions and the chromogenic reagent.

Table 2.4 Measurement of ammonia produced by the reduction of nitrite and nitrate ions.

Ions	$N\text{-}NO_x^-$/ mg L^{-1}	Zinc/ g mL^{-1}	NH_3-N/ mg L^{-1}
NO_2^-	100	0	0.0
	100	0.5	1.1
	100	2.5	1.9
NO_3^-	100	0	0.0
	100	0.5	0.9
	100	2.5	1.5

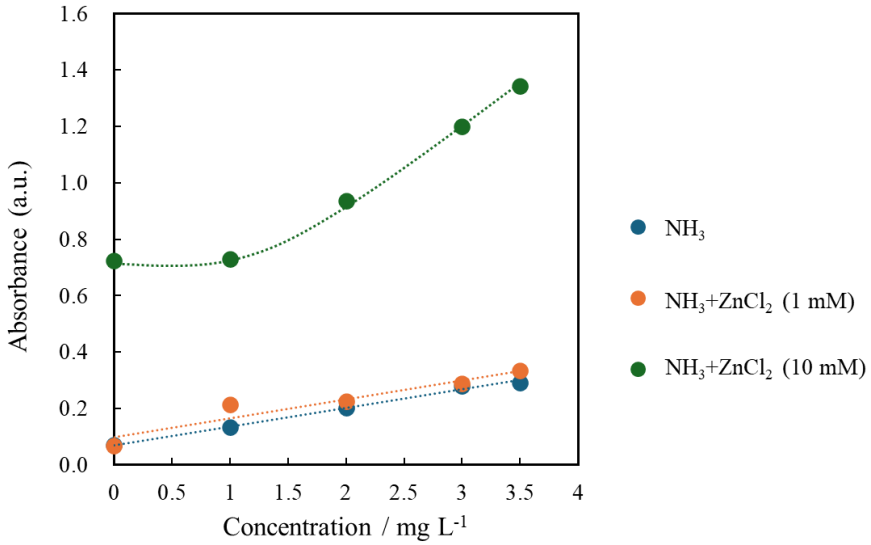

Figure 2.36 Absorbance of ammonia and zinc chloride solution

The results of (1) and (2) revealed that zinc reduction converted some of the ions into ammonia, but the amount of ammonia was too small to explain the decreased sensitivity in the presence of zinc. It is also possible that they were further reduced to nitrogen. Additionally, as shown in Chapter 2.3.3(2), the presence of zinc powder inhibited the reaction between the Griess reagent and nitrite ions. At least this fact is considered one of the factors contributing to the decreased sensitivity.

2.3.13 Analysis of natural water

With respect to the impact of zinc on the determination of nitrite and nitrate, natural water samples were analyzed using the developed μPADs and spectrophotometry to demonstrate a practical application and validate the proposed correction method. Table 2.5 shows the concentrations of nitrite and nitrate ions in natural water samples taken from wells, ponds, and a brackish lake. As seen in Table 2.5, the results for water samples are in good agreement with the results from the μPADs and spectrophotometry. The level of $N\text{-}NO_2^-$ in the brackish lake water sample was too low to be detected by the μPADs (LOD is 0.03 mg L^{-1}). This result is reasonable because spectrophotometry showed 0.01 mg L^{-1} of $N\text{-}NO_2^-$. Although the concentration of nitrate in the pond water showed a relatively large difference between the μPADs and spectrophotometry, the μPADs would

be useful to estimate concentrations of nitrite and nitrate roughly because the results showed the same order of magnitude. Conversely, it is unclear why $N\text{-}NO_3^-$ was undetectable in the spectrophotometric measurement. As expected from the results of the decreased sensitivity to nitrite ions in the presence of zinc, the level of $N\text{-}NO_3^-$ would be overestimated if not corrected using the calibration curve for nitrite with zinc treatment (see Table 2.5). We also attempted recovery tests for pond samples, revealing recovery values of 76 to 107% for nitrite and 64 to 116% for nitrate. These values would be acceptable for rough estimation, although some of the results for nitrate were slightly lower than 70%.

The tolerance limit of nitrogen formed by the combination of nitrite and nitrate in tap water is 10 mg L^{-1} in Japan. Thus, the obtained values were much lower than the tolerance limit, which means that the water samples were relatively uncontaminated.

Table 2.5 Concentrations of nitrogen in the form of nitrite and nitrate ions in natural water samples

	μPADs/ mg L^{-1}			UV-VIS/ mg L^{-1}		
	N-Nitrite	N-Nitrate with correction	N-Nitrate without correction	N-Nitrite	N-Nitrate with correction	N-Nitrate without correction
Well water 1 (Yonago)	0.18±0.29	3.10±0.90	3.75±0.86	0.20±0.00	4.79±0.00	8.80±0.00
Well water 2 (Yonago)	< LOD	-	2.84±0.56	< LOD	-	2.05±0.00
Brackish lake water (Yonago)	< LOD	-	2.37±0.54	0.01±0.00	< LOD	1.16±0.00
Pond water 1 (Yonago)	0.04±0.05	4.17±0.51	4.88±0.51	0.01±0.00	3.16±0.00	7.37±0.00
Pond water 2 (Okayama)	< LOD	-	1.31±0.47	< LOD	-	0.79±0.00
Pond water 3 (Okayama)	< LOD	-	1.26±0.71	< LOD	-	0.80±0.00

2.4 Conclusion

The μPADs were developed for the measurement of nitrite and nitrate ions contained in natural water samples. Natural water typically contains low or undetectable concentration levels of nitrite ions, so nitrate ions could be directly determined using the μPADs with a zinc reduction. When a sample contains an amount of nitrite comparable to that of nitrate, we must measure the concentration of nitrite without zinc reduction and the total concentrations of nitrite and nitrate after the reduction of nitrate to nitrite. However, we found that zinc reduction converts nitrite and nitrate to ammonia, which decreases the sensitivity to nitrite. So, the total concentrations of nitrite and nitrate ions must be corrected using an additional calibration for nitrite with zinc treatment. We proposed a correction method to measure the total concentration and validated it by comparing the calibration curves for mixtures containing nitrite and nitrate at different ratios with the calculated values using individual calibration curves for nitrite and nitrate with zinc treatment. Consequently, we successfully measured the concentration of nitrate ions in natural water samples using the developed μPADs. The results were in good agreement with those obtained via conventional spectrophotometry, i.e., the developed μPADs are expected to be useful for the determination of nitrate ions in natural water samples under the conditions of under-equipped facilities, which would be particularly useful in developing countries.

2.5 Reference

[1] Collection of Techniques for Methods of Preventing Groundwater Contamination by Nitrate Nitrogen, Ministry of the Environment **2009**.

[2] Tannenbaum, S. R.; Sinskey, A. J.; Weisman, M.; Bishop, W. *J. Natl. Cancer Inst.* **1974**, *53* 79-84.

[3] E.E. van Faassen,; S. Bahrami,; M. Feelisch,; N. Hogg, M. Kelm,; D.B. Kim-Shapiro,; A.V. Kozlov,; H. Li, J.O. Lundberg,; R. Mason,; H. Nohl,; T. Rassaf, A. Samouilov,; A. Slama-Schwok,; S. Shiva,; A.F. Vanin,; E. Weitzberg,; J. Zweier,; M.T. Gladwin,; *Med. Res. Rev.* **2009**, *2009*, 683-741.

[4] Comly, H. H. *JAMA 257* **1987**, 2788-2792.

[5] Groundwater Measurement for Fiscal Year 2022, Ministry of the Environment **2024**.

[6] Miranda, K.M.; Espey, M.G.; Wink, D.A. *Nitric Oxide* **2001**, *5* (1), 62-71.

[7] Singh, P.; Singh, M. K.; Beg, Y. R.; Nishad, G. R. *Talanta* **2019**, *191*, 364-381.

[8] Morales, J.A.; de Graterol, L.S.; Mesa, J. *J. Chromatogr. A* **2000**, *884*, 185−190.

[9] Penteado, J.C.; Angnes, L.; Masini, J.C.; Oliveira, P.C.C. *J. Chem. Educ.* **2005**, *82*, 1074-1078.

[10] Kuban, P.; Kuban, P.; Kuban, V. *J. Chromatogr. A* **1999**, *848*, 545−551.

[11] Badea, M.; Amine, A.; Palleschi, G.; Moscone, D.; Volpe, G.; Curulli, A. *J. Electroanal. Chem.* **2001**, *509*, 66−72.

[12] Nydahl, F. *Talanta* **1976**, *23*, 349-357.

[13] Margeson, J.H.; Suggs, J.C.; Midgett, M. R. *Anal. Chem.* **1980**, *52*, 1955–1957.

[14] Gine, M.F.; Bergamin F, H.; Zagatto, E. A.G.; Reis, B.F. *Anal. Chim. Acta* **1980**, *114*, 191−197.

[15] Zhang, J.; Fischer, C. J.; Ortner, P. B. *Int. J. Environ. Anal. Chem.* **2000**, *76*, 99−113.

[16] Merino, L. *Food Anal. Methods* **2009**, *2*, 212–220.

[17] Griess, P. *Ber. Deutsch Chem. Ges.* **1879**, *12*, 426-428.

[18] Rasband, W.S., ImageJ, U. S. National Institutes of Health, Bethesda, Maryland, USA, http://rsb.info.nih.gov/ij/, 1997-2012.

[19] Inagawa, A. *Bunseki* **2022**, *1*, 22-23.

[20] Christodouleas, D. C.; Nemiroski, A.; Kumar, A. A.; Whitesides, G. M. *Anal. Chem.* **2015**, *87*, 9170.

[21] Nsihimura, M.; Matsunaga, K. *Bunseki Kagaku* **1969**, *18*, 154-158.

[22] Ferreira, F. T. S. M.; Mesquita, R. B. R.; Rangel, A. O. S. S. *molecules* **2021**, *26*, 6355.

[23] Kitagawa, Y.; Hara, I.; Moriguchi, Y.; Hattori, S. Study on the Behavior and Analytical Methods of Nitrite Nitrogen in Tap Water, Osaka City Waterworks Bureau **2013**.

[24] Jayawardane, B.M.; Wei, S.; McKelvie, I.D.; Kolev, S.D. *Anal. Chem.* **2014**, *86*, 7274-7279.

[25] Ferreira, F.T.S.M.; Mesquita, R.B.R.; Rangel, A.O.S.S. *Talanta* **2020**, *219*, 121183.

[26] Teepoo, S.; Arsawiset S.,; Chanayota, P. *Chemosensors* **2019**, *7*, 44.

[27] Ratnarathorn,N.; Dungchai, W. J. *Anal. Chem.* **2020**, *75*, 487–494.

[28] Thongkam, T.; Hemavibool, K. *Microchem. J.* **2020**, *159*, 105412.

[29] Olivieri, A.C. *Anal. Chim. Acta* **2015**, *868*, 10-22.

[30] Nakamoto, K. Infrared and Raman Spectra of Inorganic and Coordination Compounds, Part A, Wiley-Interscience **2009**, *6*, p.164, 183.

[31] Carlson, R. M. *Anal. Chem.* **1986**, *58*, 1590–1591.

[32] Limousy, L.; Dutournie P.,; Hadjiev, D. *Water Environ. Res.* **2010**, *82*, 648-656.

Chapter 3

Development of μPADs for Measuring Ammonium Ions

Chapter 3. Development of μPADs for Measuring Ammonium Ions

3.1 Introduction

3.1.1 Ammonia in environmental water

In environmental waters, nitrogen is present in the forms of nitrate nitrogen, nitrite nitrogen, and ammonia nitrogen. While these nitrogen compounds serve as essential nutrients for organisms, their excessive discharge into the environment can lead to eutrophication, characterized by an overgrowth of plankton and algae, ultimately resulting in the deterioration of water quality. The primary sources of ammonia include industrial activities, the use of fertilizers, animal waste, and the decomposition of organic matter. As discussed in Section 2.1.2, nitrogen compounds are also associated with potential health hazards. Therefore, regulating nitrogen emissions in environmental waters is critical for maintaining favorable environmental conditions.

Despite these concerns, in 1978, the Ministry Ordinance on Water Quality Standards excluded ammonia nitrogen from the list of regulated water quality standards, based on the premise that ammonia nitrogen itself does not pose a direct risk to human health. However, ammonia nitrogen undergoes microbial conversion to nitrite nitrogen and nitrate nitrogen, and in aerobic aquatic environments, it is oxidized into these forms. Since nitrite and nitrate nitrogen contribute to environmental and health risks, the regulation of ammonia emissions remains a significant consideration for ensuring the preservation of water quality and overall environmental conservation.

In Japan, environmental standards regulate that the concentrations of nitrate nitrogen and nitrite nitrogen in public water bodies must remain below 10 mg L^{-1} to ensure their suitability as sources of tap water. To satisfy this requirement, emission standards specify that the combined concentration of ammonia, ammonium, nitrate, and nitrite compounds must not exceed 100 mg L^{-1}. This limit is determined as the sum of nitrite nitrogen and nitrate nitrogen concentrations, in addition to ammonia nitrogen multiplied by a conversion factor of 0.4. Furthermore, the water quality standard for ammonia nitrogen in drinking water is ideally set at less than 0.3 mg L^{-1} to ensure safety and quality.

3.1.2 Quantitative method for ammonia

Common methods for the quantification of ammonia include the indophenol method and the Nessler method; however, these techniques present several limitations, such as the use of hazardous mercury compounds, the requirement for proper waste disposal, and the necessity of distillation during the analytical process [1]. The Nessler method, in particular, is hindered by the complexity of reagent preparation, poor reagent stability, and insufficient precision and reproducibility, which restrict its applicability [2]. Similarly, the pyridine-pyrazolone method is affected by reagent instability, making it difficult to achieve accurate and reliable measurements [3, 4]. Currently, the indophenol derivative spectrophotometric method, employing salicylic acid, is widely used for the determination of ammonia in environmental water samples [5]. However, this method involves the use of sodium nitroprusside as a catalyst, which is a toxic substance, raising concerns regarding its environmental and operational safety.

In this study, a spectrophotometric method for ammonia determination, utilizing 1-naphthol and hypochlorite ions for the color reaction [1, 2], was employed with the aim of developing microfluidic paper-based analytical devices (μPADs) for simple and efficient ammonia measurement. The method demonstrated excellent linearity within the concentration range of 0.01–0.075 mol L^{-1}. Furthermore, the results of condition optimization for this method are presented and discussed in detail.

3.2 Experiment

3.2.1 Ammonia detection method

This study used the indophenol reaction with α-naphthol to detect ammonium ions. Scheme 3.1 illustrates the reaction mechanism [2]. Ammonia reacts with hypochlorite to form monochloramine. Subsequently, the reaction proceeds through one of two pathways to form naphthoquinonylchloramine. The first pathway involves α-naphthol or oxidized naphthoquinone reacting with monochloramine to produce naphthoquinonylchloramine. In the second pathway, α-naphthol and chloramine react to make 4-amino-1-naphthol. This compound then reacts with hypochlorite to make naphthoquinonylchloramine. The generated naphthoquinonylchloramine further condenses with α-naphthol to form a green indophenol-type dye. The pH of the reaction solution influences the formation rate of

monochloramine, which reaches its peak under basic conditions. If α-naphthol and ammonia react under basic conditions before adding hypochlorite, a decrease in pH occurs, leading to the oxidation of α-naphthol being prioritized and thereby inhibiting monochloramine formation [2]. Therefore, the reaction order is crucial for color development.

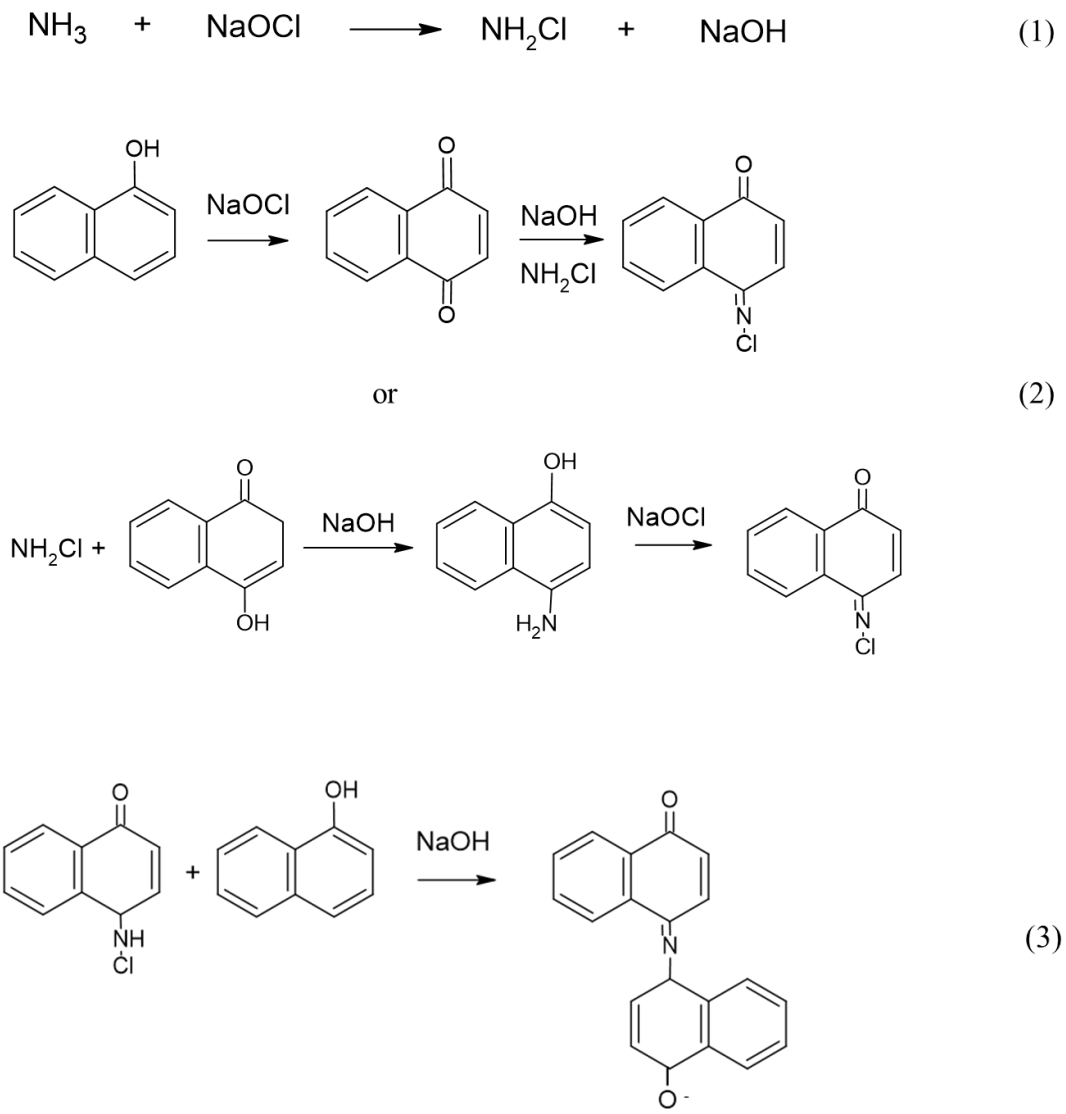

Scheme 3.1 Reaction mechanism of ammonia detection

3.2.2 μPADs design and measurement procedure

Figure 3.1 illustrates the flow channel design of the μPADs. The device comprises two hydrophilic circles that overlap when the μPADs are folded at their center, enabling the reagents in the circles to react with each other. To prepare the detection zone, 10 μL of 0.5 mol L^{-1} sodium hydroxide was added twice to one of the hydrophilic circles, followed by the addition of 8 μL of a 7% α-naphthol-acetone solution. After each addition, the reagents were dried at 120 °C for 90 s to ensure proper immobilization.

The other hydrophilic circle was treated with chloramine T, which generates hypochlorite ions upon dissolution in water. To prevent premature contact of chloramine T with water before analysis, it was suspended in toluene at a concentration of 0.03 mol L^{-1}, and 5 μL of this suspension was added to the μPADs.

The prepared μPADs were folded and placed into a holder. Subsequently, 30 μL of the sample solution was introduced into the upper layer circle. A weight was placed on the holder after sample introduction to ensure firm contact between the two layers. The detection zone (the circle containing sodium hydroxide and α-naphthol) was scanned using a flatbed scanner, and the scanned image was analyzed with a custom-developed image analysis tool. The color intensity in the detection zone was quantified using multiple color models, including RGB, HSV, Lab*, LCh, and ΔE values, providing a robust and comprehensive evaluation of the colorimetric response.

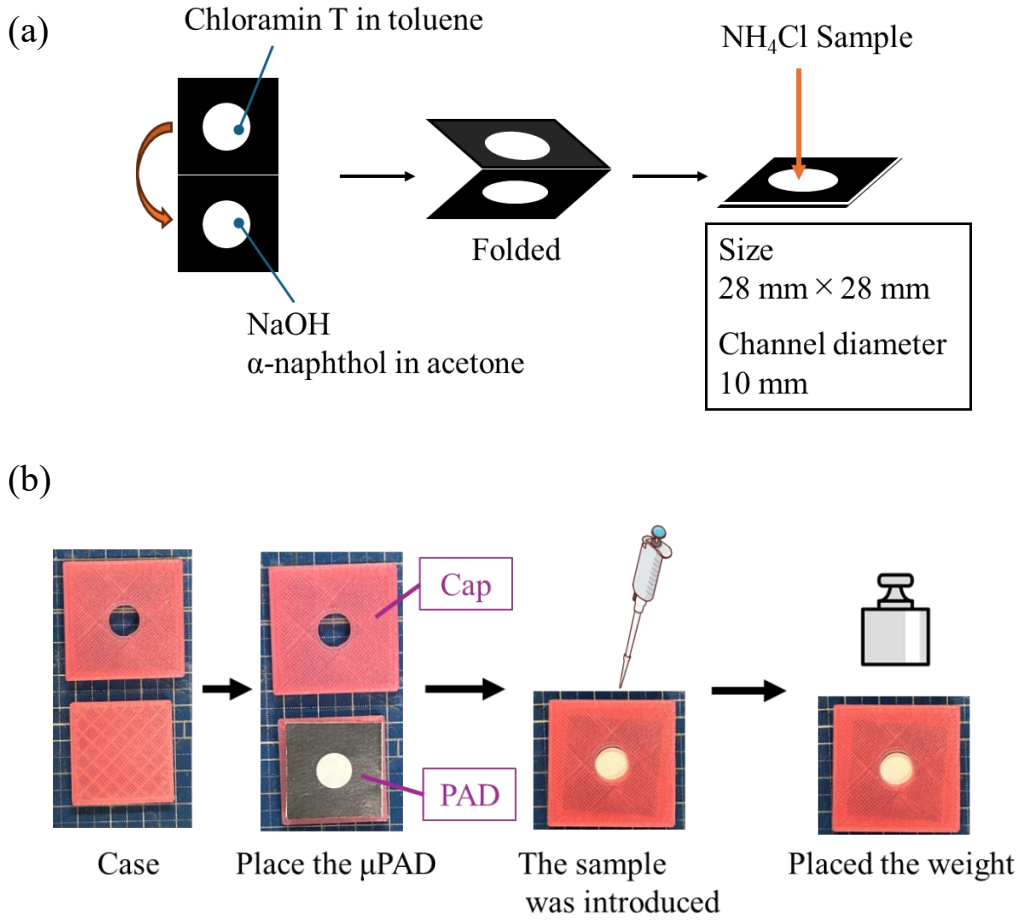

Figure 3.1 μPADs for ammonia detection

(a: design and reagent addition location, b: the case of μPADs and measurement procedure)

3.2.3 Regarding the color system

The detected zone of the scanned image was processed using a self-made image analysis tool, and the color change was quantified using the following color representation methods: (1) to (4). This chapter introduces each of them.

There are various types of color spaces and chromatic diagrams, depending on the parameters and formulas used. The systematic approach to selecting these parameters and calculation methods is called the color system [6]. Color systems can generally be classified into two categories: the "color mixing system," which represents psychophysical quantities, and the "color appearance system," which represents

perceived colors [7]. The former uses a coordinate system to represent color, while the latter displays colors in a three-dimensional color space.

(1) RGB color model

Red, green, and blue are the three primary colors of light, and by combining these colors, we can represent all colors. These colors are classified as part of the color mixing system within color spaces. The basic mechanisms of vision closely relate to the color mixing system, simplifying its numerical handling [6]. The amount of each component—red, green, and blue—defines the color. The brightness of a color is represented on a scale of 0 to 255, with 256 levels. If each element is 0, the resulting display will be black. If each element is 255, the resulting display will be white. Color images in ImageJ typically use the RGB color model.

The CIE (Commission Internationale de l'Eclairage) defines color matching functions as shown in Figure 3.2 (A) [8]. A color matching function is a plot of the mixture ratios of red, blue, and green light that appear visually similar to a test light, which is a light of a single wavelength. In the RGB system, there are regions of the wavelength spectrum where the color matching function takes negative values. Through a coordinate transformation, CIE established a new color matching function that has only positive stimulus values, called the XYZ color space (Figure 3.2 (B)) [8].

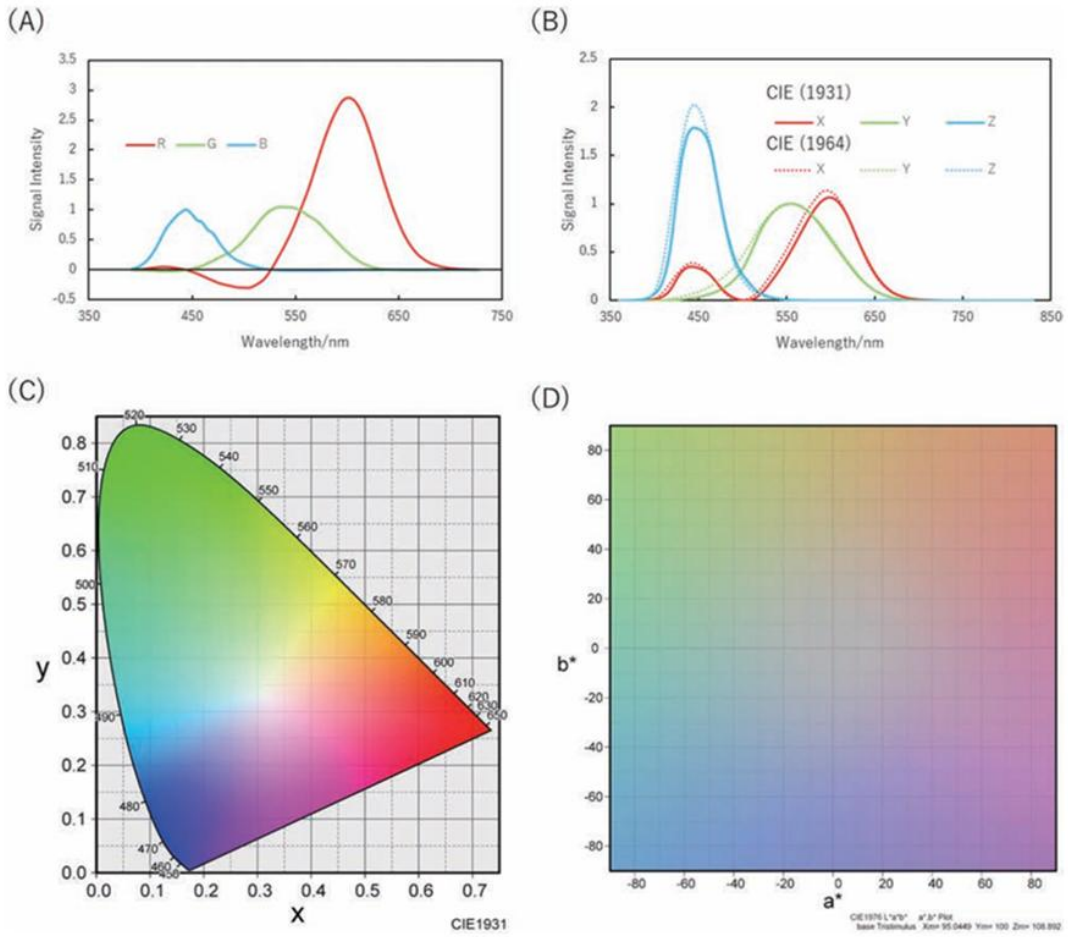

Figure 3.2 Various Color matching functions and diagrams [5]
(A: Color matching function for RGB color systems, B: Color matching functions for CIE(1931) XYZ and CIE (1964) XYZ systems, C: CIE(1931)XYZ based x-y chromaticity diagram, D: CIE(1976)L*a*b*-based color space)

(2) HSV model

Color appearance systems refer to color spaces based on how colors appear. The oldest color system, the Munsell system, was introduced in 1905 by the painter Munsell. The Munsell system, a color space notation method based on hue, value, and chroma, has undergone continuous improvement and remains widely used today.

The HSV model consists of three components: Hue, Saturation (Chroma), and Value (Brightness) and is also known as the HSB model. Alvy Ray Smith developed it in 1978 [9]. This model represents hue in a circular region and visualizes it using a conical or cylindrical space. Figure 3.3(a) uses the triangular area within the cone to represent saturation and brightness. The horizontal axis (radius) of the triangle

indicates brightness, while the vertical axis (height) corresponds to saturation. When visualized in a cylindrical space, hue changes along the outer edge of the cylinder, saturation varies with the distance from the center (radius), and brightness changes from the top to the bottom. In most cases, visualization with a cone is considered more realistic. The HSV model can be converted from the RGB color space.

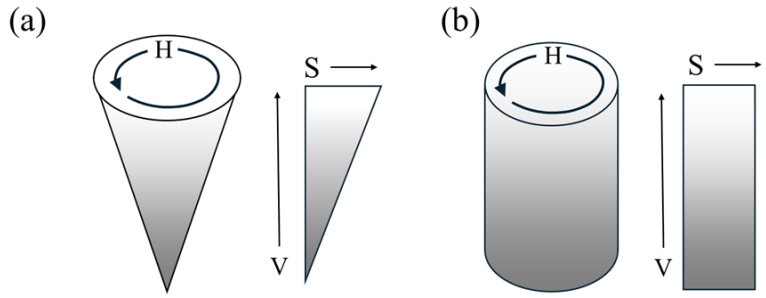

Figure 3.3 HSV color space
(a: Representation by a cone, b: Representation by a cylinder)

(3) CIE Lab color system

This color system is a type of color space designed to improve uniformity by refining the calculation method of the XYZ color system. It was established in 1976 [6]. In this system, L* represents lightness, while a* and b* denote chromatic components (Figure 3.4). A positive a* value corresponds to redness, with higher values indicating more intense red tones, whereas a negative a* value corresponds to greenness, with larger magnitudes signifying deeper green hues. Similarly, a positive b* value indicates yellowness, with greater values representing more vivid yellow tones, while a negative b* value indicates blueness, with larger negative values corresponding to stronger blue tones.

This color space is referred to as a "uniform color space" because perceptual differences in color are directly proportional to the geometric distances within the space. This ensures that variations in color are represented in a way that closely aligns with human visual perception.

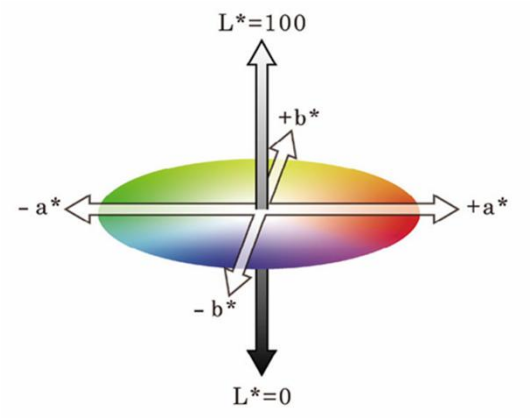

Figure 3.4 L*a*b* color space [1]

(4) CIE LCh color system

The LCh color space is a color model derived from the Lab* color space. While the Lab* color space is represented using a Cartesian coordinate system, the LCh color space utilizes polar coordinates [10]. In this system, L* represents lightness, with values ranging from 0 (black) to 100 (white). C* represents chroma, which corresponds to the distance from the central axis. A larger C* value places the color closer to the outer edge of the circle, resulting in higher vibrancy, whereas a smaller C* value indicates a more subdued or muted color.

The parameter h denotes the hue angle, where +a* (red) in Figure 3.4 is defined as 0°, and the hue progresses counterclockwise around the circle (Figure 3.5). Consequently, the range of h spans from 0° to 360°. The values of C* and h can be calculated using Equations (3.1) and (3.2).

$$C^* = \sqrt{(a^*)^2 + (b^*)^2} \qquad (3.1)$$

$$h = \tan^{-1}\left(\frac{b^*}{a^*}\right) \qquad (3.2)$$

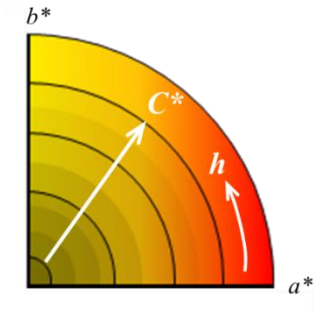

Figure 3.5 L*C*h color space

3.2.4 Materials and Equipment

α-Naphthol, sodium hypochlorite solution (3–5%), chloramine T, and acetone were procured from Sigma Aldrich Japan (Tokyo, Japan). Ammonium chloride was obtained from FUJIFILM Wako Pure Chemical Corporation (Osaka, Japan), while toluene and sodium hydroxide were purchased from Nacalai Tesque, Inc. (Kyoto, Japan). A 0.03 mol L^{-1} suspension of chloramine T was prepared by suspending it in toluene. α-Naphthol was dissolved in acetone to prepare solutions at concentrations of 5% or 7%.

Chromatography paper (200 × 200 mm, 1CHR, Whatman™) was utilized as the substrate for the μPADs. The μPADs were designed using Microsoft Office PowerPoint 2016. Wax patterns were printed onto the μPADs with a wax printer (ColorQube 8580N, Xerox, CT, USA), and the paper was then heated in an oven (EO-300V, AS ONE, Tokyo, Japan) to form hydrophobic barriers. The detection zones on the μPADs were scanned using a CanoScan LiDE400 scanner (Canon, Tokyo, Japan). For the solution-based reactions, the absorbance of the reaction product was measured with a V-730 spectrophotometer (JASCO, Tokyo, Japan).

3.3 Results and discussion

3.3.1 Color reaction in aqueous solution

Before reproducing the reaction on paper, a color reaction was carried out in a flask, and absorbance over time was measured using a spectrophotometer. A sample of 20 μL of a 1 mol L^{-1} ammonium chloride solution was put into a 25 mL volumetric flask. Then, 1 mL of 0.03 mol L^{-1} sodium hypochlorite solution was added, followed by 5 mL of 0.2 mol L^{-1} sodium hydroxide and 2.5 mL of 5% α-naphthol-acetone solution, and the mixture was stirred. Afterward, the absorbance at 740 nm was measured. Figure 3.6 displays the results. After mixing, the absorbance remained almost constant for 5 to 20 min before decreasing after 50 min. Therefore, it was determined that the reaction is relatively stable.

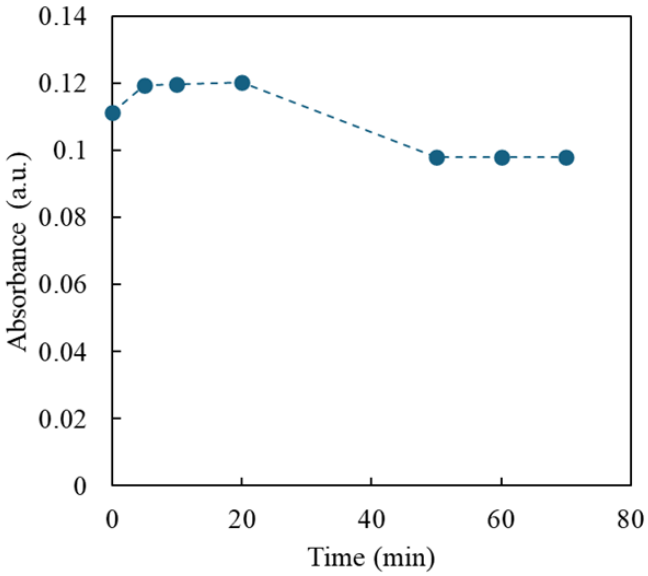

Figure 3.6 Change in absorbance over time

3.3.2 Change of color reagent

As shown in Chapter 3.2.1, the color reaction creates a green pigment when naphthohydroquinone, which is made from α-naphthol, and α-naphthol itself come together. To investigate whether stronger coloration could be obtained, 2,4-Dinitro-1-naphthol and 2,4-Dichloro-1-naphthol, which have similar structures to α-naphthol, were tested (Figure 3.7). A mixture was prepared by combining 10 μL of 2 mmol L^{-1} ammonium chloride, 1 mL of 0.03 mol L^{-1} sodium hypochlorite solution, 5 μL of 0.2 mol L^{-1} sodium hydroxide solution, and 5% solutions of either 2,4-dinitro-1-naphthol or 2,4-dichloro-1-naphthol. The color change in the presence or absence of ammonium ions was then observed. It didn't make any difference in the color whether ammonium ions were present or not, and the color wasn't stronger than when α-naphthol was used (Figure 3.8). These compounds already have functional groups at the para position, which likely prevented the reaction in Scheme 3.1(2) from occurring; thus, the reaction did not proceed.

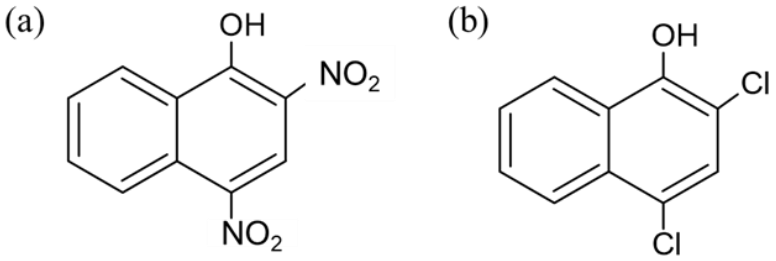

Figure 3.7 Structural formula（a: 2,4-Dinitro-1-naphthol, b: 2,4-Dichloro-1-naphthol）

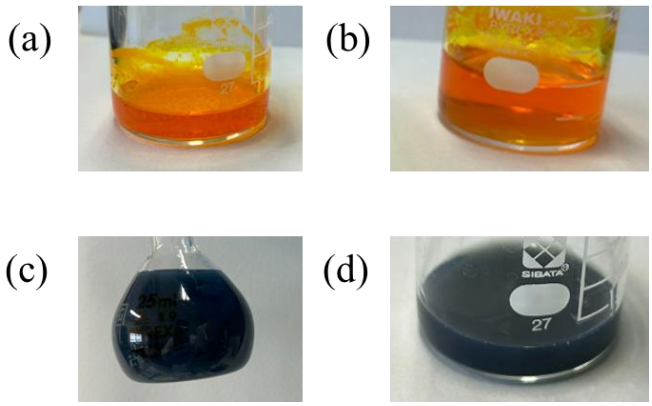

Figure 3.8 Solution color with or without ammonium ions

(a: 2,4-Dinitro-1-naphthol with NH_4^+, b: 2,4-Dinitro-1-naphthol without NH_4^+,

c: 2,4-Dichloro-1-naphthol with NH_4^+, d: 2,4-Dichloro-1-naphthol without NH_4^+)

3.3.3 Design optimization

Three different designs were created, and an attempt was made to reproduce the reaction on paper. Each reagent was pre-added to the designated area shown in Figure 3.9, and the sample was introduced to observe the color change. Consequently, the design in Figure 3.9 (b) demonstrated the strongest coloration. Figures 3.9 (a) and (c) were made so that the solution could flow horizontally. Figure 3.9 (b), on the other hand, folded the μPAD in the middle and glued the circles together so that they overlapped, which let the solution flow. It is speculated that the folded design produced stronger coloration because it provided a larger contact area with the reaction reagents (NaOH, α-naphthol). Future studies employed the folded design.

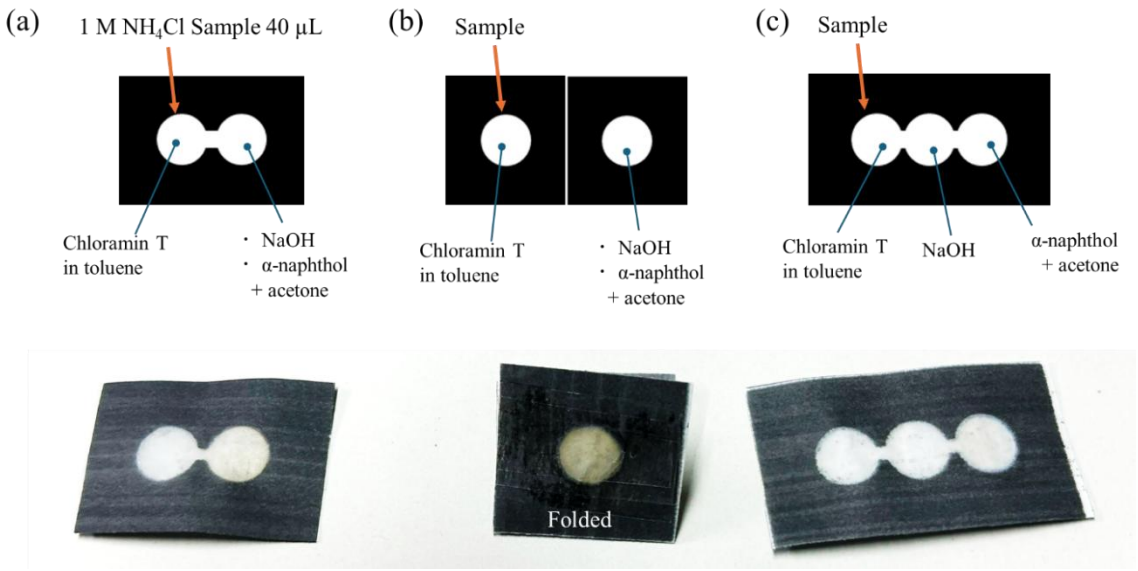

Figure 3.9 Design idea and color results

3.3.4 Reagent optimization

The optimal conditions for reagent addition were determined by considering five parameters: (1) sample volume, (2) the amount of 0.5 mol L^{-1} NaOH, (3) the amount of 0.03 mol L^{-1} chloramine T suspension, (4) the amount of 7% α-naphthol-acetone solution, and (5) the drying time of the 7% α-naphthol-acetone solution. A 1 mol L^{-1} ammonium chloride aqueous solution was used as the sample. The conditions for preparing the PADs are summarized in Table 3.1. The degree of coloration was assessed by measuring the red value, which is complementary to the green product color. A lower red value indicates a more intense green coloration.

Table 3.1 Conditions for preparation of μPADs

Conditions / Survey. item	Sample volume (μL)	NaOH volume (μL)	Chloramine T volume (μL)	α-naphthol volume (μL)	α-naphthol drying time (s)
Sample volume	10-60	20	5	8	90
NaOH volume	30	5-50	5	8	90
Chloramine T volume	30	20	3-15	8	90
α-naphthol volume	30	20	5	2-16	270
α-naphthol drying time	30	20	5	8	0-150

(1) Sample volume

Figure 3.10 (a) showed that the coloration tended to intensify as the sample volume increased. However, when 40 μL and 60 μL were introduced, some of the solution that had not dried leaked from the μPADs while scanning the detection zone. In this experiment, the red value was largest when 30 μL was used. Based on the trend of the results, this is likely an outlier, as only one measurement was taken. It was concluded that the red value of 30 μL should be between that of 20 μL and 40 μL, and 30 μL was chosen as the optimal volume, as it was the maximum amount that did not overflow from the solution.

(2) Amount of 0.5 mol L^{-1} NaOH added

Reagents were measured using a micropipette to take 5 μL, which was then added to the μPAD and dried at 120 °C. When adding 10 μL or more, 5 μL was added in multiple steps, with drying after each addition. In Figure 3.10 (b), it can be seen that the red values were nearly the same between 10 μL and 50 μL. The amount of NaOH added was set at 20 μL.

(3) Amount of 0.03 mol L^{-1} chloramine T suspension added

Chloramine T was used as a source of hypochlorite ions in this reaction. When adding 10 μL or more of the reagent, it was added in multiple steps of 5 μL each, with natural drying between each addition. It was shown in Figure 3.10 (c) that the lowest value was when 10 μL was added. However, the red value did not change significantly under the conditions used in this experiment.

(4) Amount of 7% α-naphthol-acetone solution added

Chloramine T was used as the source of hypochlorite ions in this reaction. When adding 10 μL or more of the reagent, it was applied in multiple 5 μL increments, with natural drying between each addition. As shown in Figure 3.10 (c), the lowest value occurred when 10 μL was added. However, under the experimental conditions, the red value did not change significantly.

(5) Drying time after adding the α-naphthol-acetone solution

During the optimization process, it was observed that the coloration intensity varied depending on the drying time after the addition of α-naphthol. The drying temperature was set to 120 °C. As the drying time increased, the areas where the base and α-naphthol were applied turned brown. This is consistent with the known behavior of phenolic compounds, which gradually discolor and turn brown when exposed to air [11]. It is believed that oxidation was accelerated by the high temperature, contributing to the browning.

The results of the optimization, in which drying time was varied, are shown in Figure 3.11. As the drying time increased, the red value decreased. Since the red value remained stable after 90 s the optimal drying time was determined to be 90 s.

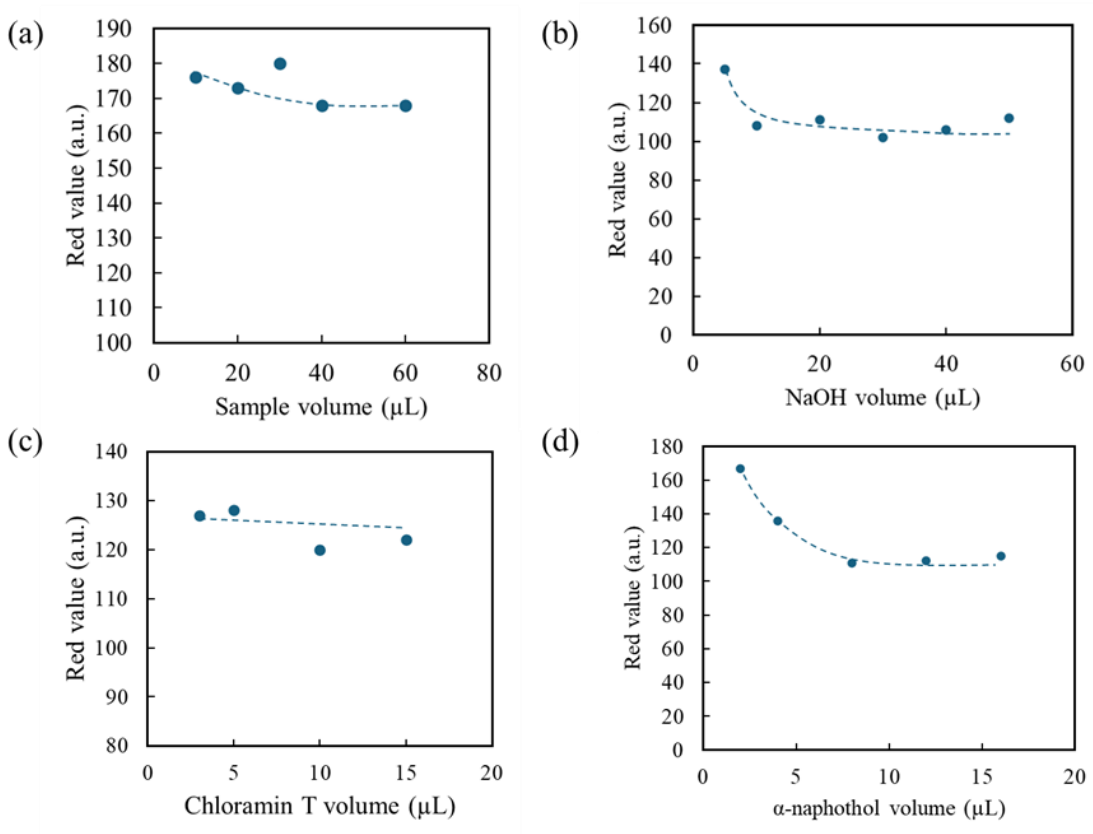

Figure 3.10 Optimization of reagent dropping volume
(a: sample, b: NaOH, c: Chloramin T, d: α-naphthol)

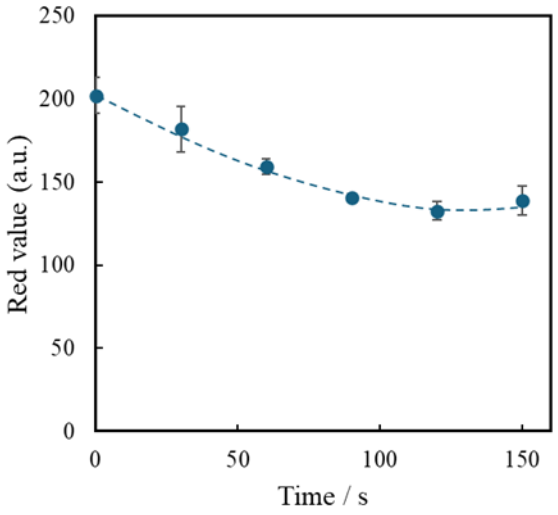

Figure 3.11 Drying time of α-naphthol

3.3.5 Effect of reaction time with Chloramine T on color intensity

As detailed in Chapter 3.2.1, the reaction in this study occurs in three distinct steps. In the first step, ammonium ions and hypochlorite ions react to form monochloramine, which subsequently drives the following reactions. To determine the optimal reaction time for reliable monochloramine formation, the reaction time between ammonium ions and hypochlorite ions was systematically varied and evaluated.

The reagents used in the experiment included 10 µL of NaOH solution (added in two aliquots), 4 µL of α-naphthol-acetone solution (added in two aliquots), and 5 µL of chloramine T, all of which were introduced to the µPADs. After a specified time had elapsed since the introduction of the 1 mol L^{-1} ammonium chloride aqueous solution, the µPADs were folded in half to allow the base and α-naphthol to react for a fixed period of 10 min.

As shown in Figure 3.12, no significant change in the red value was observed between 0 and 15 min, indicating that the reaction time did not have a substantial impact on the results. A previous study by Morita et al. demonstrated that stronger coloration is achieved when hypochlorite ions initially react with ammonium ions before reacting with α-naphthol [2]. Consequently, in this study, the sample was introduced from the side containing chloramine T while the µPAD was folded, ensuring that the reagents reacted in the order specified.

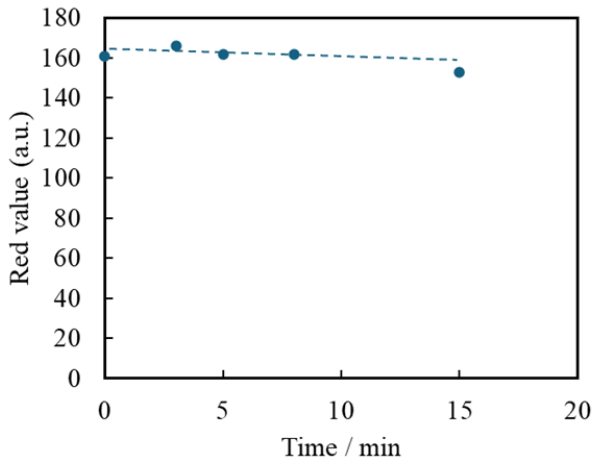

Figure 3.12 Red value depending on contact time of chloramine T and ammonium ion

3.3.6 Consideration of improving color unevenness

Occasionally, color unevenness was observed in the detection zone (Figure 3.14(a)). To address this issue, the surface of the filter paper was modified. Because of the way it is structured, α-naphthol is thought to have a negative charge. To make the filter paper surface positively charged, polydiallyldimethylammonium chloride (PDADMA) was added. Figure 3.13 displays the structures of naphthol and PDADMA. It was mixed with water to prepare PDADMA solutions of 0.1%, 1%, and 5%. 10 μL of each solution was added to the detection zone before α-naphthol was added. Afterward, the μPADs were dried at 120 °C for 90 s.

The dominant cluster ΔE of the scanned detection zone is shown in Table 3.2. The dominant cluster ΔE is an index that indicates color differences and is used to measure similarity or differences in color. A smaller value indicates more similar colors, while a larger value indicates more distinct colors. Among the results measured, no significant color unevenness, such as that shown in Figure 3.14 (a), was observed. However, the ΔE of the μPADs without PDADMA was the largest. The smallest ΔE and standard deviation were observed for the μPADs with 0.1% PDADMA added.

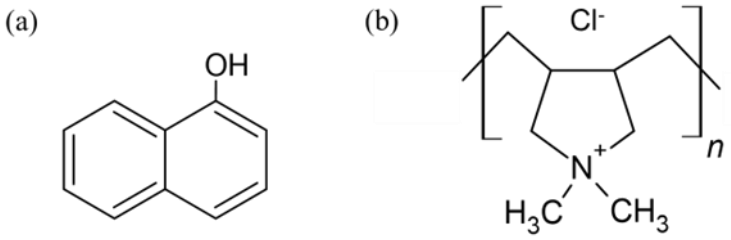

Figure 3.13 Structural formula (a: α-naphthol, b: PDADMA)

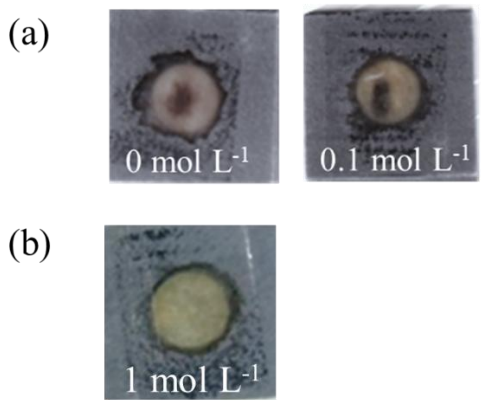

Figure 3.14 The images of Detection zone

(a: uneven color (no PDADMAC added), b: 0.1% PDADMAC added, the concentration at the bottom of image indicates the concentration of the ammonium chloride solution introduced.)

Table 3.2 Dominant cluster ΔE against PDADMAC concentration

PDADMAC concentration	Dominant cluster ΔE (Ave.)	SD
0%	10.8	2.3
0.1%	7.9	1.2
1%	8.5	2.1
5%	9.1	3.5

3.3.7 Confirmation of concentration dependency

The relationship between coloration intensity and ammonia concentration in the range of 0–0.1 mol L^{-1} was investigated. To achieve uniform coloration in the detection zone, 0.1% PDADMAC was added. Upon observing the coloration, it was found that as the ammonia concentration increased, the color shifted towards yellow-green. The coloration in the detection zone was then converted into red values, and a calibration curve was constructed (Figure 3.15). It was speculated that the red value would decrease as the green color intensity increased with the rising ammonia concentration. However, the calibration curve did not exhibit linearity with respect to the red value. The blank sample already showed a brown color with a mix of different hues, leading to a complex color mixture.

As a result, the slight changes in color could not be accurately observed using the red value. In contrast, in the nitrite ion detection described in Chapter 2, the reaction product was monochromatic, and the blank was white. As the concentration increased, the color intensity also increased, allowing for easy tracking of changes using the green value. However, in this case, due to the factors mentioned above, it was concluded that using RGB conversion was not suitable for observing the color change.

Other color spaces were explored to identify parameters that could exhibit linearity. As a result, four parameters, shown in Figure 3.16, were found to show concentration dependence.

Saturation represents the degree of vividness, with higher values indicating more vivid colors. No correlation was found in the region with low ammonia concentrations and slight color changes, but good linearity was observed in the range of 0.25-0.75 mol L^{-1}. This is likely due to the shift from dark to light colors, resulting in changes in saturation.

The hue angle (h) for a color resembling orange is approximately 45°. As the angle approaches 90°, the color shifts toward yellow, and at 180°, it turns green. Although the color appeared yellow-green to the naked eye, the hue angle data revealed that as the ammonia concentration increased, the color shifted closer to yellow. This shift is likely due to the insufficient formation of indophenol-type dyes, resulting in the production of quinones and contributing to the overall yellowish hue. The a* value is negative for green and positive for red, with higher values indicating more intense red. The b* value is positive, with larger values indicating more yellow. As the concentration increased, Figure 3.16 (c, d) shows a decrease in the red component and an enhancement of the yellow component. By constructing a calibration curve using these parameters, it may be possible to quantify the ammonia concentration effectively.

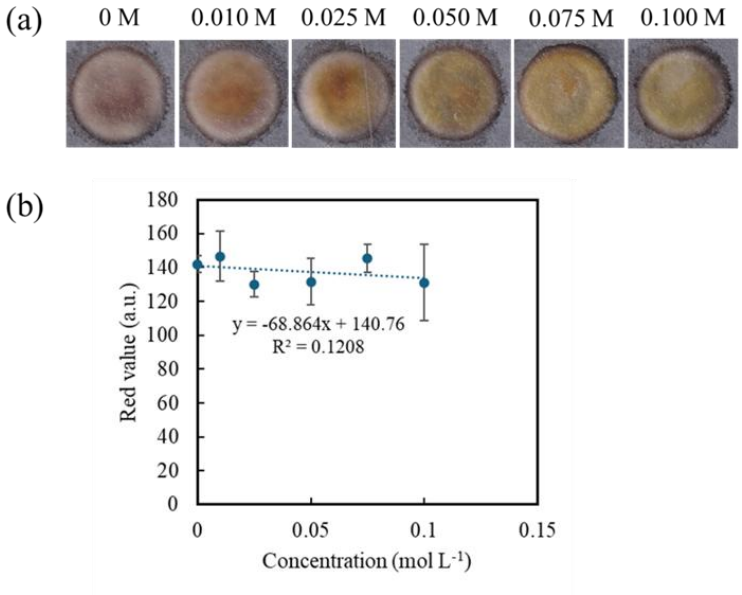

Figure 3.15 Color change due to ammonia concentration

(a: detection zone image, b: ammonia concentration relative to red value)

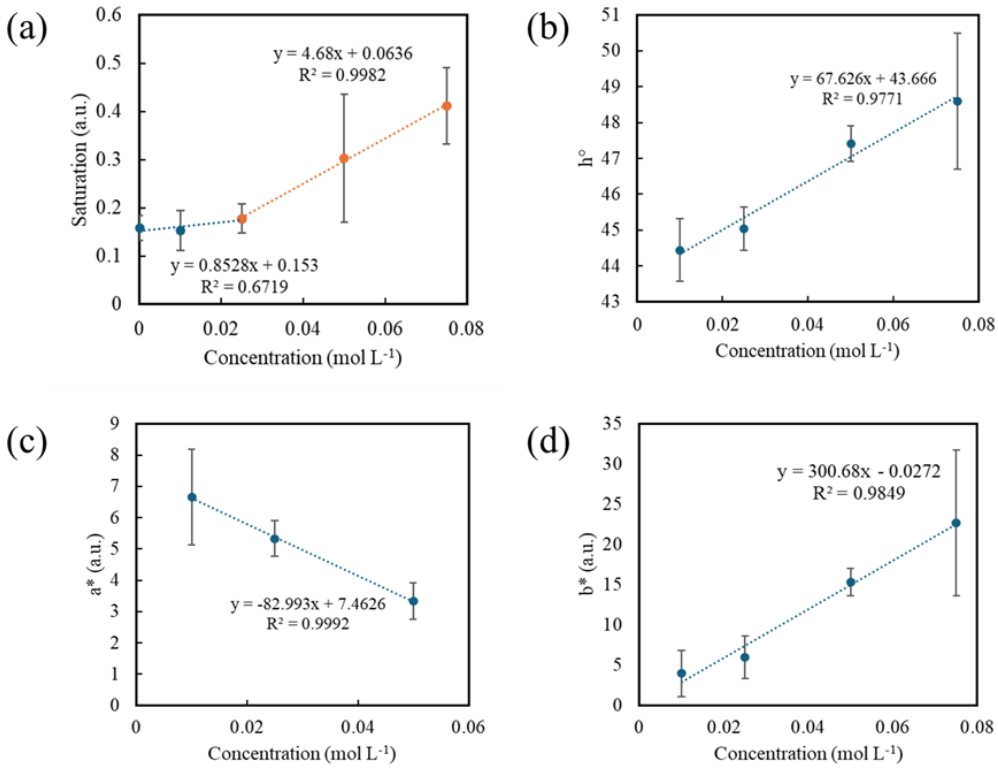

Figure 3.16 Correlation of each parameter to ammonia concentration

(a: Saturation, b: hue angel, c: a*, d: b*)

3.4 Conclusion

This study developed μPADs to measure ammonium ions. Environmental waters regulate ammonium ions because they can transform into nitrite and nitrate ions. However, conventional reagents used in such measurements are highly toxic. Therefore, this study explored simple analytical methods using reagents with minimal human toxicity. The colorimetric reaction employed the indophenol reaction with α-naphthol, and the reaction was reproduced on filter paper to confirm the concentration dependence. The products of the colorimetric reaction were complex, with various colors mixed together. By processing the data using different color spaces, correlations with ammonia concentration were found in parameters such as saturation in the HSV model, hue (h) in the L*C*h model, and a* and b* in the L*a*b* model.

Although ammonia quantification has not yet been fully realized, these parameters show significant potential for enabling simple ammonia measurements. Future efforts should focus on developing methods for accurate concentration calculations and aim to quantify ammonia in environmental waters, thereby demonstrating the practicality of this approach. This research holds promise for facilitating the simple separation and quantification of nitrogen compounds, particularly in areas with limited infrastructure and technology, such as developing countries, by integrating measurement techniques for nitrite and nitrate ions.

3.5 Reference

[1] Suekane, T.; Oshima, M.; Motomizu, S. *BUNSEKI KAGAKU* **2005**, *54* (10), 953-957.

[2] Morita, Y.; Kogure, Y. *Journal of the Chemical Society of Japan* **1963**, *84* (10), 816-823, A56.

[3] Kruse, J. M.; Mellon, M. G. *Anal. Chem.* **1953**, *25*, 1188.

[4] Leer, J. B. *Anal. Chem.* **1957**, *29*, 293.

[5] Murai, H.; Higuchi, K.; Sakai, M.; Korenaga, T.; Toei, K. *Anal. Chim. Acta.* **1993**, *261*, 345.

[6] Yokoi, K. *J. Inst. Image Inform. TV. Engnr.* **2011**, *65* (12), 1723-1725.

[7] Kotera, H. *The journal of the Imaging Society of Japan* 2004, 43, 2, 73-81.

[8] Inagawa, A.; Uehara, N. *Bull. Soc. Sea Water Sci., Jpn.* **2022**, *76*, 2-10.

[9] Smith, A. R. *ACM SIGGRAPH Computer Graphics* **1978**, 12 (3), 12–19.

[10] Nagano, C. *J. Jpn. Soc. Colour Mater.* **2016**, *89* (6), 197-202.

[11] Ogata, Y.; Morimoto, T. *Journal of Japan Oil Chemists' Society* **1965**, *14* (5), 219-228.

Chapter 4

A Facile Fabrication Method Using Rosin Spray

Chapter 4. A Facile Fabrication Method Using Rosin Spray

4.1 Introduction

There are several methods to fabricate channels for μPADs, as described in Chapter 1.2.3. The most common method is wax printing using a wax printer. The method easily fabricates hydrophobic barriers by printing paper with solid wax ink. Unfortunately, the product company discontinued the production of the wax printers in 2016, so they are no longer commercially available. Therefore, researchers have explored alternative materials for the fabrication of PADs, including bovine serum albumin (BSA) [1], hydrophobic silane [2], beeswax emulsion [3], correction pen fluid [4], glass varnish [5], and oil-based markers [6, 7]. Sgobbi et al. reported a method in 2024 to form hydrophobic barriers by substituting the gel ballpoint pen's ink with a rosin-prepared bioink [8].

Rosin is the residue that remains when the sap of pine plants is distilled. It is a transparent solid with a yellow to brown color at room temperature. A photo of its crystal is shown in Figure 4. As a material, rosin has several advantages, such as being a green natural product and having a relatively low cost. In fact, rosin is used by various industries to prevent ink from bleeding in the paper industry, as well as for oil varnishes and lacquers [9]. For everyday products, it serves as rosin bags for baseball, an anti-slip material in gymnastics and ballet shoes, and a fluff agent for the bows of stringed instruments.

Rosins are classified into abietic acid and pimaric acid types that are determined by the resin acids contained in them. The classification of resin acids is shown in Table 4.1. The resinous form softens below 85 °C, which is lower than the melting point of the resin acid alone. The main component of abietic acid-type rosin is abietic acid [10], which is soluble in alcohol, ether, benzene, and chloroform but insoluble in water.

This study proposed a facile method to fabricate μPADs using the natural product rosin as a hydrophobic barrier. The method involves spraying a solution of dissolved rosin onto masked filter paper to form hydrophilic channels, thereby enabling the fabrication of hydrophobic barriers in limited environments without the need for a power source. The study attempted to dissolve rosin in several solvents, including alcohol, acetone, and toluene. A suitable solvent was selected to form channels surrounded with hydrophobic barriers. The concentration of the rosin and the spraying condition were also optimized

by comparing the flow patterns in the channels. The method was used to fabricate acid-base titration μPADs to assess the rigidity of the channels against acid and base solutions and to compare them with those fabricated by the conventional wax printing method.

Figure 4.1 Rosin Crystals

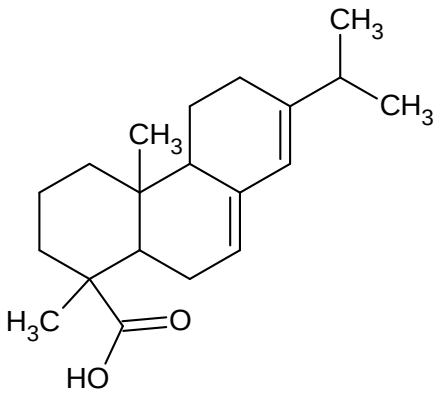

Figure 4.2 Abietic acid, the main component of rosin

Table 4.1 Components in rosin [9]

Name of resin acid		Melting point (˚C)
Abietic acid type	Abietic acid	172-175
	Levopimaric acid	172-175
	Neoabietic acid	167-169
	Palustric acid	162-167
	Dehydroabietic Acid	171-172
	Dihydroabietic Acid	176
	Tetrahydroabietic acid	173.5
Dextropimaric acid type	Textropimaric acid	217-219
	Isotextropimaric acid	162-164

4.2 Experiment

4.2.1 Materials and Equipment

Methanol, ethanol, and acetone were purchased from Sigma-Aldrich Japan (Tokyo, Japan). Rosin, phenolphthalein, sulfanilamide, citric acid, N-(1-naphthyl)-ethylenediamine dihydrochloride, nitrite ion standard solution (NO_2^- 1000 ppm) and sodium carbonate were purchased from FUJIFILM Wako Pure Chemical Co. (Osaka, Japan). Potassium hydrogen phthalate, sodium hydroxide, and toluene were purchased from Nacalai Tesque, Inc. (Kyoto, Japan). A 1% phenolphthalein solution was prepared by dissolving it in ethanol. The Griess reagent contained 50 mM sulfanilamide, 330 mM citric acid, and 10 mM N-(1-naphthyl)-ethylenediamine dihydrochloride. Natural water samples were collected from ponds in the National Institute of Technology, Yonago College.

Chromatography paper (200×200 mm, 1CHR, WhatmanTM) served as the substrate for the μPADs. The masking mold was printed using a 3D printer (XYZ printing) manufactured by XYZprinting, Inc. Polylactic acid (PLA) resin with a filament diameter

of 1.75 mm served as the material for the masking mold. The μPADs were designed using Microsoft Office PowerPoint 2016. For comparison, conventional μPADs were printed using a wax printer, Color Qube 8580N (Xerox, CT, USA), and heated at 120 °C for 1 min in an oven (EO-300V, AS ONE, Tokyo, Japan) to melt the wax so that it would penetrate to the backside of the μPADs.

4.2.2 A method for fabricating μPADs using rosin solution

The rosin crystals were crushed and ground in a mortar to make powder. The powdered rosin was dissolved in alcohol, acetone, or toluene by irradiating ultrasonic vibration. After rosin was completely dissolved, the solution was transferred into a spray bottle (Figure 4.1). A masking mold made with a 3D printer was placed in the center of a filter paper piece with the size of 100 mm x 100 mm. The mold design used is shown in Figure 4.2. The design of the masking mold was similar to that reported in a reference for acid-base titration [11]. Pencil marks indicate the position of locating the masking mold. The rosin solution was sprayed toward the center of the masking mold. After confirming that the first spray of the rosin solution had dried, it was sprayed again. The drying time was roughly 1 min, although it depends on the solvent and room temperature. The spraying and drying were repeated several times to form the rigid hydrophobic barriers. The rosin solution was sprayed on both the front and back sides of the filter paper to form a rigid hydrophobic barrier. When fabricating the μPAD for acid-base titrations, the rosin solution was sprayed five times on each side of the filter paper piece. The design of the μPAD is shown in Figure 4.4. Clear tape was attached to the back to prevent leakage of solutions. In the μPAD, the center circle serves as the sample introduction zone, and the first and second circles from the center work as the reaction zone and the detection zone, respectively. It took approximately 15 min or less to fabricate a μPAD. The operations consist of only dissolving rosin in a solvent, covering the paper substrate with a masking mold, spraying it onto the paper piece, and drying the rosin solution, which are simple and straightforward.

Figure 4.1 The spray bottle and rosin solution used

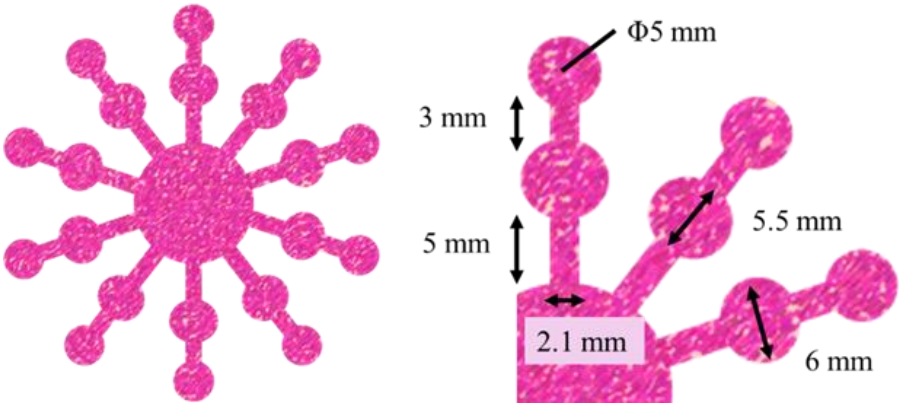

Figure 4.2 Masking mold design and each channel size

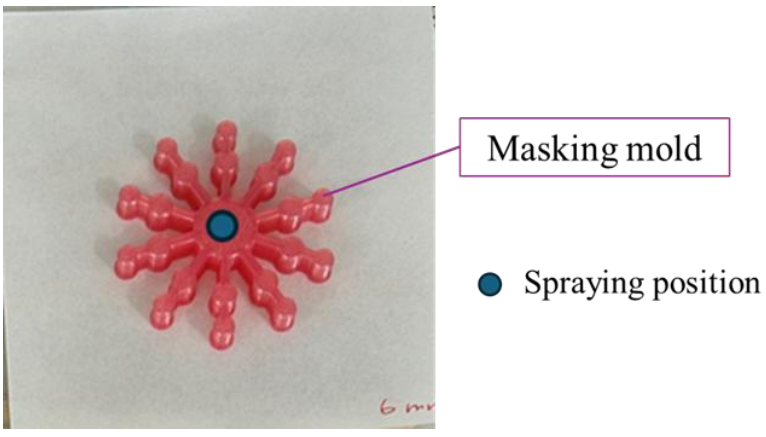

Figure 4.3 Spraying position

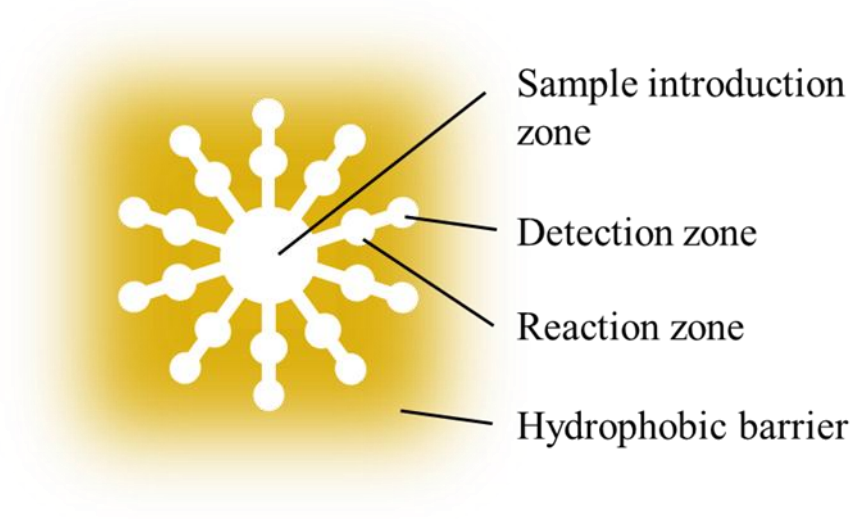

Figure 4.4 μPADs design

4.3 Results and discussion

4.3.1 Selection of solvent for rosin solution

Rosin solutions at a concentration of 50 g/L were prepared by dissolving in ethanol, toluene, acetone, and methanol as the solvent. Adding 40 μL of a methyl orange solution three times to the introduction zone of the μPAD (a total of 120 μL) proved that the hydrophilic channel had formed. The images of the μPADs after the introduction of the methyl orange solution are shown in Figure 4.5.

Solutions containing acetone or toluene clogged the spray nozzle and straw of the container, preventing continuous spraying. The high volatility of these solvents causes an increase in the viscosity of the solution and subsequent solidification of rosin. The channels formed by the toluene solution did not spread the methyl orange solution from the center to the end. This would be due to a high surface tension in toluene. Toluene has the highest surface tension among the solvents used in this study [13]. A large surface tension increases the size of the droplets [12]. When the sprayed droplets are large, they are likely to penetrate into the gap between the masking mold and the paper piece. So, the channels were closed, consequently resulting in stopping the flow in the channels. Among the four solvents, ethanol formed the finest channels, as seen in Figure 4.5a. Conversely, methanol also formed clear channels at the upper part, while the channels at the lower

part leaked the solution. An inappropriate spraying of the methanol solution might have caused the leaking at the lower part. However, ethanol provided reproducible channel fabrication, likely due to its suitable viscosity and surface tension for spraying. Therefore, ethanol proved to be a suitable solvent for the spraying method.

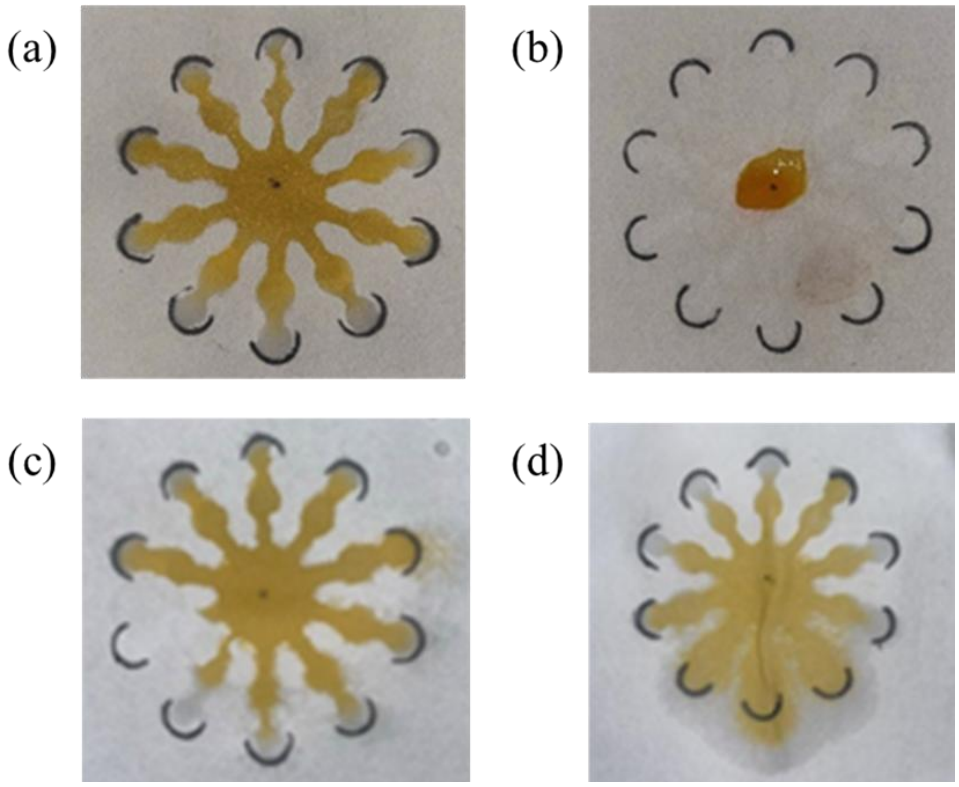

Figure 4.5 Channels made using several solvents

(a: Ethanol, b: Toluene, c: Acetone, d: Methanol)

Table 4.2 Properties of substances used as solvents

Substance	Molecular weight	Vapor pressure (mmHg at 20℃)	Surface tension (mN/m)	Boiling point (℃)	viscosity (mPa·s at 20℃)
Ethanol	46.07	44.1	22	78.29	1.20
Toluene	92.14	22	29	110.63	0.586
Acetone	58.08	181.72	23	56.5	0.322
Methanol	32.04	95.2	-	64.7	0.62

4.3.2 Optimization of concentration for rosin solution

The concentration of rosin was optimized using ethanol as the solvent. The rosin solutions with 50 g/L, 100 g/L, and 200 g/L were sprayed onto a masked filter paper 10 times on the front side and 5 times on the back side. Figure 4.6 shows a photograph after the introduction of a methyl orange solution into the fabricated μPADs. The outline of the channel was clearest, and the flow pattern was similar to that of the masking mold at 50 g L^{-1}. As the rosin concentration increased, the outline distorted. At a concentration of less than 50 g/L, the number of sprays has to increase, which elongates the fabrication time. These results determined the optimal concentration of rosin to be 50 g L^{-1}.

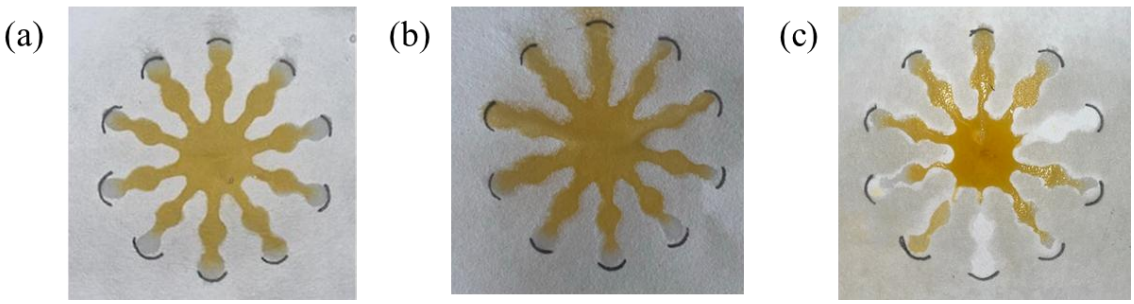

Figure 4.6 Channels with different rosin concentrations

(a: 50 g/L, b: 100 g/L, c: 200 g/L)

4.3.3 Optimization of spraying conditions

The spraying conditions investigated were: (1) thickness of the masking mold, (2) spraying location, (3) number of sprays, and (4) spraying distance.

(1) Thickness of the masking mold

Three masking molds with different thicknesses of 2 mm, 4 mm, and 6 mm were prepared to fabricate μPADs. Water was introduced into the fabricated μPADs to see the flow pattern in the channels. The results are shown in Figure 4.7. The thinner masking mold formed the narrower flow channel. Figure 4.8 shows a schematic illustration of how the masking mold blocks the spray when the thickness varies. Figure 4.8 assumes a constant distance and height from the edge of the masking mold for the solution spray. Figure 4.8 implies that a thick masking mold blocks the solution from reaching the edge of the masking mold.

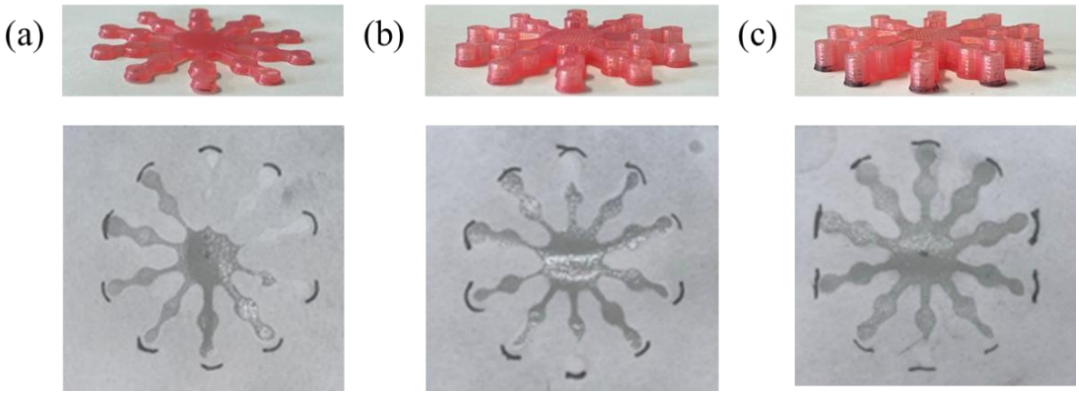

Figure 4.7 Comparison of channel shapes depending on the thickness of the masking mold (a: 2 mm, b: 4 mm, c: 6 mm)

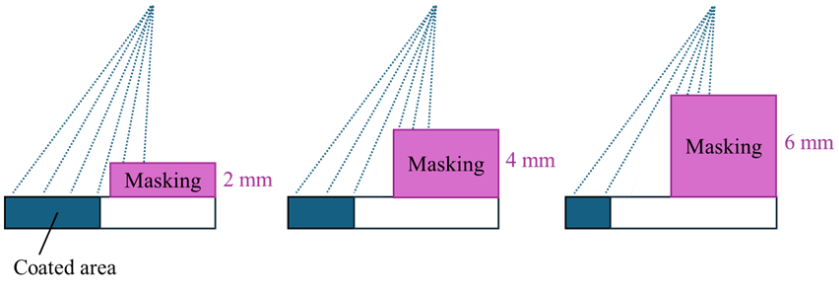

Figure 4.8 Image diagram of spray range

(2) Spraying location

The rosin solution was sprayed in three patterns as illustrated in Figure 4.9. When spraying the rosin solution from the positions depicted in Figure 4.9 (b, c), it penetrates into the gap between the paper and the masking mold, resulting in either narrowing or destroying the channel. It was found that spraying toward one point in the center of the masking mold is the best position.

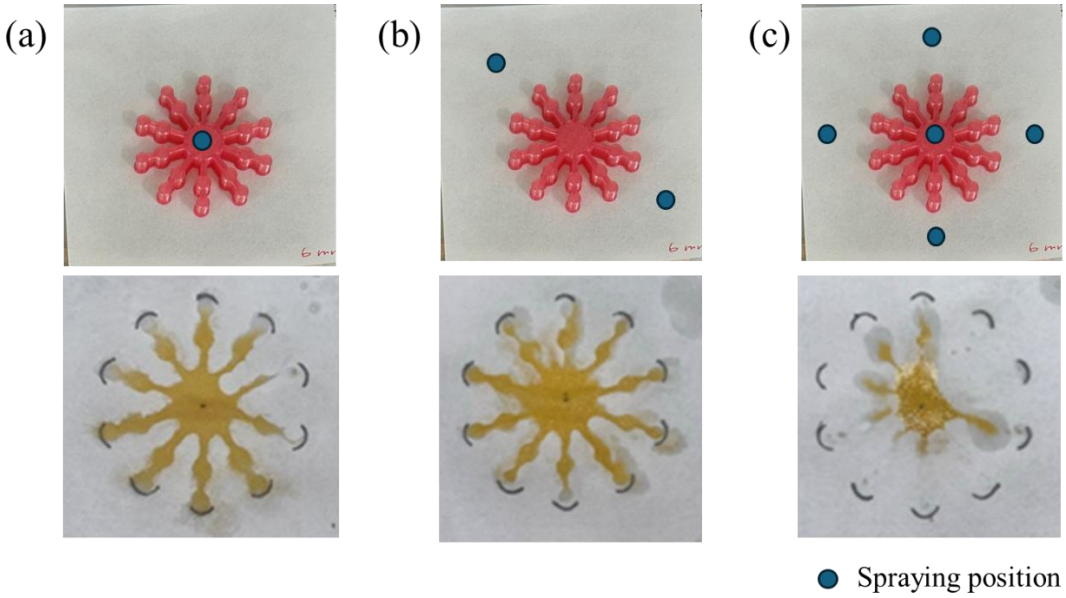

Figure 4.9 Comparison of channel shapes depending on spray location
(a: 1 place, b: 2 places, c: 5 places)

(3) Number of sprays

The rosin solution was sprayed 5, 7, and 10 times on each of the front and back surfaces. Figure 4.10 shows μPADs with methyl orange. Five sprays on each side were sufficient to form clear boundaries for the channels. Since the rosin solution is sprayed, dried, and then sprayed again to form the channel, the fewer the number of sprays, the shorter the manufacturing time. Consequently, the number of sprays was set to five.

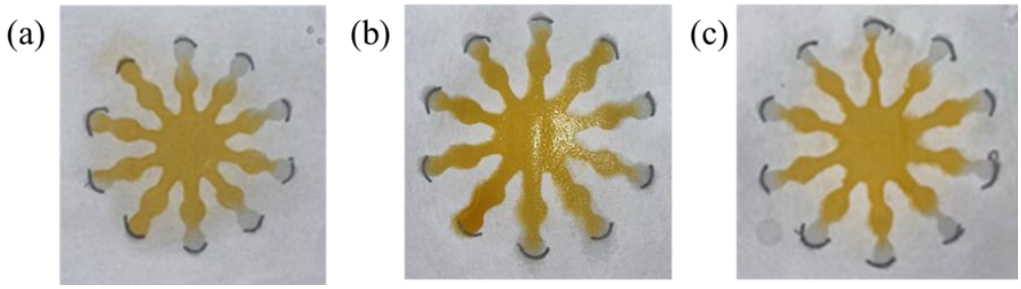

Figure 4.10 Comparison of channel shapes by number of sprays
(a: 5 times, b: 7 times, c: 10 times)

(4) Spraying distance

The distance from the filter paper to the spray was changed to form a channel. Figure 4.11 shows the μPADs after methyl orange was introduced. The longer the spray distance, the less clear the outline of the channel became. When the spray distance was short, the droplets attached to the filter paper were concentrated in a small area. Conversely, when the distance was long, the distance between the droplets increased. When the spray distance was 5 cm, the droplets were closer to each other, so they spread more easily, and the channel became narrower. When the spray distance was 15 cm, the droplets were farther apart, so the outline became blurred. When the spraying distance was 7 cm, the outline was clear and the shape was reproduced without collapsing the channel, so 7 cm was set as the optimal spraying distance.

Furthermore, as illustrated in Figure 4.11 (a, b), the methyl orange solution did not flow into the right-side channels. Specifically, in Figure 4.11 (a), the right-side connection channels were observed to be narrower compared to other channels, which may have hindered the solution from reaching the channel ends. Conversely, in Figure 4.11 (b), although the channel width was not narrow, the solution similarly failed to reach the ends of the channels, as observed in Figure 4.11 (a). Figure 4.12 presents magnified images of the channels, which appear to delineate boundaries between hydrophobic and hydrophilic zones. Despite the solution not flowing to the channel ends, the hydrophobic boundaries seem to have formed as expected. This suggests that the stopping of flow may be attributed to the bending of the PAD. To address this issue and prepare the μPAD for acid-base titration, weights were placed on the four corners of the μPAD to prevent bending.

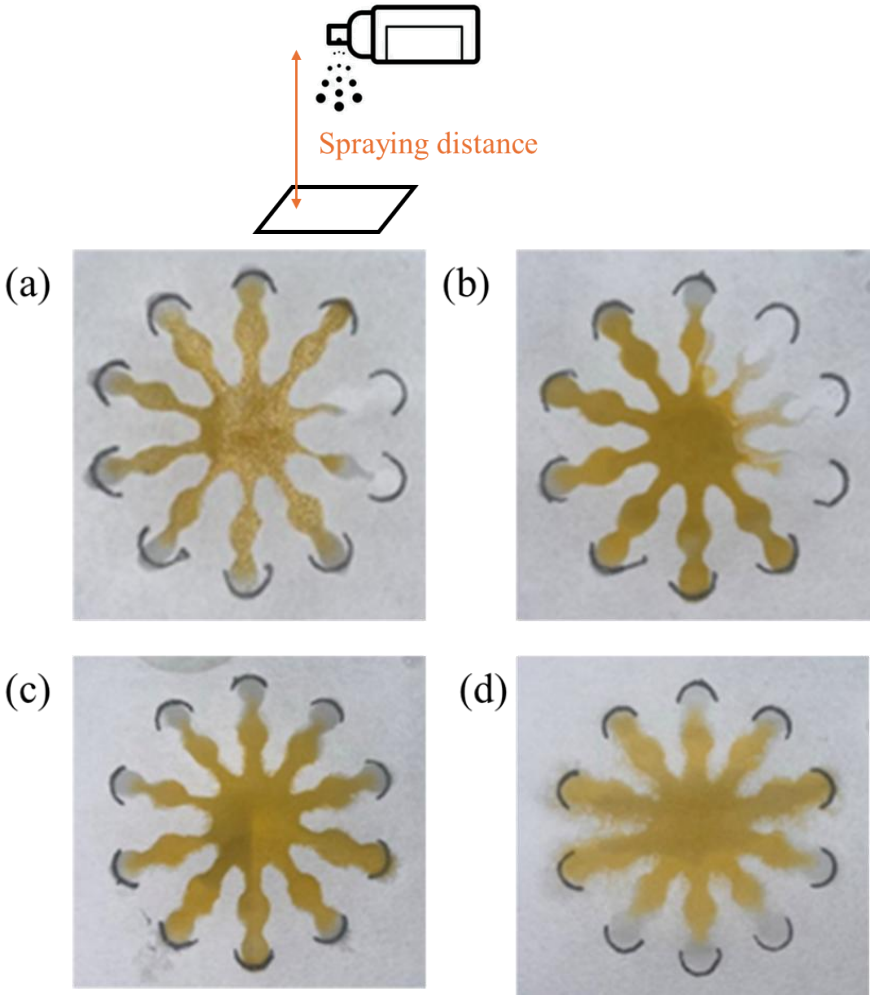

Figure 4.11 Channel shape due to different spraying distances
(a: 5 cm, b: 7 cm, c: 10 cm, d: 15 cm)

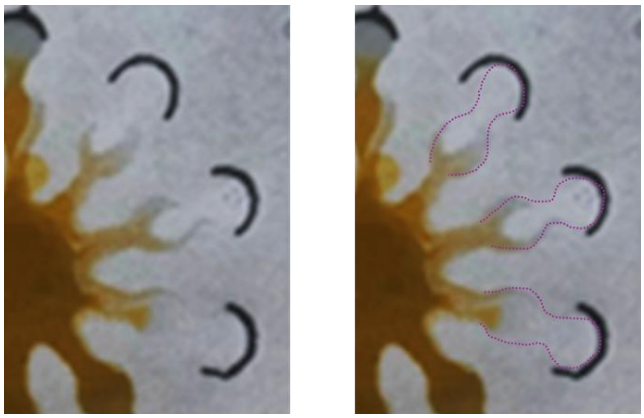

Figure 4.12 Enlarged image of the channel created with a spraying distance of 7 cm

4.3.4 Heat treatment

Rosin melts when heating it from 90 to 150 °C, depending on the type. Since the softening point of rosin is generally below 85 °C, the paper was heated in an oven set at 120 °C for 1, 3, and 5 min. In this experiment, the rosin solution was sprayed onto the front surface of the filter paper, and the drying process was repeated 10 times to coat the surface. The methyl orange solution was introduced into the fabricated μPADs, and the channel shape was confirmed.

When wax ink is used as a hydrophobic barrier, the longer the heating time, the more the wax melts and spreads, narrowing the channel. However, when comparing Figures 4.13 (a) and (c), no significant difference in the channel shape due to the heating time was observed. It is thought that the amount of rosin applied was minimal, so it did not spread any further. Although a channel could be formed even with a heating time of 1 min, a slight outflow from the tip of the channel was confirmed, so it was determined that a heating time of 3 min is preferable. The slight difference in the channel shape is most likely due to the angle of the rosin solution spray, rather than the heating.

The masking mold must align reproducibly when spraying rosin solution from both sides. If spraying and heating can be accomplished under the same condition without moving the μPADs, they can be fabricated more easily by spraying from one side and heating treatment as in this case.

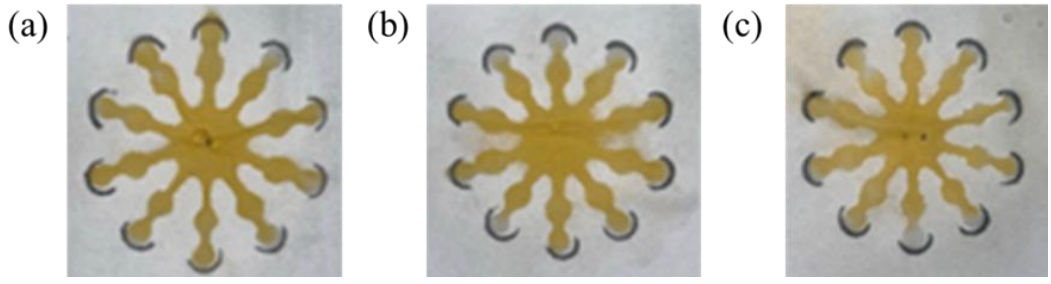

Figure 4.13 Comparison of flow channel shape by heating time
(a: 1 min, b: 3 min, c: 5 min)

4.3.5 Evaluation of resistance to acid and base

To evaluate the resistance of the hydrophobic barrier to acidic and basic solutions, an acid and a base were introduced into the fabricated μPADs. The results, presented in Figure 4.14, show the behavior of the μPADs when water, 1 M hydrochloric acid, and 1 M sodium hydroxide were used as samples. When an acidic sample was introduced, the flow channels retained their shape, similar to the case with water. In contrast, the introduction of a basic sample broke the flow channels. Consequently, an investigation was conducted to determine the pH threshold at which the flow channels could maintain their structure.

The pH of the 1 mol L^{-1} sodium hydroxide solution was measured using pH test paper and found to exceed pH 11. The solution was subsequently diluted to prepare solutions with concentrations of 0.1 mol L^{-1} (pH 10–11), 0.01 mol L^{-1} (pH 9–10), 1×10^{-3} mol L^{-1} (pH 8–9), and 1×10^{-4} mol L^{-1} (pH 8). The experimental results are presented in Figure 4.15. In Figure 4.15 (a), the solution flowed through the channels extending in 10 directions; however, the channel widths increased, indicating the breakdown of the hydrophobic barriers. In contrast, the flow channel structures were preserved in Figures 4.15 (b–d). It should be noted that, in Figure 4.15 (b), no solution flowed in the left-side channel. This phenomenon is likely attributable to excessive absorption of the rosin solution, which may have resulted in channel blockage, but not due to the broken channels. As neither leakage nor breakdown of the flow channels was observed when introducing basic solutions with pH below approximately 10, it can be concluded that the fabricated μPADs are suitable for use with aqueous solutions with a pH of approximately 10 or lower.

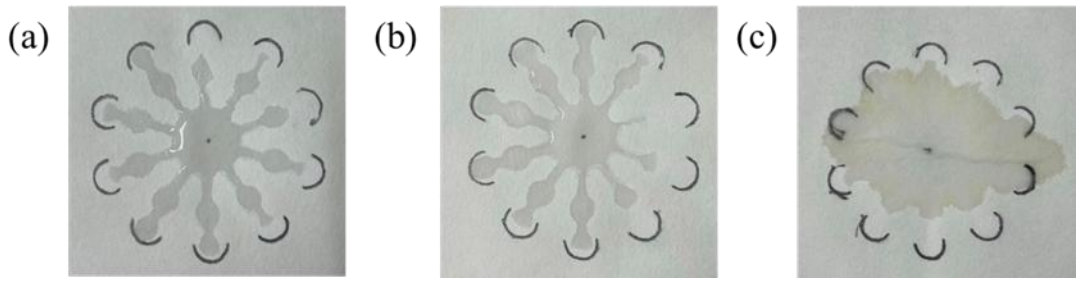

Figure 4.14 μPADs with acid or base

(a: Water, b: HCl, c: NaOH solution)

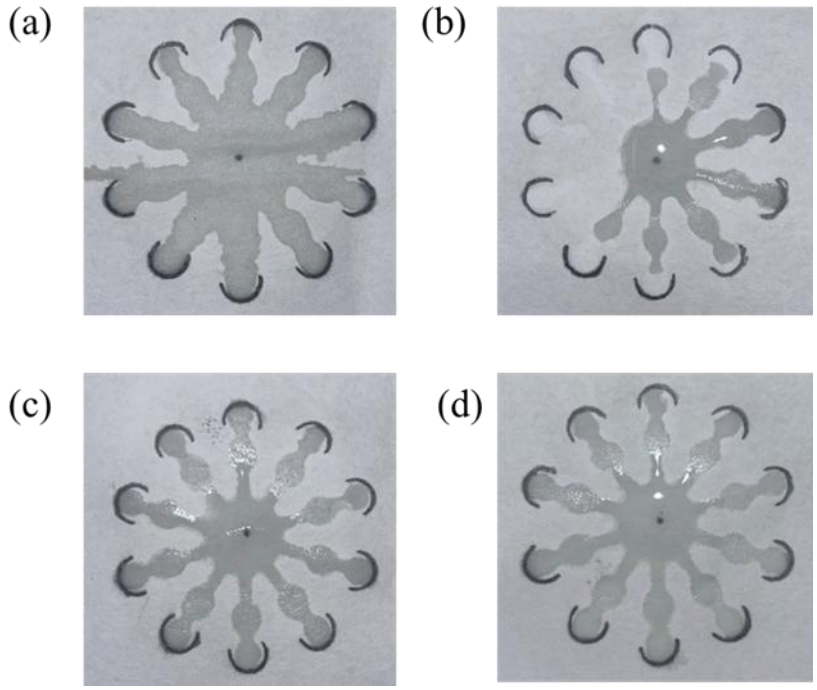

Figure 4.15 μPADs with various concentrations of base

(a: 0.1 mol L^{-1}, b: 0.01 mol L^{-1}, c: 1×10^{-3} mol L^{-1}, d: 1×10^{-4} mol L^{-1})

4.3.6 Comparison with μPADs fabricated using a wax printer

The performance of μPADs was evaluated by conducting (1) acid-base titration and (2) nitrite ion concentration measurements, and the results were compared with those obtained by conventional methods.

(1) Acid-base titration

The acid-base titration μPADs were fabricated based on the method reported by Karita et al. [11], employing a similar design for the μPADs produced using both a wax printer and the developed fabrication method. The reagents required for the titration reactions were pre-added to the designated locations, as indicated in Figure 4.16. The primary standard solutions were prepared at ten concentration levels, with dilution intervals of 1/10 or 1/100. A volume of 2 μL from each concentration was introduced into the reaction

zone twice. The values displayed next to the detection zones indicate the concentrations of the added primary standard solutions. Sodium carbonate solution and potassium hydrogen phthalate solution were used as the primary standard substances. Phenolphthalein, at a concentration of 0.25%, was employed as the indicator. A volume of 1.5 μL was added to the detection zone twice. Subsequently, 40 μL of the sample solution was introduced into the sample inlet three times, so the total volume is120 μL. The samples used in the titration were 0.5 mol L^{-1} HCl or 0.04 mol L^{-1} NaOH solution. The results obtained from these experiments are shown in Figure 4.17.

In Figure 4.17 (a), the hydrochloric acid did not flow along with the channel fabricated with rosin barriers. This means that additions of the basic standard solutions to the reaction zones break the flow channels of the μPADs fabricated using the developed method. Conversely, as shown in Figure 4.17 (b) where the acidic standard solutions were added to the reaction zones and a 0.04 mol L^{-1} NaOH solution was used as the sample, the flow channel remained the designed shape; however, phenolphthalein exhibited a color change in all detection zones. In contrast, for the μPADs fabricated using the wax printer, a color change was observed only in detection zones corresponding to concentrations below 0.04 mol L^{-1}. Namely, the reason for the incorrect detection is independent of the neutralization reaction.

In Figure 4.17 (a), the hydrochloric acid did not flow along the channel fabricated with rosin barriers. This indicates that the addition of basic standard solutions to the reaction zones destroyed the flow channels fabricated with rosin. Conversely, as shown in Figure 4.17 (b), when acidic standard solutions were added to the reaction zones and a 0.04 mol L^{-1} NaOH solution was used as the sample, the flow channel maintained its intended shape. However, phenolphthalein exhibited a color change in all detection zones. In contrast, for μPADs fabricated using the wax printer, a color change was observed only in detection zones corresponding to concentrations below 0.04 mol L^{-1}.

These discrepancies in detection accuracy in the μPADs fabricated with rosin barriers can be attributed to differences in channel widths compared to those fabricated using wax printing. The wider flow channels produced by the developed method likely resulted in a higher sample flow rate to the detection zones. Consequently, the base may have reached the detection zones before complete neutralization occurred in the reaction zones, leading to phenolphthalein turning red across all detection zones.

In the wax printer method, the wax is melted by heating, resulting in the flow channel being smaller than the printed size. Under the conditions of the developed method in this case, a flow channel of a size similar to or slightly wider than that of the masking mold was formed, which led to the observed difference from the conventional method.

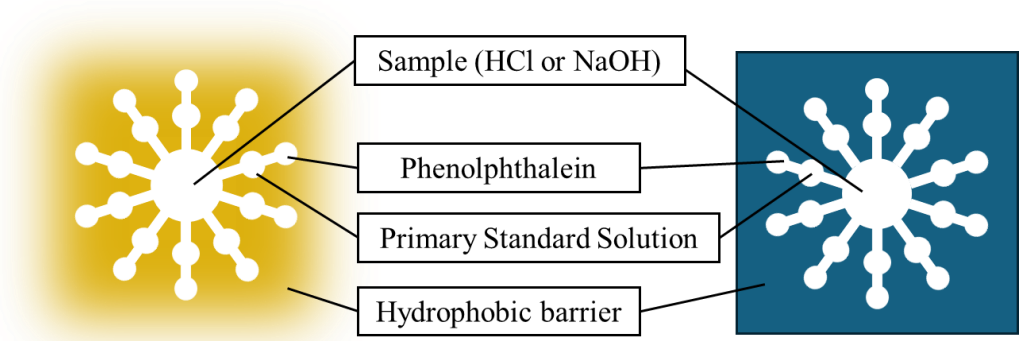

Figure 4.16 Added reagents and their location

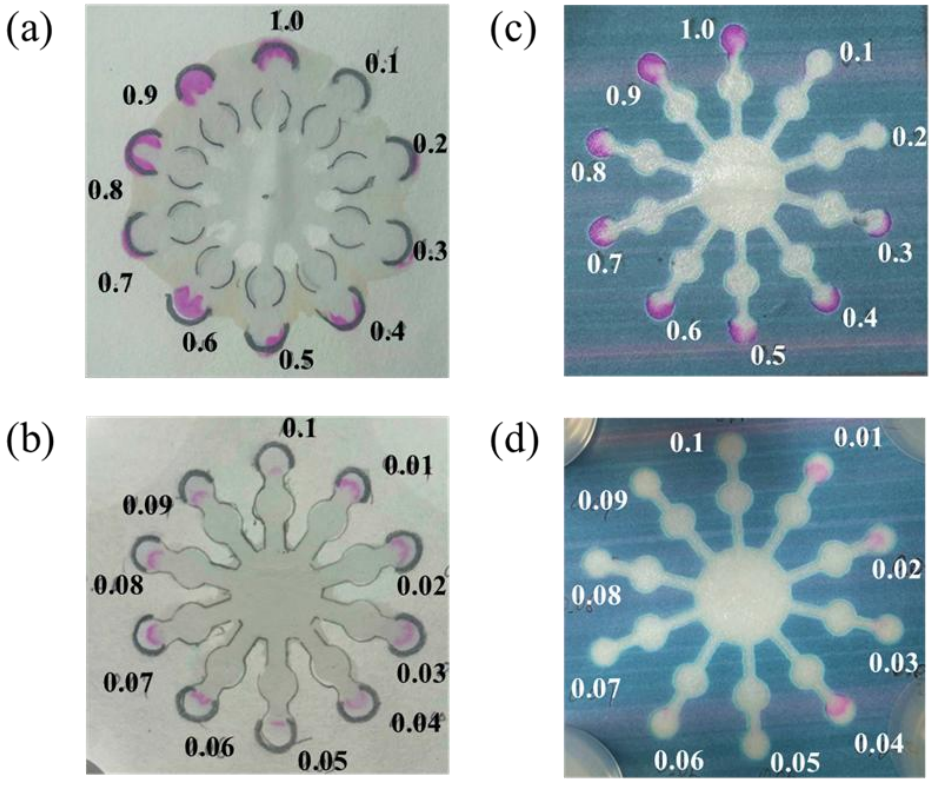

Figure 4.17 Comparison of titration results

(a, b: 0.4 M HCl, c, d: 0.04 M NaOH solution)

(2) Colorimetric measurement of nitrite

Nitrite ions were measured with reference to the paper by He et al. [2]. The sample was collected from a pond in the National Institute of Technology, Yonago College campus, and three spiked samples with different concentrations were prepared by adding nitrite ions to the sample. The spike samples were made by mixing pond water with standard solutions at the concentrations shown in Table 4.18 in a 1:1 ratio, and 2 µL was added to the circles at the ends of each channel (Figure 4.18). A total of 120 µL of Griess reagent was introduced in three increments of 40 µL into the center, and after 5 min, the absorbance was calculated from the intensity of the developed color, and a calibration curve was constructed. Table 4.3 displays the concentrations derived from the calibration curve. The µPADs made by wax printing demonstrated a higher detection sensitivity and could detect lower concentrations, while the values for Samples 3 and 4 were nearly identical. Moreover, the µPADs made using rosin were closer to the estimated values. At this level of measurement, the differences between the respective µPADs were minimal, indicating that they provide results comparable to those obtained by the conventional method.

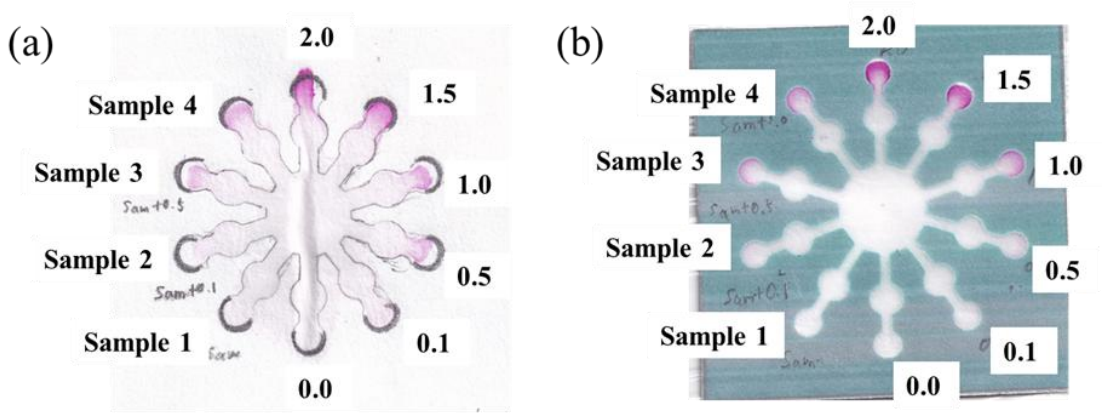

Figure 4.18 Comparison of nitrite ion measurement

(a: Rosin µPADs, b: Wax ink µPADs)

Table 4.3 NO_2^-N concentrations in environmental water and spiked samples

Sample	Estimated value (mg L^{-1})	Rosin μPADs (mg L^{-1})	Wax ink μPADs (mg L^{-1})
1 (Pond water)	-	ND	ND
2 (Pond water + 0.1 mg L^{-1} NO_2-N)	Pond water + 0.05	ND	0.2
3 (Pond water + 0.5 mg L^{-1} NO_2-N)	Pond water + 0.25	0.3	0.4
4 (Pond water + 1.0 mg L^{-1} NO_2-N)	Pond water + 0.5	0.6	0.7

4.4 Conclusion

Natural rosin worked as a hydrophobic barrier for a facile μPADs fabrication method where its solution dissolved in an organic solvent was sprayed to form the flow channels. When acids or bases of various concentrations were introduced into the fabricated flow channels, it was confirmed that the flow channel shape was maintained in aqueous solutions with a pH of 9 or lower. Acid-base titrations were attempted using the μPADs fabricated by the developed method. Although the results were inconsistent with those obtained by the wax printing method, the flow channels were proven to be usable, albeit with some limitations regarding pH conditions. To eliminate the difference from the wax printing method, it is necessary to control the flow channel width by reconsidering the spraying conditions. The spraying method developed in this study uses rosin, which is relatively inexpensive and does not require the purchase or maintenance of special equipment. Therefore, it holds potential for use in regions with limited resources, such as developing countries.

4.5 Reference

[1] Walia, S.; Bhatnagar, I.; Liu, J.; Mitra, S. K.; Asthana, A. *Int. J. Biol. Macromol.* **2021**, *193*, 1617−1622.

[2] He, Q.; Ma, C.; Hu, X.; Chen, H. *Anal. Chem.* **2013**, *85* (3), 1327-1331.

[3] Thongkam, T.; Hemavibool, K. *Microchemical Journal* **2020**, *159*, 105412.

[4] Varsha, V.; Aishwarya, S.; Murchana, S.; Naveen, G.; Ramya, M.; Rathinasabapathi, P. J. *Microbiol. Methods* **2020**, *174*, 105962.

[5] Silva-Neto, H. A.; Jaime, J. C.; Rocha, D. S.; Sgobbi, L. F.; Coltro, W. K. T. *Anallytica Chimica Acta* **2024**, *1297*, 342336.

[6] Nie, J.; Zhang, Y.; Lin, L.; Zhou, C.; Li, S.; Zhang, L.; Li, J. *Anal. Chem.* **2012**, *84* (15), 6331−6335.

[7] Armenta, S.; Esteve-Turrillas, F. A.; Herrero-Martínez, J. M. *J. Chem. Educ.* **2020**, *97*, 3852-3857.

[8] Romanholo, P. V. V.; de Andrade, L. M.; Silva-Neto, H. A.; Coltro, W. K. T.; Sgobbi, L. F. *Anal. Chem.*, **2024**, *96*, 5349-5356.

[9] Yamada, B. *J. Soc. Mater. Sci., Jpn.* **1967**, *16* (169), 800-808.

[10] Fiebach, K.; Grimm, D. *Ullmann's Encyclopedia of industrial Chemistry* **2000**, *31*, 477-494.

[11] Karita, S.; Kaneta, T. *Anal. Chem.* **2014**, *86*, 12108.

[12] Sato, K.; Hirose, T.; Furuya, O. *Journal of the Visualization Society of Japan* **2006**, *26* (7), 62-68.

[13] Kobayashi, T. *J. Jpn. Soc. Colour Mater.* **2017**, *90* (9), 324-332.

Chapter 5

General Conclusion

Chapter 5. General Conclusion

This thesis investigated the development of a simple analytical method using μPADs to measure nitrogen compounds, which are considered nutrients, in environmental water on-site. Additionally, in response to the discontinuation of wax printers, the author explored a simple fabrication method for μPADs.

The μPADs for nitrite and nitrate measurements determined their concentrations in actual environmental water samples. In the optimization study, the finding indicated that the use of zinc as a reducing agent resulted in the incomplete reduction of nitrate ions. Moreover, the study clarified that the presence of zinc decreased the detection sensitivity of nitrite ions. Furthermore, the decreased sensitivity depended on the ratios of nitrite and nitrate ions in the solution. These results indicated the need for correction formulas to estimate the concentrations of both nitrite and nitrate ions. The μPADs yielded results comparable to traditional methods, demonstrating the practicality of the proposed measurement technique. The μPADs measurement allows samples collected in the field to be measured directly by simply dropping them on the μPADs without the need for complex procedures. Moreover, it can be safely disposed of, as no pretreatment is required, making it a high-throughput array analysis method.

The measurement of ammonium ions was based on the reactions of monochloramine formation and the oxidation of α-naphthol in the μPADs. The results demonstrated that the color change of the reaction product was complex, necessitating further investigation to enable reliable quantification of ammonium ions for environmental analysis. In this study, key experimental parameters were identified to achieve concentration-dependent color changes. The findings suggest that further research, particularly the integration of a suitable color processing method, will enable the accurate quantification of ammonium ions. Once the μPAD method for ammonium ion detection is fully established, it could offer a simple, on-site measurement solution, providing an environmentally friendly and less burdensome alternative for both environmental monitoring and human health.

It was demonstrated that the application of a rosin solution facilitates the fabrication of hydrophobic barriers. While rosin is both inexpensive and readily available, its use is limited by the types of reagents and the pH range of the sample. Under conditions with a pH of 9 or lower, the channel shape remained stable, confirming its potential as a suitable flow channel material. However, when applied to titration experiments using μPADs, strict control over channel width was required, necessitating further investigation. Subsequent experiments for nitrite quantification revealed that the μPADs fabricated with rosin successfully facilitated the use of flow channels for rough estimation of nitrite concentrations, making them suitable for screening purposes.

This study addressed several challenges associated with the on-site environmental analysis of nitrogen compounds in natural water, focusing on simple operation, portability, and cost reduction through the use of μPADs. The developed μPADs aim to resolve these challenges, contributing to the achievement of specific Sustainable Development Goals (SDGs). The author believes that this research will advance the field of analytical chemistry and solve environmental problems in resource-limited settings, particularly in developing countries where access to both skilled personnel and advanced technology is restricted.

Acknowledgements

In writing this thesis, I received tremendous support and cooperation from many people, and I would like to express my sincere gratitude to all those who contributed to this research.

In particular, I would like to deeply thank Professor Takashi Kaneta of the Graduate School of Natural Science and Technology at Okayama University for his guidance throughout this research. Without Professor Kaneta's outstanding guidance and consistently accurate advice, this research would not have been possible. Furthermore, I am grateful for the opportunity to present at international conferences, an experience that greatly contributed to my confidence and personal growth. I learned a tremendous deal from exchanging ideas and interacting with people across borders and disciplines. Beyond the laboratory, I also learned a lot from Professor Kaneta, and it was his character that allowed me to approach the research with sincerity and carry it out to this point. I express my heartfelt thanks.

I would like to express my heartfelt gratitude to Associate Professor Nobuyuki Takeyasu and Assistant Professor Kaewta Danchana of the Graduate School of Natural Science and Technology at Okayama University for their guidance on research methodology, presentations, and thesis writing, as well as for the many insightful discussions we had on a daily basis. I am also grateful for sharing their passion for research with me.

I would also like to extend my thanks to the members of the thesis review committee, including Professor Takayoshi Suzuki and Associate Professor Nobuyuki Takeyasu, for their valuable feedback and advice from various perspectives. I deeply appreciate the time they took out of their busy schedules to provide guidance.

I am also thankful to Dr. Toshiyuki Tanaka, Senior Researcher at the Tottori Institute of Industrial Technology Center, for his technical support during Raman spectroscopy measurements and for his assistance with experiments and data analysis.

I would like to express my sincere gratitude to Professor Shoji Motomizu of the Graduate School of Natural Science and Technology at Okayama University for his valuable opinions and for providing me with information that broadened my

perspective. I deeply appreciate his constant care and guidance every time we met.

I would like to extend my sincere gratitude to Professor Kaoru Aoki, Associate Professor Yusuke Date, Technical Staff Eiichi Hino, and Associate Professor Takatoshi Fujii at the National Institute of Technology, Yonago College for their guidance in research and for their invaluable support in securing funding, which allowed me to smoothly advance my research activities. I am deeply grateful for their ongoing assistance throughout the course of this study.

I also deeply appreciate the students of Yonago College, who conducted experiments alongside me and shared the challenges and joys of the research. Naoto Arimatsu, Tamaki Miyawaki, Keisuke Yamamoto, Yuto Misaki, and Shinichiro Hiroyoshi contributed to the research on nitrite and nitrate ions. Soichiro Ida assisted with the research on ammonium ion measurements. Saya Yoshida collaborated on the study of a simple μPADs fabrication method using rosin.

Furthermore, the members of the Analytical Chemistry Laboratory at Okayama University provided valuable insights during our weekly discussions, which greatly contributed to the success of this research. Even though our time together was brief, it proved to be a valuable resource for me. I sincerely thank them all.

This research was supported by a grant from JSPS KAKENHI (Grant Number JP23K04830), and I would like to express my sincere gratitude for this support.

Finally, I am deeply grateful to my husband, Umeda Shota, and my family for their support, which allowed me to focus on my research. Thanks to their constant encouragement, I was able to bring my doctoral thesis to completion. I truly appreciate all the support they have given me.

Please accept my sincerest thanks to everyone involved in this work. I dedicate this acknowledgment to each and every one of you.

March 2025

Mika Isoyama

List of Publications

Referred paper

1. Reduction with zinc — impact on the determination of nitrite and nitrate ions using microfluidic paper-based analytical devices
   M. I. Umeda, K. Danchana, T. Fujii, E. Hino, Y. Date, K. Aoki, T. Kaneta
   Transactions of the Talanta Open, Vol.10, Paper No. 100347 (2024).

2. Development of a simple method for measuring ammonia in environmental water
   S. Ida, M. I. Umeda, T. Fujii, E. Hino, Y. Date, K. Aoki, K. Danchana T. Kaneta
   Proceedings of the *6*th INTERNATIONAL ENVIRONMENTAL CHEMISTRY CONGRESS symposium, The Society of Turkish Chemist Society, p.74 (2024).

3. A facile fabrication method for microfluidic paper-based analytical devices using natural resins
   S. Yoshida, M. I. Umeda, T. Fujii, E. Hino, Y. Date, K. Aoki, K. Danchana T. Kaneta
   Proceedings of the *6*th INTERNATIONAL ENVIRONMENTAL CHEMISTRY CONGRESS symposium, The Society of Turkish Chemist Society, p.75 (2024).

Other Papers

1. オンサイト環境分析のためのマイクロ流体ペーパー分析デバイス
   梅田美華，金田隆，分析化学，Vol.73, No.9, pp.433-439 (2024).

2. Effect of Electrospun Nanofibrous Film on Drilling-Force Reduction for Fine-Hole Drilling in Metals
   Y. Date, H. Sunaba, Y. Oyama, T. Sato, T. Yamawaki, M. I. Umeda, T. Fujii, E. Hino, K. Aoki, M. Goto
   Tribology Online, Vol.19, No.4, pp.381-386 (2024).

3. Separation and fractionation of glutamic acid and histidine via origami isoelectric focusing
   K. Danchana, N. Yamashita, M. I. Umeda, T. Kaneta
   Journal of Chromatography A, Vol.1706, Paper No. 464247 (2023).

4. 高温水蒸気による炭化けい素繊維結合型セラミックスの腐食挙動
青木 薫, 伊達 勇介, 藤田 剛, 藤山 淳平, 礒山 美華, 藤井 貴敏, 日野 英壱
耐火物誌, Vol.75, No.5, pp.173-177 (2023).

5. 湖底耕耘による底質環境改善効果
藤井 貴敏, 伊達 勇介, 日野 英壱, 礒山 美華, 青木 薫
環境技術, Vol.51, No.2, pp.93-98 (2022).

6. 減圧下で氷温水処理した炊飯米の物性
伊達 勇介, 勝部 諭紀, 角田 直輝, 福間 康文, 礒山 美華, 藤井 貴敏, 日野 英壱, 青木 薫
氷温科学, Vol.23, pp.1-7 (2022).

7. 氷温技術を用いたワイン醸造　その 1　氷温乾燥および氷温減圧乾燥によるブドウの高糖度化
伊達 勇介, 藤井 雄三, 藤井 貴敏, 日野 英壱, 原 美咲, 加川 庸一, 礒山 美華, 福間 康文, 小田 耕平, 青木 薫
氷温科学, Vol.17, pp.16-20 (2015).

8. 氷温水処理した炊飯米の物性と食味　～保温と冷凍の影響～
藤井 貴敏, 藤井 雄三, 伊達 勇介, 日野 英壱, 嘉村 茅夏, 礒山 美華, 福間 康文, 小田 耕平, 青木薫
氷温科学, Vol.17, pp.11-15 (2015).

International Conference

1. Development of a simple method for measuring ammonia in environmental water
   S. Ida, M. I. Umeda, T. Fujii, E. Hino, Y. Date, K. Aoki, K. Danchana T. Kaneta
   The *6*th INTERNATIONAL ENVIRONMENTAL CHEMISTRY CONGRESS, The Society of Turkish Chemist Society, No. PP-10 (Trabzon, 2024-11).

2. A facile fabrication method for microfluidic paper-based analytical devices using natural resins
   S. Yoshida, M. I. Umeda, T. Fujii, E. Hino, Y. Date, K. Aoki, K. Danchana T. Kaneta
   The *6*th INTERNATIONAL ENVIRONMENTAL CHEMISTRY CONGRESS, The Society of Turkish Chemist Society, No. PP-11 (Trabzon, 2024-11).

3. Preparation and evaluation of boron sensing material composed of chromotropic acid in layered double hydroxide
   K. Yoshida, Y. Date, M. I. Umeda, T. Fujii, E. Hino, K. Aoki
   The *6*th INTERNATIONAL ENVIRONMENTAL CHEMISTRY CONGRESS, The Society of Turkish Chemist Society, No. PP-23 (Trabzon, 2024-11).

4. Development of a simple method for measuring nitrate ions in natural water samples
   Mika I. Umeda, Takatoshi Fujii, Eiichi Hino, Yusuke Date, Kaoru Aoki, Danchana Kaewta, Takashi Kaneta
   Pure and Applied Chemistry International Conference 2024, The Chemical Society of Thailand, No. AC-O-22, (Bangkok, 2024-01).

5. Observation of cell blebs immobilized on a glass substrate by total internal reflection fluorescence microscopy
   Mika Isoyama, Takashi Kaneta
   Asianalysis XIII, The 13th conference on analytical sciences, The Chemical Society of Thailand, National Research Council of Thailand, Research group of the University of Malaysia, The Japan Society for Analytical Chemistry, The Japanese Association for Flow Injection Analysis, No. OR-76 (Chaing Mai, 2016-12)

Domestic Meeting

1. 環境水中の窒素化合物計測のためのペーパー分析デバイスの開発
   礒山 美華, 藤井 貴敏, 日野 英壱, 伊達 勇介, 青木 薫, Danchana Kaewta, 金田 隆
   日本分析化学会第 73 年会，No. D2008 (名古屋市，2024-09).

2. 環境水中の亜硝酸イオンおよび硝酸イオンの簡易計測法の開発
   礒山 美華, 藤井 貴敏, 日野 英壱, 伊達 勇介, 青木 薫, Danchana Kaewta, 金田 隆
   日本分析化学会第 72 年会，No. 1D-101 (熊本市，2023-09).

3. ガラス基板上への細胞小胞固定の全反射蛍光顕微鏡観察
   礒山 美華，金田 隆
   日本分析化学会第 65 年会，No. C3001 (札幌市，2016-09).